Democratic and Popular Republic of Algeria

Ministry of High Education and Scientific Research

University of Ferhat Abbas Setif1

THESIS

Presented at Faculty of Sciences

Department of Physics

To obtain the degree of

Doctor

Option: Applied Physics

By

Narimane Dahdouh

Title

Radiobiological assessment of radiotherapy treatment plans

:Discussed publicly at 27 / 09 / 2025 with the board of examiners

S.Houamer	**Professor**	**Univ. Ferhat Abbas Setif 1**	**President**
Z.Chaoui	**Professor**	**Univ. Ferhat Abbas Setif 1**	**Thesis Director**
A.Dib	**Professor**	**Univ. Scienc. Thec. Oran1**	**Examiner**
A.Belafrites	**Professor**	**Univ. Mohamed seddik Benyahia Jijel**	**Examiner**
A.Betka	**M.C.A**	**Univ. Ferhat Abbas Setif 1**	**Examiner**

"To all those who have fought or are still fighting cancer, I truly hope that this modest work will bring you a sense of hope, and accept it as a small token of support and solidarity"....

Contents

Acknowledgments

First and foremost, I want to express my deepest gratitude to God for granting me the resilience to endure and the courage to conquer all challenges.

I want to express my profound gratitude to my thesis supervisor, ***Pr. Zine El Abidine Chaoui****. He introduced me to the Fortran language and made major contributions to the programming of radiobiological models. His technical expertise in writing articles has been invaluable, and he instilled in me the essential values of being a dedicated researcher. Through his guidance, I learned the importance of seriousness, discipline, and patience. I truly appreciate his unwavering support and attentiveness throughout this journey. Thank you for your exceptional guidance.*

I would also like to express my gratitude to ***Dr. Saad Khoudri****, who heads the medical physics unit at the Setif Cancer Center, and* ***Dr. Ismail Zergoug****, who heads the medical physics unit at ONCOPOLE L'espoir Center in Oran. Their generosity in providing me with access to patient databases has been invaluable in completing this thesis. I am also thankful for their valuable feedback and guidance throughout this process.*

I am deeply thankful for the valuable guidance provided by ***Pr. Khelil Boumama*** *during my doctoral work. His advice has been invaluable, and I am truly honored to have had the opportunity to know and learn from him.*

I would like to express my sincere gratitude to the members of the Physics Department at the Cancer Center of Setif for contributing to an enriching working experience. Particularly the medical physicists and the oncologist, Dr. Hamzi.

Finally, I would like to express my sincere gratitude to the jury member for graciously agreeing to evaluate my work.

Dedication

This thesis is dedicated

*To my beloved father **ABED EL HAFID**, who not only taught me middle school mathematics but also dedicated his life to sharing the wonders of science. Even after retiring, he continues to give and inspire. He still takes an interest in the students he once taught, selflessly sacrificing everything for our education and happiness.*

*To my dear mother **BEN IGHIL FATIMA**, who dedicated her life to us and imparted the essential values of life, who wholeheartedly devoted herself to caring for her children, who made countless sacrifices for my happiness, even at the expense of her own.*

The depth of my love and respect for you cannot be captured by any words or phrases. Your unwavering support, guidance, and advice have meant the world to me, and I am forever grateful.

*To my husband **MESBAH HAMZA**, I would like to express my love and gratitude to you for your unwavering support and encouragement, even in your own unique but deeply heartfelt way.*

*To my grandson **ILYES**, who has brought so much joy and sweetness into my life.*

To my sister Louisa and brothers Belkacem, Massinissa, and Lounes, I dedicate this work to you as a testament to my deep affection for you. Life without you would be lacking.

To all my beloved family: Mesbah Nacer Eddin and Nechadi Dalila, …, friends, and relatives: Dr. Dahdouh Nadjib, and Dahdouh Sarah, …who have offered support and assistance, near and far, as I completed this work.

In loving memory of my grandfather, may God have mercy on him, whose passion for science inspired us all.

List of Figures

Chapter I

Chapter II

Chapter III

Chapter IV

List of Tables

Chapter I

Chapter II

Chapter III

Chapter IV

List of abbreviation

IMRT: Intensity-modulated radiation therapy

MIT: Monoisocentric technique

DIT : Dual isocentrique technique

H&N cancer: Head and neck cancer

VMAT: Volumetric intensity-modulation arc therapy

TCP: Tumor control probability

NTCP: Normal tissue complication probability

LQ: linear quadratic

DNA: Deoxyribonucleic acid

OAR: Organ at risk

ICRU: International Commission on Radiation Units and Measurements

IAEA: International Atomic Energy Agency

PTV: planning target volume

GTV: Gros tumor volume

CTV: clinical target volume

RCF: repopulation correction factor

FSU: functional subunits

PSA: prostate-specific antigen

EBV: Epstein-Barr Virus

BED: biological effective dose

LKB: Lyman-Kutcher-Burman

CV: Critical volume

FSU: Functional sub-units

UTCP: Uncomplicated tumor control probability

DVH: Dose-volume histogram

3D-CRT: Three-dimensional conformal radiation therapy

TPS: Treatment planning system

EUD: Equivalent uniform dose

TRU: Tissue-rescuing units

CSV: comma-separated value

RTOG: Radiation Therapy Oncology Group

EORTC: European Organization for Research and Treatment of Cancer

LENT: Late Effects Normal Tissue Task

SOMA: subjective, objective, management and analytic

CTCAE: Common Terminology Criteria for Adverse Events

MRI: Magnetic resonance imaging

AOM : Acute otitis media

COM : Chronic otitis media

RS: Relative seriality

LM: logistic model

BS: Brainstem

SC: Spinal cord

OC: Optical chiasm

RON: Right optical nerve

LON: Left optical nerve

RME: Right middle ear

LME: Left middle ear

RP: Right parotid

LP: Left parotid

RL: Right lens

LL: Left lens

EQD: Equivalent uniforme dose

Introduction

The pursuit of a reliable indicator for assessing the response of normal tissues to specific radiation doses during and after radiotherapy remains a significant topic of discussion among radiobiologists. This challenge continues to be a focal point within the field. In recent years, indicators have been developed as radiobiological models. These predictive assessments aim to identify various clinically measurable radiobiological characteristics crucial for personalizing radiotherapy, thereby enhancing treatment quality while minimizing associated morbidity.

These models are essential tools for evaluating and selecting the most effective radiotherapy treatment plans. Additional important factors include: the dose delivered by the treatment accelerator, the spatial distribution of the dose, and the quality indices of dosimetry. The predictive radiobiological models include parameters in their equations. It is therefore essential to thoroughly understand the biological information behind these parameters through mathematical modeling. Several endpoints of the major dose-limiting organ are evaluated to predict early and late effects fitted by these parameters, using our elaborated in-house program (Radbio-For) and an effective optimized tool for isotoxic plans.

In this thesis, we aim to provide a comprehensive overview of the significance of various radiobiological models, supported by analyses conducted to predict in a precise and personalized way the early and late effects of different cancers at different stages caused MV photon beams in healthy tissues during external radiotherapy. Furthermore, it suggests alternate fractionation schedules to optimize the treatment plan and possibly reduce the period of treatment.

Upon reviewing the historical context, it is evident that external photon beam radiation therapy has played a crucial role in treating localized cancer. Various techniques and modalities have been employed; however, the available literature indicates that none of these studies utilized radiobiological tools to assess the effectiveness of 7-field and 5-field IMRT plans for prostate cancer, as well as to predict the different pneumonitis toxicities associated with MIT and DIT in treating the breast cancer. This thesis will discuss the analysis of these two searches in detail.

Procedure for Completing the Thesis:

The work has been divided into four stages. The first stage involves developing a program that integrates all the radiobiological models discussed in this work. This program aims to manage execution time, unify the data types used, and prevent the need for any conversions of dose and volume units between different programs.

In the second stage of the process, radiobiological models serve as criteria for comparing various external radiotherapy treatment techniques and modalities. This comparison aims to identify the most effective approach that preserves the organs at risk and ensures optimal control of the target treatment. The third stage focuses on predicting toxicity levels by assessing multiple endpoints related to late and severe toxicity in the various organs at risk. This analysis establishes important dose constraints that influence toxicity predictions and studies the reliability of expected radiation-induced late complication calculations in advanced H&N cancers and prostate cancer. Lastly, the fourth stage is dedicated to optimizing treatment plans, to minimize side effects on the identified organs at risk, thereby allowing for a more personalized approach to radiotherapy for individual patients.

Chapter I: Bases of Clinical Radiobiology

I. Clinical radiobiology

Clinical Radiobiology Processing Contact between a given physically absorbed dose and the resulting dose biological responses are related to factors that influence this relationship. Although the term tolerance is often (wrongly) used when discussing radiotherapy toxicity, it is important to recognize that there is no dose below its zero-complication rate: there is no clear limit to tolerance. A wide range of doses is seen in clinical practice at which the risk of a given radiation reaction increases from 0% As the dose increases to 100% (ie, dose-response relationship).

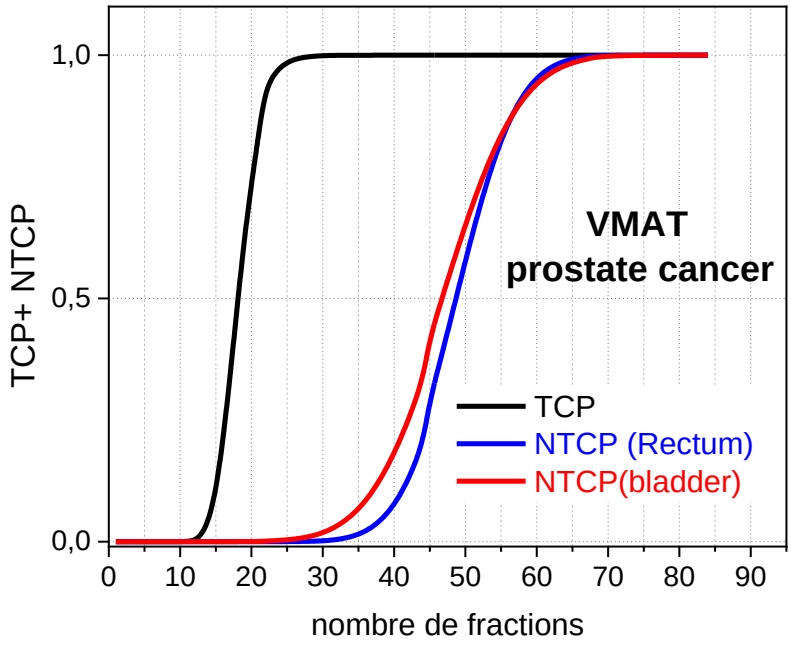

Figure I.1: Calculated TCP and NTCP of late rectal toxicity grade ≥ 2 of rectum and late bladder toxicity using presented program Radbio-For.

The specific event that may or may not occur at some point after irradiation is called an endpoint **(Bentzen 2018)**. The dose-response concept of radiation endpoints is almost integrated into our definition: to classify a phenomenon as a radiation effect, we never or rarely see it after zero doses, and in almost all cases, at very high doses post-dose. Different approaches to characterize endpoints in normal tissue are discussed in more detail.

II. Classical radiobiology

Radiation biology is the study of the effects of ionizing radiation on cells and organisms. Radiation modeling combines radiation physics and living cell biology. The most basic unit of an organism is the cell. The latter consists of different biological materials. The most important part of all cells is the nucleus, which contains the genetic material that controls the cell's response to any stimulus.

Cells are generally divided into somatic cells that can undergo mitosis and germ cells. The type of division germ cells undergo is called meiosis, which occurs in two stages. The first step is meiosis, in which a diploid parent cell divides to form a haploid daughter cell. During the second stage of meiosis, haploid daughter cells; one from the male parent and one from the female fuse to form a diploid daughter cell **(Ohkura 2015)**.

When a cell is exposed to radiation, the radiation passes through the cell and a certain amount of energy is deposited in the cell. Cells can be damaged by acting as a "resistance". The interaction between radiation and cell molecules produces excitation and ionization. Generally, two cellular effects occur during the interaction between cells and radiation: direct effects and indirect effects.

Radiation damage to the human body is usually not immediately apparent, like burns or cuts. The timescale on which radiation damage manifests depends on the intensity of radiation exposure, the total exposure time, and the characteristic radiation sensitivity of the tissue. Physical realization of radiation damage can be divided into early tissue response and late tissue response **(Andrea et al. 2007, Podgorsak 2005)**.

i. Early effects :

Early effects of radiobiological damage appeared within 3 months of radiation therapy/exposure. They mainly result from burning or a depletion of the number of cells capable of reproduction or repair in the irradiated tissues and only appear in the presence of doses large enough to destroy many of these cells.

The tissues most sensitive to acute effects are renewal tissues, such as the basal layer of the skin (mucosa), bone marrow, and stem cells in the crypts of the small intestine. Complications that can manifest as early effects of radiation exposure include edema, inflammation, hemorrhage, and denudation of epithelial and hematopoietic tissue. The acute middle ear otitis displayed in the figure below has been selected as the

evaluation endpoint for both ears following head and neck cancer radiotherapy in all study patients.

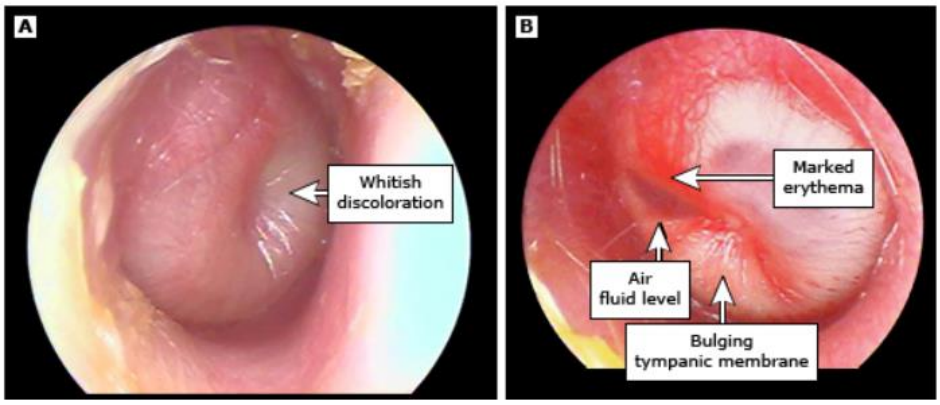

Figure I.2: Example of a white tympanic membrane caused by acute otitis media. **(A)** Protruding tympanic membrane with minimal erythema; **(B)** Protruding tympanic membrane with prominent erythema at the malleus handle and an air-fluid level on the upper anterior part of the tympanic membrane. *Courtesy of Alejandro Hoberman, MD. Graphic 63268 Version 6.0© 2023 UpToDate, Inc. and/or its affiliates. All Rights Reserved.*

ii. Late effects :

The late effects of radiation damage are chronic in nature concerning normal tissue and clinical radiation therapy. These include mutagenic and carcinogenic effects, considered stochastic phenomena resulting from random molecular alterations of individual cells, the frequency of which increases as a linear function of the dose.

Delayed effects may be caused by stem cell depletion, radiation damage to stromal tissue components, or repeated radiation damage to overlying tissue. Delayed responses have long-term effects on organ physiology. Fibrosis, ulceration, atrophy, obstruction, or stenosis are some examples of symptoms associated with advanced chronic radiation injury **(Chapman et al. 2016)**. An example of a late complication used in our evaluation of prostate cases has been illustrated in

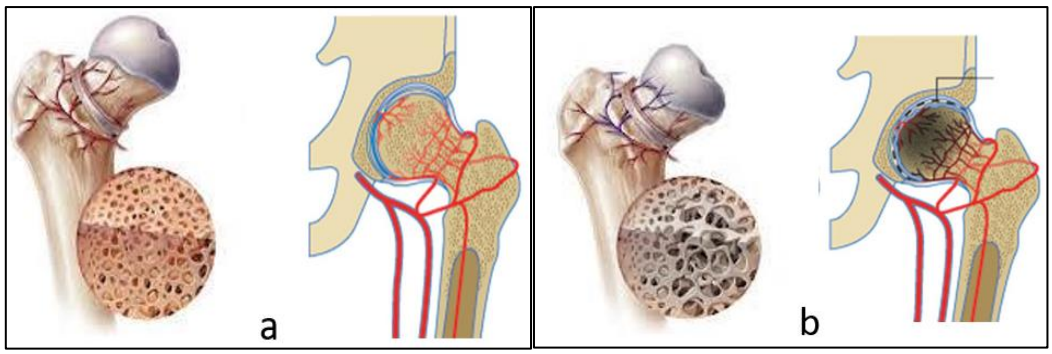

Figure I.3: a) Healthy femoral head and **b)** femoral head with avascular necrosis.

the following figure, in cases of Grade 5 necrosis, bone death occurs in the femoral head due to a defect in bone vascularization. As a result, the affected bone becomes extremely fragile and is more prone to fracturing than healthy bone **(Burman et al. 1991)**.

iii. Prolonged germinal effects :

Radiation damage can be fully repaired, leading to programmed cell death or genetic mutation. DNA damage due to free radicals interacting with chromosomes can sometimes lead to incomplete repair, resulting in mutation rather than apoptosis. This affects the germ cells of the organism **(Podgorsak 2005)**. The effects of this type of radiation damage continued and became visible in the second generation.

Around the early 1980s, significant advances were made in the theory of radiobiology, focused on the linear quadratic (LQ) model and the associated α/β ratio; it was believed that α/β was generally high (~10 Gy) for the destruction of tumor clonogenic and low (~3 Gy) for dose-limiting 'late' normal tissue complications. These were the very important characteristics of classical radiobiology **(Williams et al. 1985, Fowler 1989, Steel 2002, Steel 2007)**.

1. 5Rs of radiobiology :

Is rooted in 5 primary biological factors also called the five Rs of radiotherapy:

i. **Radiosensitivity:** The damage to different cell types (tumor or organ at risque) varies, for a given single dose of radiation. This characteristic plays an important role in determining the response of cells to a given dose of ionizing radiation **(Andrea et al. 2007, Withers 1975, Steel 1993)**.

ii. **Repair:** The instant after a finite amount of radiation damage occurs in a living cell, cell diagnostics detect abnormal DNA strand breaks and initiate a very sophisticated repair mechanism. However, the time it takes for a full repair (mostly but not always) depends on the type of cell and the extent of damage encountered.

iii. **Repopulation:** Cell proliferation is advantageous for OARs and a disadvantage as far as radiotherapy treatment of tumors is concerned **(Withers 1975)**. While clonogenic cells that survive irradiation can repopulate tumors by proliferating and/or reducing cell loss. During fractionated radiation therapy, clonogenic tumor cells can repopulate, reducing the effectiveness of the treatment.

iv. **Redistribution:** The proliferating cell population throughout the cell cycle phases increases cell destruction from fractionated processing **(Withers 1975)**.

v. **Reoxygenation:** Hypoxic cells occur during a fractional course of treatment **(Fleet 2006)**, making them more radiosensitive to subsequent doses of radiation. Thus, damage to the same set of cells in subsequent fractions is likely to be higher as they are rendered radiosensitive. This is another factor contributing to the adaptation of fractionation in radiotherapy.

III. Modern radiobiology

In 1999, Duchesne and Peters estimated a very low value of the α/β ratio (1.5 Gy in a confidence interval of 0.8 Gy and 2.2 Gy) for the prostate location, after that several studies confirmed this value **(Brenner et al. 1999, Duchesne et al. 1999)**. In parallel with other authors who in turn calculated a very high value for the α/β ratio **(Nahum et al. 2003, Orton 2004, Valdagni et al. 2005, Williams et al. 2007, Nickers et al. 2010)**. This estimate has contributed to the birth of another meaning of radiobiology.

In this study, we examined the effect of changing the alpha/beta ratio on the surviving fraction of tumors treated with VMAT technique using 76 Gy/2Gy per fraction regime. The range of Alpha/beta ratio values is 1.5 to 5 Gy, which is generally lower than the generic 10 Gy value for prostate tumors. We observed an increase in the number of dead cancer cells when the ratio decreased. Compared to classical radiobiology we can see that prostate cancer tumors are more sensitive to fraction size or number of fractions, in accordance with the literature, we favor the hypofractionated regime over the conventional regime see Figure I. 3.

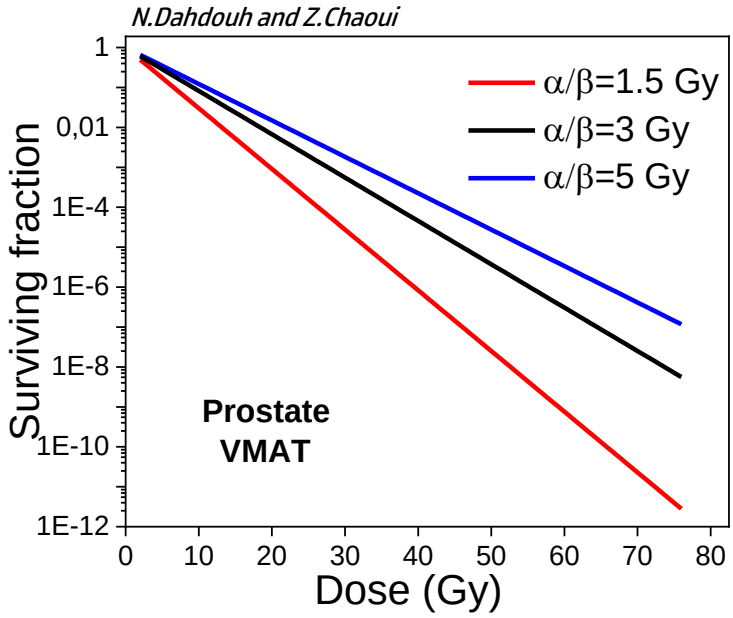

Figure I.4: Radiation survival curves for a population of prostate tumors treated with VMAT technique using presented program Radbio-For.

1. The new Rs of radiobiology:

In addition to the 5Rs of classical radiobiology, other properties of cells are very important to understanding the way tumor- and normal tissue cells behave in response to radiation exposure. These properties are enumerated below.

vi. **Irradiated volume:** The irradiated volume of an organ must be taken into account as an important parameter that determines the clinical consequences of tissue exposures **(Doerr 2009a, Doerr et al. 2014)**.

vii. **Restoration:** Long-term restoration of normal tissue, impacting tissue tolerance at long intervals of months to years after initial exposure **(Doerr 2009b)**.

viii. **Radiopathology (molecular):** Thorough knowledge of the process of molecular/tissue radio pathology is a major prerequisite for the identification of early biomarkers of the risk of development of later macroscopic tissue effects, as well as for the development of biologically based interventional strategies for modifying such effects **(Doerr 2009c)**.

ix. **Remove (non-target) effects.**

IV. **Fractionation:**

The fractionation is the division of the total prescribed dose into smaller doses. Usually, the fractions are equal in size (dose) and spread evenly over a given treatment period. Classic fractionation (5 sessions of 2 Gy per week) had been developed empirically by the first generation of radiotherapists at the beginning of the century. It is remarkable to note that even today, the most cutting-edge radiobiologists agree that this scheme often achieves the best possible compromise between antitumor efficacy and toxicity toward healthy tissues **(Nahum et al. 2018)**. Fractionation helps normal tissues recover from sub-lethal damage.

Joiner and van der Kogel from 2009 until 2019 studied the radiobiology of normal tissues and the effect of changing fraction sizes on normal tissue responses. However, this question was asked in the early 1980s because they established that the variation and change in a dose per fraction of radiation treatment can affect early and late normal tissue reactions **(Nahum et al. 2018, Bentzen 2018)**. Five categories of fractionation exist today: Hypofractionation, Conventional fractionation, Hyper-fractionation, Accelerated fractionation, and Protracted fractionation **(Dale et al. 2007)**.

Hyperfractionation refers to fractions less than 2 Gy per session, and is still at the stage of therapeutic trials, to precisely define its place in clinical practice. There is currently only one formal indication outside this framework: tumors with a very fast doubling time because only hyperfractionation then makes it possible to deliver a high dose in a short time (accelerated treatment) see Figure I. 4.

Hypofractionation is of fraction size greater than 2 Gy/fraction, it can be very widely recommended in the case of palliative irradiation, because of its simplicity and its effectiveness.

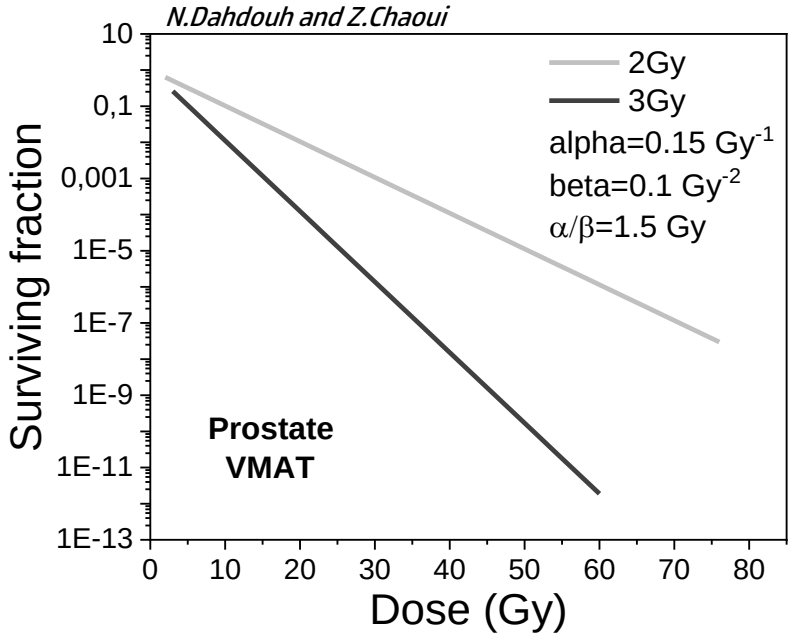

Figure I.5: Surviving fraction in the function of the prescribed dose, light gray presents the 76 Gy/2 Gy per fraction and in dark gray 60 Gy/3 Gy per fraction regimen, using presented program Radbio-For.

On the other hand, in case of treatment of large volumes (in particular digestive) in patients whose expected cure rate is high, this technique has a risk of causing an increase in late complications, and should a priori be avoided. In the case of treatment of smaller volumes (head and neck or breast), it seems possible to be able to develop "hypofractionated" protocols allowing local control identical to that obtained by the classic scheme, without a significant increase in late complications, provided to choose with the greatest care the parameters (dose, spread, fractionation) of the irradiation.

Accelerated and Protracted fractionation is defined as a total weekly dose greater than 10 Gy and a total weekly dose less than 10 Gy, successively **(Bentzen 2018, Dale et al 2007)**.

V. The place of radiobiology in radiotherapy (the contribution of radiobiological models and parameters in the evaluation of radiotherapeutic treatment plans).

Biology has contributed to the development of radiation therapy at three different levels, Based on theoretical and experimental studies of irradiation. The first is to produce ideas that provide a conceptual basis for radiation therapy, to identify the

mechanisms and processes by which tumors and normal tissues respond to radiation, and to help explain and observe these phenomena. Examples are knowledge of reoxygenation, hypoxia, repopulation of tumor cells, or DNA damage repair mechanisms. Also, biology can develop new approaches to radiation therapy or treatment strategies such as hypoxic cell sensitizers, targeting agents, high linear energy transfer radiation therapy, accelerated radiation therapy, and hyper fractionated radiation therapy **(Bentzen 2018)**.

Moving to the more specific which are protocols that consider recommendations for choosing a clinical radiation therapy schedule. For example, formulas for changes in fractions or dose rate, or recommending whether chemotherapy should be used concurrently or sequentially with radiation. We can also include a method to predict the best treatment for an individual patient (individualized radiotherapy) under this heading.

There is no doubt that radiobiology is very productive in generating new ideas and identifying potentially exploitable mechanisms. A variety of new therapeutic strategies have been developed, but unfortunately, few have produced significant clinical benefits to date. Regarding the third level listed above, the newer conversion formula is based on the linear quadratic (LQ) equation and appears to be successful. Beyond that, however, laboratory science can guide radiation therapists who are limited in choosing specific regimens due to insufficient theoretical and experimental models: it is always necessary to rely on clinical research for final regimen selection.

VI. Radiotherapy treatment plans modalities.

1. Intensity Modulated Radiation Therapy (IMRT)

This irradiated technique is a highly technical procedure. It consists of varying the shape of the irradiation beam during the same session to adapt to the shape and volume constraints of the organ to be treated. In general, recommendations for prescribing, recording, and reporting special external photon beam therapy techniques, such as IMRT, should be consistent with previous ICRU recommendations. In particular, the same definitions of terms and concepts should be used whenever possible. However, each treatment's clinical and technical uniqueness must be considered **(Karia 2018, Grégoire et al. 2011)**.

The present work consists of analyzing the treatment plans of the three localizations nasopharynx, breast, and prostate for cohorts of patients treated by radiotherapy. Because of the advancement of computer technology, radiation therapy has developed into a computer-assisted three-dimensional treatment plan to ensure consistency in radiotherapy planning across centers. The ICRU Report 83 (ICRU, 2010) builds on concepts and definitions previously presented in ICRU Reports 50 (ICRU, 1993a) and 62 (ICRU, 1999) where the IMRT optimization process is described in detail. This report updates the concept of dose ratio from a single spatial point ratio to a dose-volume ratio, coined the terms planning target volume (PTV), gross tumor volume (GTV), and clinical target volume (CTV), and defined the upper and lower dose limits to the above volumes relative to the prescribed dose. In addition, it includes reports on uniformity and uniformity indices and absorbed dose uncertainty **(Karia 2018)**.

GTV refers to visible tumors and its delineation aims to identify the demonstrable extent of the tumor and its location (see Figure). The GTV should also include any involved lymph nodes or noticeable spread to adjacent tissue areas. Surrounding the GTV is the CTV which is GTV plus a margin that will cover the microscopic spread of cancer. Adding a margin to the GTV to create the CTV is a matter of clinical evaluation by biopsy or judgment based on experience which should take into account microscopic infiltrations of disease outside of the GTV **(Burnet et al. 2004)**.

The concepts of gross tumor volume (GTV) and clinical target volume (CTV) remain important. However, the GTV description aims to determine the detectable extent of the tumor and its location (visible tumor), also including any involved lymph nodes or apparent spread to adjacent tissue areas. The CTV is the volume of tissue containing detectable GTVs and/or subclinical malignancies considered therapy-related with some probability of occurrence and a boundary covering the microscopic spread of cancer. Adding a margin to the GTV to create a CTV is a matter of clinical assessment by biopsy or empirical judgment, which should account for microscopic infiltration of disease beyond the GTV **(Grégoire et al. 2011, Burnet et al. 2004)**. Some of the anatomical structures like the bony cortex, muscle fascias, and ligaments act as barriers and limit microscopic tumor infiltration.

The PTV includes the CTV to ensure that the prescribed dose is delivered to the entire CTV while ensuring that no part of the CTV is under-dose.

2. Volumetric intensity-modulation arc therapy (VMAT)

VMAT is one of the treatment techniques used in radiotherapy, it is considered one of the best treatment techniques, particularly for prostate and head and neck cancers. It consists of delivering the dose to the tumor during continuous 360° rotation **[Bedford et al. 2009]**.

This technique is based on two principles:

- Modulation of the intensity of the delivered dose.
- 360° rotation of the beams to match the shape of the tumor.

Treatment can be performed in a single rotation, or in two rotations, with the possibility of modulating collimator rotation speed and dose rate as well as continuously moving blades with speed variability.

3. Three-dimensional conformal radiotherapy (3D-CRT).

The concept of conformal radiotherapy (3D-CRT) has emerged as a result of significant advancements in imaging technologies, including CT, MRI, and PET. Additionally, improvements in computing and collimation equipment enable us to deliver radiation treatments that are increasingly tailored to the specific dimensions of the target volume. These developments enhance the precision and effectiveness of radiotherapy **(Purdy 1999, Poncyljusz et al. 2016, Viani et al. 2019)**.

3D conformal radiotherapy is an advanced technique that facilitates the precise targeting of treatment areas utilizing three-dimensional reconstructed images. This method encompasses three essential phases: the acquisition and processing of 3D images, the planning of the treatment, and the execution and verification of the treatment process. The current development of this technique necessitates several critical components:

- ✓ Implementation of procedures to ensure the reproducibility of treatment, which includes effective patient immobilization and contention methods.

- ✓ Utilization of three-dimensional imaging to capture all irradiated volumes, primarily through CT scans, with the potential for supplementary imaging techniques such as MRI, PET, and image fusion.
- ✓ Precise delineation of target volumes and critical organs, ensuring the application of appropriate safety margins.
- ✓ Customized beam collimation and ballistic calculations, which involve tailored shielding and specialized collimators, grounded in a three-dimensional evaluation of dose distribution across various volumes, including GTV, CTV, PTV, and organs at risk.
- ✓ Rigorous control of treatment reproducibility through monitoring techniques such as portal imaging.

This comprehensive approach is essential for enhancing the effectiveness and safety of the treatment process **(Purdy 1999, Mazonakis et al. 2022)**.

XI. The LQ formula for cell survival

The Linear Quadratic (LQ) is originally an empirical model used to fit radiation chromosome damage and radiation-induced suppression of broad bean growth and development **(Lea et al. 1942, Gray et al. 1951)**, This model is currently the most widely-used radiation effect formulation **(Fowler 1989)**. The LQ model represents a major advance in describing the killing of cells by ionizing radiation, especially in the radiation therapy of cancer. For a set of cells, each with the same radiosensitivity, the LQ model predicts the fraction of survival of irradiated cells depending on the dose ‘d’, according to the (relation 1):

$$SF=\frac{N_s}{N_0} = \exp\{-\alpha d - \beta d^2\} \quad \text{(1)}$$

The LQ expression can be written as:

$$-\text{Ln (SF)} = \alpha d + \beta d^2 \quad \text{(2)}$$

where: No is the initial number of cells (tumor clonogens), and N_s is the mean number of surviving cells after a radiation dose d. The coefficients α and β represent Radiosensitivity parameters **(Chapman 2003, Nahum et al. 2015)**.

The coefficient α describes "single-hit" killing (i.e. irreparable) also relates to the direct radiation damage, and β describes cell killing due to the combination of two independent sublethal lesions and is mostly DNA damage consisting of single-strand breaks. The two parameters (α and β) depend on the phase of the cell cycle; when the

LQ model is applied to "asynchronous" cell populations, which is the standard case in organisms and laboratories, the resulting alpha and beta must be averaged over the cell cycle **(Nahum et al. 2015)**. The magnitude of β relative to α can determine the increment of effect with increasing dose per fraction, particularly at high doses per fraction.

The basic LQ model is highly applicable to in vitro and in vivo data, it may require additional functionality or modification to more fully describe the clinical practice and other factors such as repopulation and other physiological changes during treatment. That is another challenge for the future.

1. **Biological effective dose**

The BED is defined as the physical dose required for a given effect without repopulation, its concept is derived from the LQ model which was proposed by Chadwick et al in 1973, in which radiation cell kill (E) is expressed as derived earlier in (**equation 3**). Considering the effect of fractionation, - log (surviving fraction), E, yields:

$$E = -\log_e(SF) = n * (\alpha d + \beta d^2) \quad \text{(3)}$$

The total prescribed dose D can be expressed as 'n' equal-sized fractions of dose 'd'; thus, dividing both sides by α:

$$\frac{E}{\alpha} = D\left\{1 + \frac{\beta}{\alpha} d\right\} \quad \text{(4)}$$

$$BED = D(1 + \frac{\beta}{\alpha} d) \quad \text{(5)}$$

The expression $(\frac{E}{\alpha})$ was invented after that as the biologically effective dose (BED) by Fowler in 1989, where he incorporated the overall treatment time factor in the LQ model equation and introduced the concept of BED, which is responsible for the revival of the use of mathematical models in the radiobiology of radiation therapy **(Dale et al. 2007)**.

The biological dose delivered by a particular combination of each partial dose and the total dose is measured by BED (**Equation 5**) of each tissue characterized by a specific α/β ratio. However, for a constant total dose (D), the BED will increase with an increase in dose per fraction. The concept of using the BED is to equalize two treatment regimens by keeping the same effect on normal tissues and the same quality of tumor control or by increasing the quality of treatment, On the other hand, to compare different fractionation schedules.

The increment in BED being greater for tissues possessing low α/β values and equal if a total dose D_1 delivered in n_1 fractions each of dose d_1, is equivalent to the biological effect of a dose D_2 in n_2 fractions of dose d_2. This is demonstrated in (**equation 6**):

$$D_1\left[1+\frac{d_1}{\frac{\alpha}{\beta}}\right]=D_2\left[1+\frac{d_2}{\frac{\alpha}{\beta}}\right]\ldots\ldots\ldots\ldots\ldots\ldots\ldots\ldots\ldots\ldots\ (6)$$

The problem with radiotherapy is the repopulation, which cannot be overlooked when treating cancer. Fowler and Harari in 2000 thought of integrating the value of repopulation into the BED equation.

$$BED=nd\left[1+\frac{d}{\alpha/\beta}\right]-KT\ldots\ldots\ldots\ldots\ldots\ (7)$$

$$BED=nd\left[1+\frac{d}{\alpha/\beta}\right]-K(T-T_K)\ldots\ldots\ldots\ldots\ldots\ldots\ldots\ (8)$$

Where **T** is the overall treatment duration and **K** is the daily BED equivalent of repopulation expressed by Gy per day (high for squamous cell carcinoma and small for radioresistant tumor, as in the case of most breast and prostate cancers). The term K is obtained by dividing the conventional RCF (repopulation correction factor) ($0.693/T_{eff}$) by the parameter α.

Here we assume continuous repopulation, for example, the repopulation proceeds at a constant rate throughout the entire treatment time. For tumors that repopulate in a quasi-steady state after a significant time lag of T_K days, the repopulation is called repopulation modified $K(T-T_K)$, we can use equation (8) which is valid only if $T>T_K$. For short fractionation schedules with $T<T_K$, the RCF could be omitted altogether, as there is relatively little repopulation (because if $T<T_K$ then, by definition, the standard model assumes no RCF).

The validation of a treatment plan may require a change in the treatment regimen, Fowler was the first to introduce this using the BED. In terms of personalization of radiotherapy, our work is more important, since the BED is better for the optimization of all patients and how to change from one regimen to another to set the best treatment plan and not to personalize radiotherapy. Fowler calculated hypofractionated regimens that are equivalent to the standard regimen for early-stage breast, prostate, and head and neck cancer. But for advanced-stage cancer, the hypofractionated regimen cannot be used because of late toxicities, for that reason we favored the hyperfractionated regimen

with an interval of 6 hours between two sessions on the same day so that patients can withstand the early toxicities.

XII. Mathematical modeling

1) The definition of a model in general.

It is a mathematical function that passes through the experimental points. It allows making interpolations and extrapolations (more or less well). Three standard formulations are used in the literature: logistic, Poisson, and Probit dose-response models. To decide whether one model fits the observed data better than another.

A mechanistic assumption builds a logical system based on a theory. However, the design begins with modeling simple processes, governed by basic theoretical knowledge, and complex processes are mathematically combined into a complex mechanical model. Next, the model needs to be validated with known outcome/response data and refined to improve predictive accuracy for example Marsden model and relative seriality. A model can also be empirical (phenomenological) supported by experiment and observation but not necessarily supported by theory, this model aims to quantitatively account for the different outcomes that are expected from observed system behavior. Its equation is fitted to the data observed or recorded. A goodness-of-fit metric associated with the model fitting process indicates the predictive power of the model, for example, the LKB model.

XIII. Organ architecture

The simplest representation of an organ is that it is composed of independent functional subunits (FSUs), which can be defined structurally like the nephron of the kidney or operationally like the FSU of the skin. In addition, it was suggested that FSUs had either parallel or serial organizations **(Withers et al. 1988)**.

1. Parallel architecture: These are organs in which many or all subunits must be inactivated to cause organ failure. Typical examples of organs with a parallel architecture are the lungs, kidneys, and liver.
2. Serial architecture: or tabular architecture, the function of the entire organ depends on the function of each FSU. Inactivation of only one FSU may result in clinical side effects in the downstream part of the organ in a binary response pattern. For example, the spinal cord, and the Brain stem.
3. Serial-parallel architecture: Since the FSUs are considered (by definition) to be independent of one another. For example, the bladder and rectum.

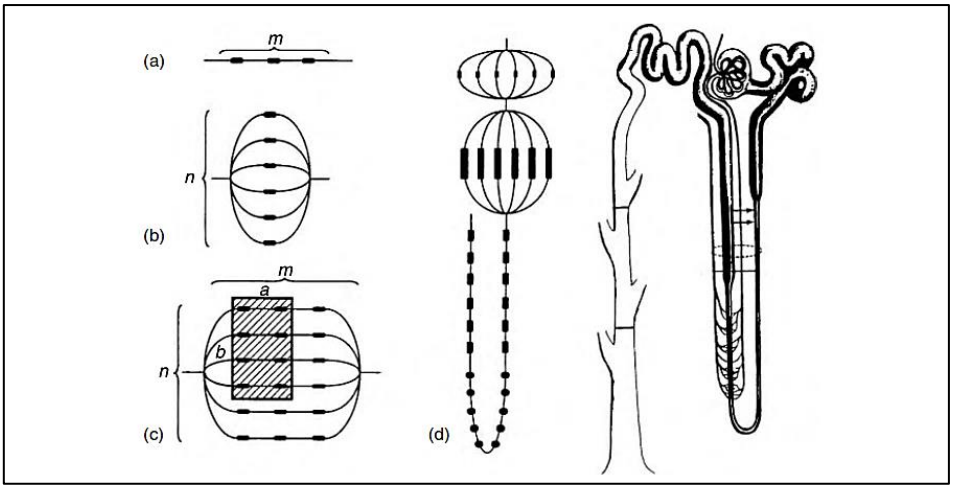

Figure I.6: schematic illustration of the concept of (a) series, (b) parallel, and (c) serial-parallel or organization of functional subunits in an organ; (d) a nephron (Serial-parallel).

XIII. Radioanatomy of the three locations selected in this study.

1. Breast anatomy

a. Breast situation

The **breasts** are paired structures located on the anterior-superior of the thorax, on both sides of the sternum in front of the pectoral muscles (between the 3rd and the 7th rib), and the nipple is located at the level of the 9th vertebra. In a standing position, under the influence of its weight, the breast falls slightly, which creates the inframammary sillion between the lower half of the breast and the thorax. A single breast can be divided into four quadrants: upper outer (UO), upper inner (UI), lower outer (LO), and lower inner (LI) by two perpendicular planes intersecting at the nipple **(Fwu et al. 2015)**.

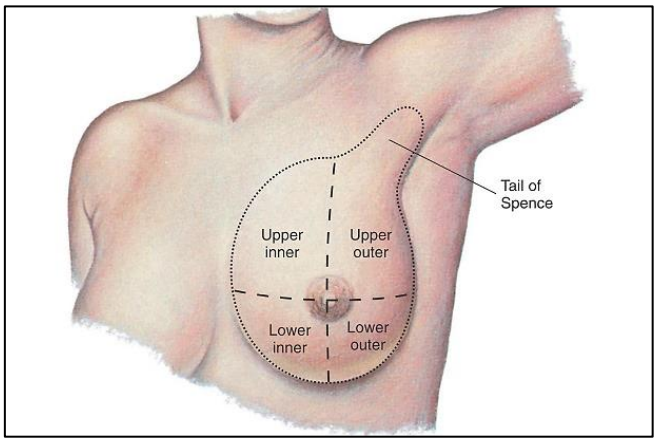

Figure I.7: The four quadrants of a single breast

b. Breast structure

The breast has two configurations: the external configuration consists of 3 concentric circular zones: peri areolar skin, areola, and nipple. The internal configuration comprises two zones **(Ellis et al. 2013, Pandya et al. 2011)**.

- The mammary gland is yellowish-gray in appearance. It is made up of tubule-alveolar parenchyma, surrounded by dense adipose connective tissue. It is organized into some twenty lobes, with each lobe made up of 20 to 40 lobules, and each lobule containing 10 to 100 alveoli.
- The alveolus is the secretory unit of the gland, with each draining via intralobular ducts to form lobules that unite to form glandular lobes, which drain through milk ducts.

The milk ducts converge on the nipple, widening to form the lactiferous sinuses the lactiferous sinuses, then narrow and emerge at the level of the nipple pores **(Cooper 1840)**.

c. Breast cancer

The process of breast cell evolution from normal to cancerous is unknown, but recent studies using molecular technology suggest breast cancer is a heterogeneous disease. About 95% of breast cancers are initially hormone-dependent, regardless of a woman's menopausal status **(Pasqualini 2002)**. The chosen cancer type for this study is adenocarcinoma, although various types of breast cancer can be found in the literature **(Greene et al. 2006, Compton et al. 2012, Weigelt et al. 2010)**.

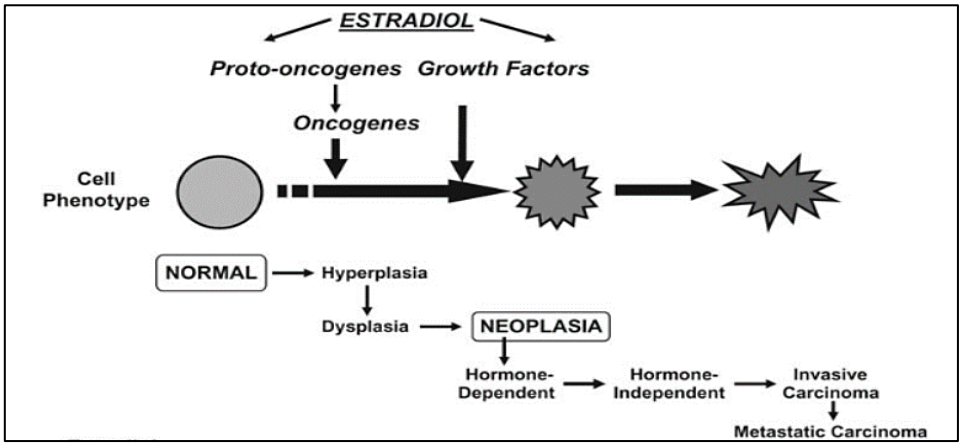

Figure I.8: The process of how a normal breast cell can transform into a cancerous cell over time **(Pasqualini 2002)**.

2. Prostate anatomy

a. Prostate situation and structure

The prostate is a fibromuscular glandular organ surrounding the prostatic urethra. The prostate secretes acid phosphatase, plasmin, citrate, amylase, prostate-specific antigen (PSA), and prostaglandins (**Fine et al. 2011)**. These secretions make up 20 to 30 percent of the semen volume. The prepared solution is rich in enzymes that nourish and prevent spermatozoa (**McNeal 1980**, **McLaughlin et al. 2005)**.

The prostate weight of a normal adult is around 20 to 25 grams and is approximately 3 cm in high, 4 cm in wide, and 2 cm in thick. It is located at the bottom of the bladder and surrounds the proximal urethra. In this position, it lies on the urogenital septum between the rectum and the pubic symphysis (**Fine et al. 2011)**.

b. Prostate cancer

Prostate cancer is a frequently diagnosed form of male cancer. Studies conducted on deceased individuals have revealed that as men age, most of them will develop microscopic cancer cells in their prostate gland.

These cells are often referred to as "latent" prostate cancer, and this occurs in populations with both high and low risk for the invasive form of the disease. However, only a small percentage of men will develop invasive prostate cancer. Therefore, while prostate cancer is prevalent, it will only be a minor factor in the overall health and eventual death of most men **(Bray et al. 2018, Mohan et al. 1998)**. The third cancer after those of the lungs and colon to affect men is prostate cancer. This type of cancer affected some 2.3 million Algerians at the end of 2017 and still growing until 2022 **(Warkentin et al. 2005)**.

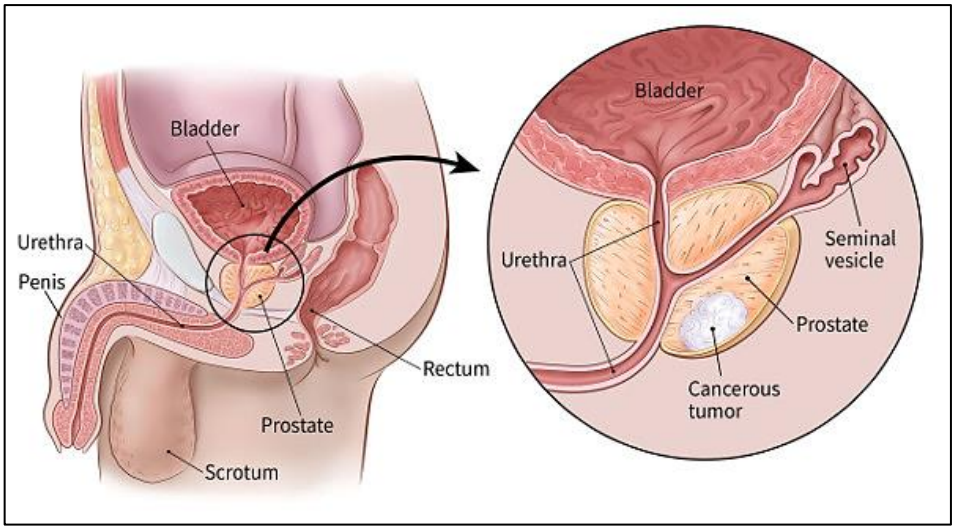

Figure I.9: Illustration showing the location of a cancerous tumor inside the prostate gland.

3. Head and neck (nasopharynx)

a. Nasopharynx situation and structure

The nasopharynx is the uppermost region of the pharynx, situated between the base of the skull and the soft palate. It links the nasal cavity to the oropharynx and contains the adenoids and openings of the Eustachian tube. Clinical conditions that can occur here include nasopharyngeal carcinoma and adenoidal hypertrophy **(Cody 1969)**. The nasopharynx has a height of around 4 cm and an A-P (anterior-posterior) diameter of about 2 cm **(Lyman 1985)**.

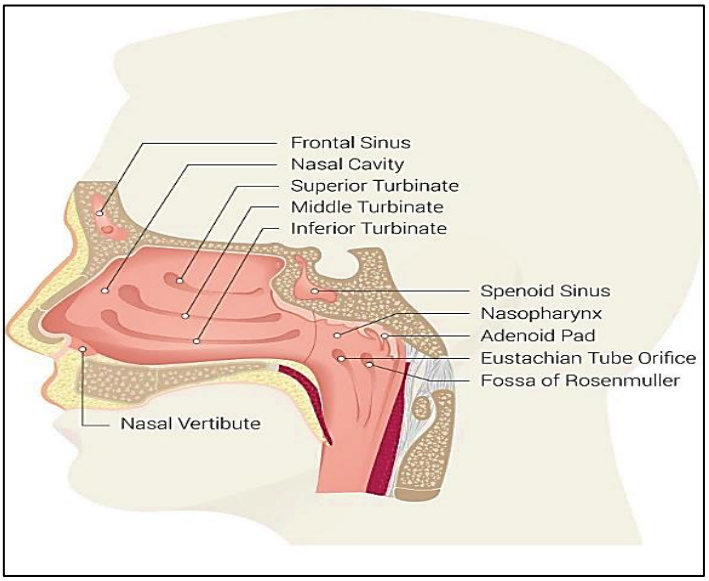

Figure I.10: Anatomy of the nasal cavity including the nasopharynx situation **(Semenenko et al. 2008)**.

Two major functions of the nasopharynx are very important:

- ✓ The nasopharynx connects the nasal passages to the larynx and trachea via the oropharynx, as part of the upper airway system.
- ✓ Muscles in the nasopharynx regulate the opening of the eustachian tubes, which help balance air pressure between the middle ear cavity and the nasopharynx.

b. UCNT (Undifferentiated carcinoma of Nasopharyngeal type)

Undifferentiated Carcinoma Nasopharyngeal Type (UCNT) is a type of tumor that originates from the epithelium and is prevalent in several regions of the world, particularly among well-defined ethnic groups. The tumor has a multifactorial etiology that is yet to be fully understood, but it is known to be associated with the Epstein-Barr Virus (EBV), making it an ideal model for studying viral carcinogenesis in humans. Despite being highly responsive to radiation therapy and having a high rate of local control, the cancer's rapid growth and aggressive metastasis often lead to treatment failure **(Altun et al. 1995)**.

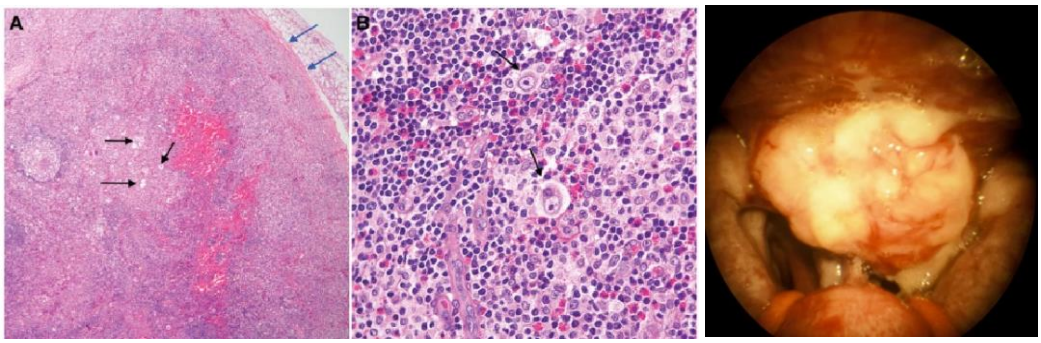

Figure I.11: A metastatic case of undifferentiated carcinoma of nasopharyngeal type (UCNT) was found in a cervical lymph node, displaying a unique Hodgkin-like morphology. The lymph node showed scattered lacunar cells resembling Hodgkin's lymphoma cells (black arrows) and was enclosed by a fibrous capsule (blue arrows, 40x magnification). The UCNT displayed Hodgkin-like lacunar cells, occasional hemophagocytosis (black arrows, 400x magnification), and was embedded in a Hodgkin-like background. On the right, a real figure of UCNT is shown.

4. Organs at risk

To complete our study, we have selected specific organs at risk which are listed in the table below. Our assessment is based on the available data and requirements that

we need to meet. However, the large number of organs at risk has limited our study. We have prioritized the most common organs at risk for breast and prostate cancer, taking into account the specific localizations. To evaluate the organs at risk of UCNT cancer, we have followed the order of priority on the IMRT planning template. However, we have not calculated the NTCP of organs with priorities lower than 250.

PTV	Organ at risk used in this study	Dose constraints
Breast	Lungs	V10Gy < 40% ; V20Gy ≤ 35% V30Gy ≤ 20%
	Heart	V10Gy <30% ; V20Gy <5% Dose moyenne < 5Gy
prostate	Bladder	V60 < 50% ; V70 <25%; Dmax, D2% < 80Gy
	Rectum	V60 < 50% ; V70 <25%; Dmax, D2% < 76Gy
	femoral heads	V50 < 10 %
Nasopharynx	The spinal cord	D2% < 54 Gy ; 1 % < 60Gy
	The brainstem	D2% < 45 Gy ; 1cc < 50Gy
	The optic chiasm	D2% < 54 Gy ; 1 % < 60Gy
	Right and left optic nerves	D2% < 54 Gy ; 1 % < 60Gy
	Right and left middle ears	D2% < 54 Gy and never exceed 60 Gy
	Right and left parotid glands	Dm < 26 Gy ; V30 < 50 %
	The right and left lens	Dm < 10 Gy ; D2 < 12 Gy

Table I.1: Organs at risk and the associated dose constraints.

Chapter II: Radiobiological indexes TCP, NTCP, and UTCP modeling.

I. Tools for evaluating radiotherapeutic treatment plans.

Qualitative and quantitative analysis tools can be placed in the evaluation of treatment radiotherapy plans. The usual tools are related to the dose delivered by the treatment accelerator (UM and the dose calculated at the isocenter) or to the spatial distribution of the dose (hot spots, three-dimensional maximum dose, gamma index, depth yield, and the correction factor). Usual dosimetric quality index tools (tumor volume coverage index, dose homogeneity index in tumor volume, dose conformation index to tumor volume, and geometric conformation index), and tools related to the volume distribution of the dose: cumulative and differential dose volume histogram and the biological indices TCP, NTCP, and UTCP. On the other hand, the more unusual and original use of comparison tools such as differential DVH is characterized by its standard deviation, the gamma index, the gamma pixel histogram, and a correction factor calculation test **(Chaikh 2012)**.

This study used the radiobiological indices to evaluate the different treatment plans. However, compared to the dose constraints and controlling the effects, it is possible to have an increased value of NTCP despite the dose constraints being respected, it is necessary to do serious radiotherapy to maintain the low value of NTCP.

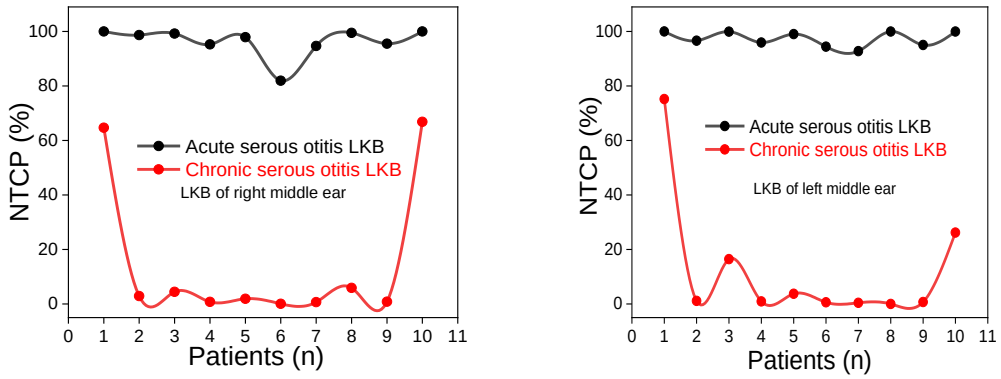

Figure II.1: Complication of acute serous otitis in all patients except patients 1, 3, and 10 excluded from the discussion.

II. Dose Volume Histogram (DVH)

1. Differential dose volume histogram

The differential DVH represents the volume as a function of the dose dV/dD. We can consider pictorially that it displays the portions of the total volume of the

irradiated structure receiving doses defined as intervals of similar widths. However, for a dose interval between (d-s and d+s) the differential DVH calculates the volume which receives a dose included in this interval, where '**d**' is the dose value. Differential DVH is characterized by its peak representing the largest volume receiving the same dose. Ideally, the entire target volume should receive the prescription dose and would be represented by a vertical segment with no volume receiving a lower or higher dose.

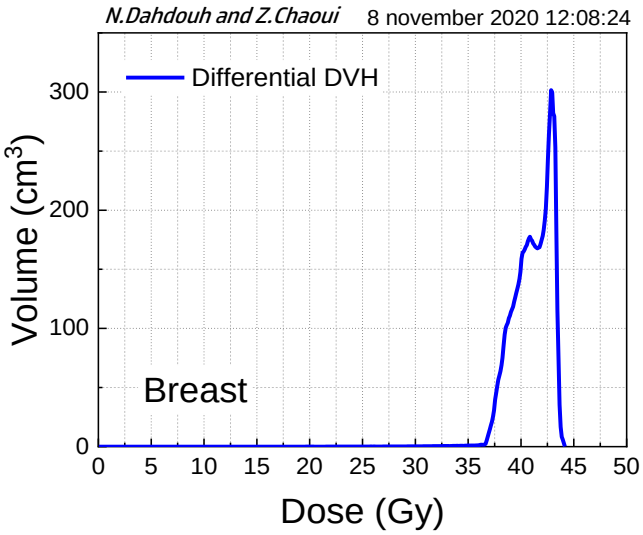

Figure II.2: Differential DVH of breast cancer treated with the 3D-CRT technique at the Setif Cancer Center.

In the differential DVH plot, the Y-axis represents the differential volume of the structures receiving the dose dV/dD, which is indicated in cm^3/Gy. The X-axis represents the doses. The analysis of the differential dose volume histogram (DVH_d) makes it possible to directly identify the position of the dose peak which represents the dose received by the largest percentage of volume, and the width of the interval around this peak.

The width of the interval presents the homogeneity of the dose distribution in the volume. It is characterized by the standard deviation given by the following equation:

$$\sqrt{\frac{\sum_{j=1}^{VL}(D(j)-Dmoy)^2}{VL}} \quad \text{..... (9)}$$

Where: D (j) is the relative dose in the lesion voxel j, D_{moy} is the relative average dose in the lesion, VL is the lesion volume in elementary voxels, and the standard deviation

depends on the shape of the differential dose volume histogram: the narrower it is, the dose is more homogeneous if the standard deviation is small. Thus, we can use the standard deviation to evaluate the uniformity of the dose in the volume studied (the more the dose distribution is concentrated over a small dose interval, the more uniform it is).

2. Cumulative "HDVc" Dose Volume Histogram

The cumulative DVH represents a structure's relative or absolute volume that receives a dose equal to or greater than a defined dose. The figure below illustrates the cumulative DVH graph routinely used for radiotherapy planning; the Y axis represents the proportion of the total volume of structures receiving a particular dose indicated in percentage or cm^3. The X-axis represents the indicated dose in percentage or absolute dose. On a cumulative DVH, the ideal treatment plan is characterized by the fact that 100% of the volume to be treated receives 100% of the prescribed dose.

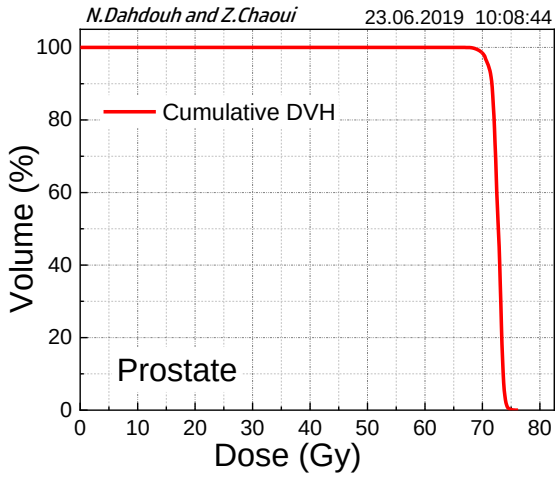

Figure II.3: Cumulative DVH of prostate cancer treated with the VMAT technique at the ONCOPOL L'espoir center.

In reality, a part of the volume always receives more or less than 100% dose. We can distinguish two sub-volumes: the partial volume of the "PTV" target volume receiving doses lower than 95% which is considered as the under-dosed volume, and the partial volume of the target volume receiving doses higher than 107% which is considered overdosed volume. The analysis of the dose-volume histogram makes it possible to compare: the average dose (D_{moy}), the minimum dose (D_{min}), the maximum dose (D_{max}), the volumes (expressed in % or cm^3) receiving at least a certain dose (V_{dose})

[writing adapted to OARs]; and the doses (expressed in % or gray) received by a given volume expressed as a percentage of the target volume to be treated (D_{vol} as a percentage).

III. Definition of the radiobiological indices TCP, NTCP, and UTCP.

There are many techniques for evaluating radiotherapeutic plans, including evaluating DVHs and calculating many quantitative biological indices such as EUD, TCP, NTCP, and UTCP **(Boyer et al. 2002)**.

The Probability of Tumor Control "TCP" and the Probability of Complication of Normal Tissue "NTCP" are mathematical regression models of dose-volume histograms. These biological models related to the dose-volume histogram can be used to compare different treatment plans. The limited performance of radiobiological models in terms of prediction (due to the lack of clinical data, and availability of tissue radiobiological parameters, etc.) and computation times incompatible with current practice have put these models under use. Recently, radiobiological software tools have been integrated, as an option, into radiotherapy planning systems (TPS) **(Boyer et al. 2002, Chaikh et al. 2020)**.

IV. The EUD Uniform Dose Equivalent

A uniform equivalent dose (EUD) is a dose that, when applied uniformly to the tumor volume, has the same biological effect (i.e. local control) as DVH on the tumor volume from which it originated **(Boyer et al. 2002)**. The original concept of EUD was defined only for the target organ and was based on cell survival predicted by a linear quadratic model. The simplest expression for computing the value of this quantity is the one developed by Niemierko **(1997)**, given by:

$$\text{EUD} = 2\ \text{Gy}\ \frac{Ln\left(\sum_{i=1}^{N} v_i SF_2^{\frac{D_i}{2}}\right)}{Ln\ (SF_2)} \quad \text{..... (10)}$$

To calculate the EUD for a given treatment regimen, values must be derived for the differential DVH in tumor volume, the α/β ratio describing the biological endpoint of interest, and the clonogenic fraction for survival after 2 Gy (SF2).

Further modifications are required to include the effects of cell proliferation and other complications in the simple model of the preceding EUD equation, and then introduce the generalized EUD (EUDg) as a phenomenological model that can be applied to tumor and normal tissues. The clear advantages of EUD, especially its generalized form (EUDg), make it a popular choice for optimizing parameters in radiotherapy treatment planning. EUDg is given by the following equation:

$$\text{gEUD} = \left(\frac{1}{N}\sum_{i=1}^{N} D_i^a\right)^{1/a} \quad \text{..... (11)}$$

where:

D_i: is the dose in voxel i.

N: is the number of voxels in the region of interest.

a: is the volume parameter that is linked to the seriality of the organ considered.

V. Tumor control probability (TCP)

Two types of TCP models category are generally used, namely, phenomenological models (which are mathematical representations that are not based on underlying physical principles) and mechanistic models (which attempt to model the actual clinical situation of the eradication of all tumor cells) **(Boyer et al. 2002)**. Clinical data show that TCP has a sigmoid relationship with dose **(steel 2007a)**.

1. TCP calculation models

a. The fundamental Poisson TCP model

Also called the simple Poisson model calculates the number of living tumor cells capable of dividing indefinitely after irradiation **(Avanzo et al. 2010)**. This model assumes that the radiation delivered in each treatment session remains constant. When the radiation dose varies within the target area, the probability of controlling the tumor is calculated as the combined probability for each sub-volume Vi within the target area (GTV), with each sub-volume receiving its total radiation dose Di.

$$Tcp = \left(\frac{1}{2}\right)^{\sum_i vi\, exp\left[\frac{2}{ln2}\gamma_{50}\left(1-\frac{D_i}{D_{50}}\right)\right]} \quad \text{..... (12)}$$

Where γ50 is the dose-response curve obtained by fitting the clinical dose-response data and the dose D_{50} which controls 50% of the tumor.

b. The Improved Marsden Model

The TCP model corresponds to the survival rate of the tumor cells and calculates the number of tumor cells capable of dividing indefinitely and still alive after irradiation. This model was derived using Poisson statistics and the Linear Quadratic (LQ) model **(Chang et al. 2016, Nahum et al. 2001, Wang et al. 2019)**.

Population variability in radiation sensitivity was incorporated into the model **(Avanzo et al. 2010)**. This is modeled as a Gaussian distribution $g(\alpha)$ of α_j values with mean $\bar{\alpha}$ and standard deviation σ_α.

$$g(\alpha) \equiv exp\left(-\frac{(\alpha-\bar{\alpha})^2}{2\sigma_\alpha^2}\right) \quad \text{(13)}$$

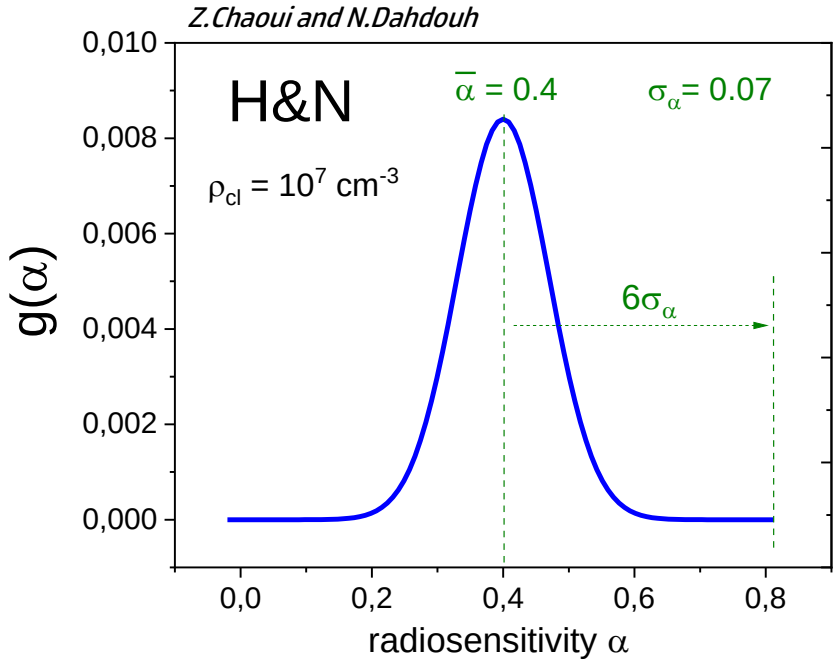

Figure II.4: The Gaussian function of the calculated head and neck example in the function of the radiosensitivity 'α' showing the standard deviation variation σ_α using presented program Radbio-For.

The Poisson TCP model has several additional radiobiological factors.

$$TCP = \frac{1}{\sigma_\alpha\sqrt{2\pi}}\int_0^\infty exp\left(\sum_i -\rho_{cl}V_i exp\left[-\alpha_i D_i\left(1+\frac{\beta}{\alpha}\,d_i\right)\right]\right) exp\left[\left(-\frac{(\alpha-\bar{\alpha})^2}{2\sigma_\alpha^2}\right)\right] d\alpha \quad \text{....(14)}$$

We can assume that the tumor volume is given by a series of subvolume V_i receiving a fraction dose d_i and total dose D_i. ρ_{cl} is the density of clonogenic cells in this volume.

For H&N, $\rho_{cl} = 10^7\ cm^{-3}$; σ_α = 0.07 with a mean value $\bar{\alpha} = 0.4$ **(Avanzo et al. 2010)**; with a width of 12 σ_α the integral of the gaussian distribution is 1 for few iterations.

c. EUD based TCP

This model also known as the logit or Niemierko model to calculate tumor control probability (TCP based on EUD) **(Gay et al. 2007)**. Niemierko proposed a parametrization of dose-response characterizations using the logistic function. The values of 'γ_{50}' and 'a' describing the dose-response curve should be obtained by fitting the clinical dose-response data to the *EUD*-based TCP model **(Gay et al. 2007, Chang et al. 2016)**.

$$EUD = \sum_{i=1}(V_i D_i^a)^{1/a} \quad \text{..... (15)}$$

$$TCP = \frac{1}{1+\left(\frac{TCD_{50}}{EUD}\right)^{4\gamma_{50}}} \quad \text{..... (16)}$$

when the tumor is homogeneously irradiated, the TCD_{50} is the tumor dose to control 50% of the tumors. D_i is the total dose in the subvolume V_i.

VI. Normal Tissue Complication Probability (NTCP)

The NTCP is a sigmoid function that relates tumor dose to the likelihood of radiation damage in healthy tissue **(Boyer et al. 2002)**. This model represents a particularly important index for classifying treatment plans, which often determines the acceptability of a treatment plan, and whether the normal tissue tolerance has been met or exceeded **(Steel 2007a)**. A Gaussian function is a common model of side effect probability density. Other models apply different mathematical functions, e.g., Statistical Poisson or regression models. NTCP models for various side effects in different organs are based on dose-volume histogram (DVH) data. They are determined by adjusting the parameters of mathematical models of the NTCP to the actual side effect profiles, which have been determined in the respective clinical studies.

Six models of complication probability in normal tissues have been proposed since 1978. All of these models are based on parameters whose value must be optimized according to patient monitoring databases **(Zhu 2013)**. Most NTCP models do not explicitly describe dose-by-fraction effects to minimize the number of parameters. Jian

Zhu **(2011)** compared these models to select those with the best predictive capacity for the case of prostate cancer.

1. NTCP calculation models

a. Lyman-Kutcher-Burman NTCP model

The Lyman-Kutcher-Burman model or the LKB model is the most used in the calculation of the probability of complications in normal tissues since it produces an error function that predicts a 50% probability of complications. The latter was integrated into the treatment planning system (Pinnacle) following the parameter values proposed by Burman et al. **(1991)** and Emami et al. **(1991)**.

- **The case of a homogeneous dose**

$$NTCP = \frac{1}{\sqrt{2\pi}}\int_{-\infty}^{t} e^{\frac{-t^2}{2}} dt \quad \ldots\ldots (18)$$

$$t = \frac{D_{eff} - TD_{50}}{mTD_{50}} \quad \ldots\ldots (19)$$

$$D_{eff} = \sum_i^M \left(\frac{V_i}{V_{ref}} EQD_i^{1/n}\right)^n \quad ; D_{eff} = \left(\sum V_i D_i^{1/n}\right)^n \quad \ldots\ldots (20)$$

Where:

D_{50}: The dose linked to a 50% probability of having toxicity would cause complications in 50% of the population

V_{ref}: A reference volume, which in many cases will be the (entire) volume of the organ.

m: A parameter representing the slope of the dose-response curve.

n: The volume exponent in the power law that relates the tolerance doses for uniform irradiation of uniform whole and partial organs. D_i is the total dose in the subvolume V_i and the effective dose D_{eff} is sometimes referred to as *EUD*.

Since low values of the n-parameter for healthy tissues or organs mean a strong dependence of NTCP on volume (or equivalently a strong dependence of the probability of toxicity on dose). The table above presents the different cases of the value of ‘n’ **(Steel 2007a, Zhu 2013)**.

The value of n is close to the unity	The value of n is close to zero
The volume effect is large	The volume effect is small
NTCP correlates with a mean dose	The NTCP correlates with the maximum dose
Parallel Architecture	Serial architecture

Table II.1: The value of the parameter n which represents the volume effect.

- **The case of an inhomogeneous dose**

Due to the requirement of uniform partial irradiation, the above approach will only apply to a limited number of treatments, namely those in which the organ is treated with opposing parallel fields.

The previous three equations do not apply in this case if the dose distribution is not in a simple, idealized examination, in which one section of an organ receives a known uniform dose and the next receives no dose. To use the LKB model in the more general case of an inhomogeneous dose in the organ or tissue of interest, it would be desirable to convert the non-uniform histogram to a uniform equivalent. Two methods for transforming a non-uniform histogram have been suggested **(Kutcher et al. 1991, Steel 2007a)**.

i. The method of the interpolation: proposed by Lyman here the histogram is transformed into a uniform with a volume equal to the organ's total volume and a maximum dose less than or equal to the maximum dose of the organ **(Lyman et al. 1987)**.
ii. The effective volume method: proposed by **(Kutcher et al. 1991)** in this last technique, the transformed uniform histogram has a volume less than or equal to the volume of the whole organ, and a maximum dose equal to the maximum dose delivered to the organ.

Both procedures usually lead to the same NTCP **(Kutcher et al. 1991)**.

A conceptual equivalent formulation of the LKB model **(Lyman 1985, Kutcher et al. 1989**) was proposed by Mohan et al. **(1992)**. The model describes the sigmoidal dose-response curve of normal tissues using the following probit forms equation (19, 20). To evaluate eq. (18), a simple form is used **(Semenenko et al. 2008)**.

$$NTCP = \frac{1}{2}\left[1 + erf\left(\frac{t}{\sqrt{2}}\right)\right] \quad \text{..... (21)}$$

We have used the nearly-best rational approximations to evaluate the error function provided by Cody **(1969)**.

b. The relative seriality model or Kallman model:

This model represents an alternative attempt to construct a quasi-mechanistic model for healthy tissue complication probability (NTCP) that explicitly considers an organ's structure or architecture. These are FSUs and/or (tissue-rescuing units) TRUs. These units are arranged in series, parallel, or series-parallel combinations (Serial-parallel architecture) **(Steel 2007a, Källman et al. 1992)**.

The model includes a parameter "s" which reflects the degree to which the functional subunit (FSU) architecture is considered serial (s=1) or parallel (s=0).

$$NTCP = [1 - \prod_i [1 - P(D_i)^s]^{V_i}\ ]^{\frac{1}{s}} \quad \text{.. ..... (22)}$$

$$P(D_i) = 2^{-exp\left(e\gamma\left(1-\left(^{D_i}/_{D_{50}}\right)\right)\right)} \quad \text{.. ..... (23)}$$

where: **s** is a parameter describing the relative seriality of the organ or tissue (s= 1/n), **EUD** is the uniform equivalent dose, $\mathbf{V_i}$ is the volume of the organ receiving the dose di, $\mathbf{P(D_i)}$ is the probability that no cell survives (probability of damage), and **v** is the fractional volume of the subunit.

- **Organs organized in series**

In the case of uniform irradiation of N functional subunits FSUs and no radiation on the rest, the probability of eradicating at least one functional subunit FSU is given by this equation:

$$\text{NTCP} = 1 - (1 - P)^N \quad \text{.. ..... (24)}$$

P: is the probability of eradicating a single functional subunit.

As the number of irradiated FSUs increases (i.e., the volume of irradiated organs increases), the sigmoid response shifts to the left, and the likelihood of complication increases. Therefore, for the serial case, the dose-response curve of the whole organ can be shown to uniquely determine the volume effect of the organ (**Källman et al. 1992)**.

The NTCP of an organ consisting only of "m" serial subunits with a local response Pi, would be given by:

$$\text{NTCP}=1-\prod_{i=1}^{m}(1 - P_i) \quad \text{.. ..... (25)}$$

- **Organs organized in parallel**

Kidneys, livers, and lungs behave as parallel organs. Because the functional subunit number (FSU) is always large in these organs. For organs organized in parallel, the complication occurs if the fraction of eradicated FSU exceeds a threshold, in this case, the so-called functional reserve (varies according to a population of patients) of the organ, such as liver function which differs according to an example of patient age and alcohol consumption as well as radiosensitivity which may vary across a patient population **(Steel 2007a, Källman et al. 1992)**.

The functional reserve of an organ can be defined by the fraction rather than the number of eradicated FSUs. Whereas for an organ with "n" parallel subunits with a local response Pj the NTCP is given by this equation:

$$\text{NTCP}= \prod_{j=1}^{n} P_j \quad \ldots\ldots\ldots\ldots\ldots\ldots\ldots\ldots \quad (26)$$

- **Organs organized in serial-parallel**

For an organ with an "n*m" matrix of subunits in parallel and series, the overall probability of complication would then be given by:

$$\text{NTCP}= \prod_{j=1}^{n}\left[1 - \prod_{i-1}^{m}(1 - P_{ij})\right] \quad \ldots\ldots\ldots\ldots\ldots\ldots\ldots\ldots \quad (27)$$

OAR	serial	parallel	Serial-parallel
Breast	/	Lung	Heart
Prostate	/	Femoral head	Rectum, Bladder
nasopharynx	Brainstem, Spinal cord, optical chiasm, optical nerve, middle ears.	Parotid gland	lens

Table II.2: The classification of the organs at risk used in this study.

c. EUD-based NTCP

This model also knowen as Niemierko model or logit model. The model assumes logistic dose response for the whole organ at risk after inhomogeneous dose distribution **(Gay et al. 2007)**. Instead of the actual nonuniform dose distribution, an equivalent uniform dose leading to the same biological effects is used. It is described by;

$$NTCP = \frac{1}{1+\left(\frac{TD_{50}}{EUD}\right)^{4\gamma_{50}}} \quad \ldots\ldots\ldots\ldots\ldots\ldots\ldots\ldots \quad (28)$$

The dose giving a 50% probability of complication if the organ is irradiated uniformly in its entirety is given by the TD_{50}, and the slope of the dose-response curve is described by γ_{50}.

In the literature, other models with numerous parameters often lead to significant parameter correlation and ambiguity in biological interpretation. For instance, for NTCP calculation, we come across individual-based and population-based variants of the CV model **(Warkentin et al. 2004)**, Simple maximum dose (SMD) **(Uzan et al. 2012)**, Schulthesis model, and Parallel model **(Niemierko et al. 1993, Wolbarst et al. 1982, Jackson et al. 1993)**. Similarly, for TCP, we find a model that utilizes linear-quadratic cell kill and the formalism developed by Zaider and Minerbo to account for repopulation **(Zaider et al. 2000)**.

VII. Uncomplicated tumor control probability (UTCP)

Represents the therapeutic window that defines the dose level enabling the tumor to be controlled while effectively protecting healthy tissues. In its simplest form, it is given by **(Ågren et al. 1990, Frometa-Castillo et al. 2020)**;

$$\mathrm{UTCP} = \mathrm{TCP}(1 - \mathrm{NTCP}) \quad (29)$$

To account for multiple normal tissues, we adopted the following formulas **(Ågren et al. 1990)**:

$$\mathrm{UTCP} = \mathrm{TCP} - \mathrm{P};\ \mathrm{P} = 1 - \prod_1^{\mathrm{i}}(1 - \mathrm{NTCP_i}) \quad (30)$$

Where $NTCP_i$ is the probability of injury to each normal tissue of interest *i*.
A more sophisticated model includes a correlation parameter δ to describe the fraction of patients for whom tumor and normal tissue complications are statistically independent.

VIII. Calculation programs

Over the last twenty years, several software packages have been developed to implement various NTCP and TCP models. These include BIOPLAN, which was written in Visual Basic **(Sanchez-Nieto et al. 2000)**; a series of Matlab modules created by Warkentin et al. **(2004)**, TCP_NTCP_CALC **(Warkentin et al. 2004)**, BioSuite which is a new program invented by Uzan and Nahum 2012 replaced BIOPLAN **(Uzan et al. 2012)**, and RADBIOMOD another program published by Chang et al **(2016)**.

Our goal is to develop a user-friendly research tool that computes the NCTP or TCP of a specific treatment plan, to generate more interest in this field of research.

1. RADBIOMOD

RADBIOMOD has been developed in Microsoft Excel (Visual Basic for Applications) as the programming language to implement the biological model. This executable requires the user to enter DVH data for a target volume of interest or normal tissue in a tabular format, with dose in the first column and volume in the second column. The default DVH format used by RADBIOMOD for calculations is the differential format. RADBIOMOD can also convert cumulative DVH to differential values if necessary. Standard units are dose (Gy) and volume (percent).

Most commercial treatment planning systems (TPS) can export the DVH in tabular format (.dat, .txt, .csv, etc.) which can then be copied and pasted into RADBIOMOD, to calculate TCP, NTCP, EUD, and UTCP.

2. BioSuite

BioSuite is a graphical interface that provides tissue response data for all types of tissue (healthy, cancerous), and enables optimization of the treatment plan, taking into account the size and number of fractions. The BioSuite package is provided as a compressed ZIP file that contains an executable file, parameters for common endpoints and tumor types (cited in text files), exercise sheets, and DVH examples.

The DVH used by this executable is described in absolute and CSV format (.csv), with dose in cGy in the first column and volume in cm^3 in the second column. The Endpoints pane allows operators to view, modify, delete, and add endpoints defined by a set of parameters for the model used to perform the biological assessment.

Many parameters are used as input to these models, describing how different tissues respond to ionizing radiation. In all cases, the parameters of the model must be determined by fitting its predictions to in vivo experimental data or, less preferably, to in vitro.

3. Eudmodel.m

It is a calculation program code on Matlab, which is based on the phenomenological model proposed by Niemierko. The program can be downloaded from:

http://www.ecu.edu/radiationoncology/downloads.htm or save the code **(gay et al. 2007)** as a Matlab function named <eudmodel.m>.

The square brackets "[]" used in this section are used in Matlab to define matrices. In the command window and command prompt, type: dvh= [column's number; row's number] to create the variable dvh. The matrix dvh represents cumulative DVH, rather than differential DVH, and is structured as follows: the first column corresponds to the increasing dose in percentage or absolute format values, and the second column to the corresponding relative or absolute volume values. This program internally converts the cumulative DVH to the differential DVH required by the mathematical model. Furthermore, the rest is just a matter of following the instructions in the code according to the user's needs.

4. Radbio-For

Radbio_for is a programming language used for numerical computation and scientific research. It serves as an input for the final output of an executable. To use Fortran, the user must provide basic cumulative DVH data for the target volume and normal tissues of interest in the form of a two-column file (.dat). The first column should contain the dose in Gy, while the second column should contain the total volume of the structure receiving this dose in %. The program has several calculation models integrated into it, making it a versatile tool for various applications. The radiobiological models integrated into each program are shown in the following table:

Programs	NTCP models	TCP models	EUD or UTCP model
BioSuite	- LKB model - Relative seriality - Simple maximum dose (SMD)	- Marsden including sublethal damage repair - Marsden including accelerated repopulation - LQ Poisson	/
RADBIOMOD	- LKB model - EUD-based NTCP	- Modified zaider-minerbo TCP - EUD-based TCP	- EUD - UTCP
Eudmodel.m	- EUD-based NTCP	- EUD-based TCP	- EUD
Radbio-For	- LKB model - Relative seriality - EUD-based NTCP	- Marsden including sublethal damage repair - Marsden including accelerated repopulation - Simple LQ Poisson	- EUD - UTCP

	- Modified zaider-minerbo TCP - EUD-based TCP

Table II.3: The integrated radiobiological models into different radiobiological programs.

IX. TCP and NTCP calculation.

Radiobiological models are used to predict and prevent severe grade 3-4 or moderate grade 1-2 toxicity. They can also assist in comparing various techniques, regimens, treatment modalities, and plans that have the same target dose and fractionation. For example, in a recent study, we conducted two comparisons between different treatment techniques. These comparisons are described below.

4. Monoisocentric and dual isocentric techniques comparison.

a. Radiation Treatment Planning

To carry out this part of the work, we selected four clinical cases of patients with breast cancer and undergone a mastectomy. For each patient, we constructed two treatment plans one with the monoisocentric technique (MIT) and the other with the dual isocentric technique (DIT). Those patients were treated with the conventional 46 Gy with 2 Gy per fraction regimen. Each of the patients received the same treatment indications, which included irradiation of two PTVs:

- PTV1= the left chest wall noted PTV46
- PTV2= the volume of the supra- and sub-clavicular lymph nodes noted PTVn.

To achieve the recommended critical OAR constraints to the heart (average dose to the heart less than 5 Gy) and lung (ipsilateral lung V20 ≤ 35% and V30 ≤ 20%), while 95% corresponds to the dose was given to 95% of the PTV **(Ardiet et al. 2007, Noël et al. 2022)**. All planes were calculated using a 3 mm dose calculation grid.

b. Monoisocentric and dual isocentric techniques

The monoisocentric technique uses a single isocenter for all the beams, bringing all the beams together around a single point (the junction point of all the fields). The use of a single isocenter for the entire treatment is the only way of guaranteeing this junction at each treatment session, thereby facilitating and speeding up the treatment session at the same time and enabling better dose distribution at the target volume and

junctions, while sparing surrounding healthy tissue as much as possible **(Banaei et al. 2015, Wadasadawala et al. 2022)**.

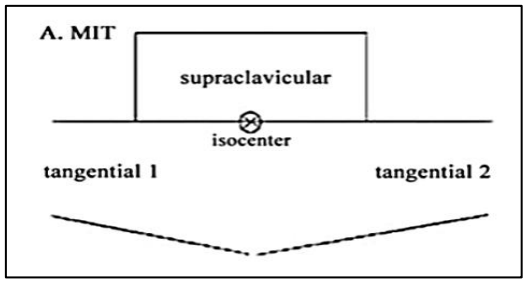

Figure II.5: Schematic illustration of the monoisocentric technique.

In contrast, the dual isocentric technique uses separate, independent beams, with a different isocenter for each beam, one placed at chest wall level and the other at lymph node level. This means that the patient has to be positioned in turn for each field, which creates problems of junction between the different irradiation beams, while at the same time lengthening the time the patient spends on the table.

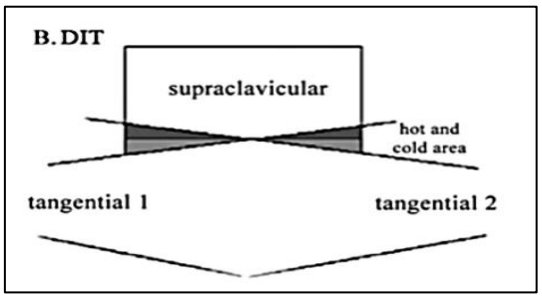

Figure II.6: Schematic illustration of the dual isocentric technique and the appearance of hot and cold zones.

c. Materials and methods

In this comparison, we used the EUD-based TCP and NTCP program proposed by Gay et al. **(2007)**, and the different parameters identified in the literature for the target and the organs at risk are listed in the table below **(Emami et al. 1991, Okunieff 1995)**. An example of the DVH of a patient included in this study is shown in the figure.

Parameters	**a**	**γ_{50}**	**TCD50**	**α/β**
PTV	-7.2	1.7	39.3	10
OAR	**a**	**γ_{50}**	**TD50**	**α/β**
Heart	1	2	24.5	3
Lung	3	3	50	3

Table II.4: The identified parameters used in the breast comparison calculation.

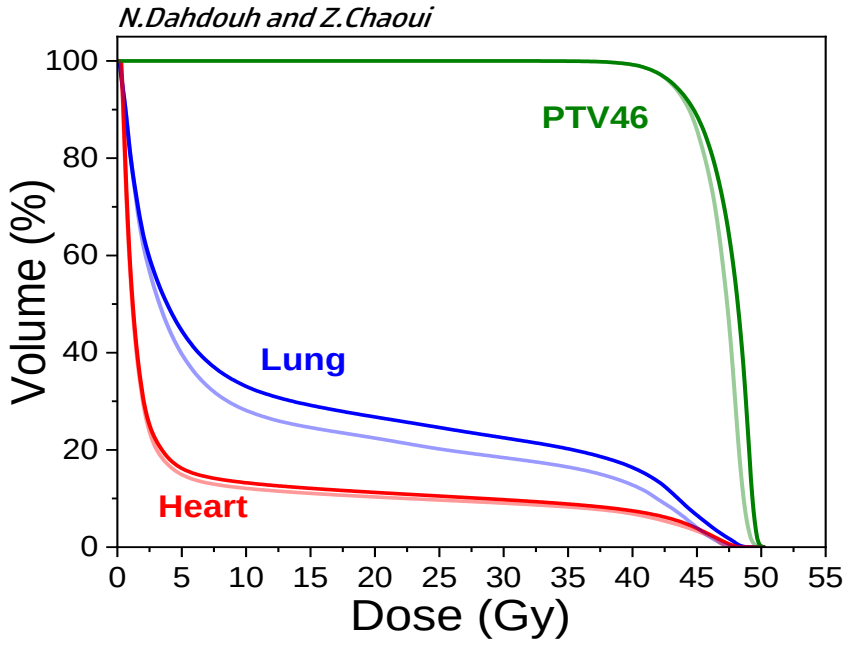

Figure II.7: The light DVH curves present the dual isocentric technique and the dark DVH curves present the monoisecentric technique in treating breast cancer.

d. Results and discussion

A dosimetric assessment took place before the radiobiological analysis. The following tables summarize the PTV results and the organs at risk. A plus (+) means that a patient presents favorable results for a technique.

Point de dose	DIT	MIT
Dmax=2%		++++
Dmin= 98%	+++	+
D95%	++	++
D50%	+	+++

Table II.5: The dose points calculated by the two PTV techniques.

From the table we notice that the D2% and the D50% are more respected in the mono-isocentric technique than the dual isocenteric, where the D98% is more respected in the dual isocenteric technique than the monoisocentric, and the two techniques present the same performance for D95%. Likewise for the dose constraints of the organs at risk according to the table we note that the monoisocentric gives clearly better results while sparing the lung as much as possible. Regarding the dose volume V10Gy and the

mean dose, the two techniques provide similar results while for the volumes V20Gy and V30Gy the mono-isocentric protects the heart better.

Dose constraints	Heart		Lung	
	DIT	MIT	DIT	MIT
V10Gy	++	++		++++
V20Gy	+	+++		++++
V30Gy		++++	+	+++
Mean Dose	++	++		

Table II.6: The dose constraints of the two organs at risk, heart, and lung, calculated by the two techniques.

This dosimetric evaluation allowed us to conclude that the monoisocentric technique is better than the dual isocentric technique. However, it is not sufficient to control these outcomes simultaneously through dosimetric factors alone; radiobiological factors also appear to be critical for evaluating and optimizing treatment plans. And make sense of the difference between dose constraints and predicting the side effects of irradiation on organs at risk. The normal tissue complications and the tumor control probabilities calculation are given in the figure below.

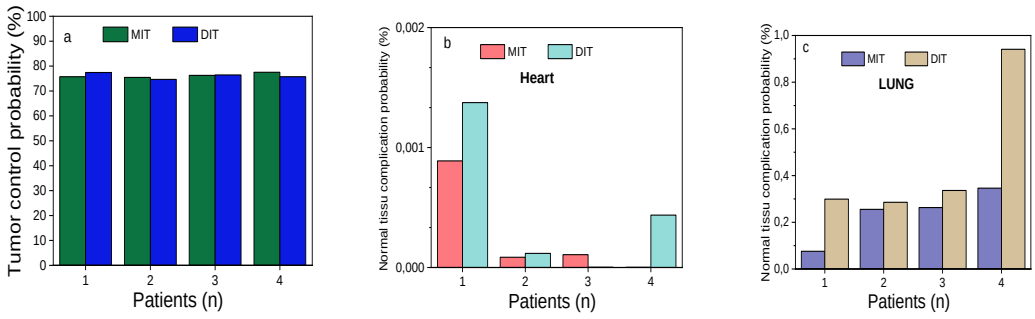

Figure II.8: Calculated NTCP and TCP values for both MIT and DIT respectively.

The NTCP value calculated for the heart using the monoisocentric technique is lower than that calculated using the dual isocenteric and almost less than 1% see figure. Emami et al. It was also noted that pericardial inflammation would be less than 15% at mean cardiac doses below 26 Gy **(Emami 2013)**. As a numerical example (patient 1), in our study, the mean dose calculated with both MI and DIT are 5.673 Gy and 6.106 Gy, respectively (see figure DVH). This result is in good agreement with the Astudillo

et al study, which reported 0-1 for heart NTCP for this mean dose range **(Astudillo et al. 2025)**. Also, for the lung, Emami et all estimated the pulmonary inflammation risk at 5% for V5 less than 42% and 10% when V20 was less than 31%. In our study, the V5 was 39.70% and 44.47%, and the V20 was 22.42% and 26.74% for MIT and DIT, respectively. The calculated NTCP was 0.08% and 0.3%. Therefore, MIT is superior to DIT in terms of compliance with dose constraints, which explains the NTCP values obtained by both techniques.

The TCP calculated in this study did not show a significant difference between the two techniques MIT and DIT, in most cases it follows the D95% value, as a numerical example the two patients 1 and 2, for both MIT and DIT techniques the D95% value of the patient 1 was 43.14% and 43.27% and for patient 2 was 43.94% and 43.03%, respectively. The TCP value for patient 1 was 75.73% and 77.44%, while for patient 2, it was 75.44% and 74.65% for MIT and DIT techniques, respectively.

5. Comparison between 5 fields and 7 fields IMRT treatment plans.

a. Radiation Treatment Planning

This study aimed to compare two different treatment techniques for prostate cancer based on radiobiological aspects. The study did not involve the prediction of toxicity for the two organs at risk (the rectum and bladder). The criteria for selection of patients with low-risk prostate cancer included Gleason score 6 or less, serum prostate-specific antigen [PSA] concentration 10 ng/mL or less, and local stage cT2a or less. On the other hand, patients with intermediate-risk prostate cancer had a Gleason score of 7 or 10 ng/mL < [PSA] ≤ 20 ng/mL, or local stage cT2b without high-risk features.

Sixteen patients of varying ages were selected for the study and treated with a hypofractionation regimen that prescribed a dose of 60 Gy in 20 fractions with 3Gy/session. The dose constraints proposed by Brenner et al. **(2018)** for the rectum were V46 Gy ≤ 30% and V37 Gy ≤ 50%, while for the bladder, the constraints were V60 Gy ≤ 5%, V48 Gy ≤ 25%, and V41 Gy ≤ 50.

b. Five and seven fields IMRT treatment plans.

The treatment plans called 5-field and 7-field both use 18 MV energy but with different angles of incidence and numbers. For the 5-field plan, the gantry angles used are 36°, 100°, 180°, 260°, and 324°, connecting LAO, LPO, Posterior, RPO, and RAO in sequence for treatment. The 7-field plan uses gantry angles of 0°, 40°, 80°, 120°, 240°, 280°, and 320° combined with Anterior, LAO1, LAO2, LPO, RPO, RAO2, and

RAO1. For each patient, the sliding window IMRT technique (dynamic mode) is chosen for MLC.

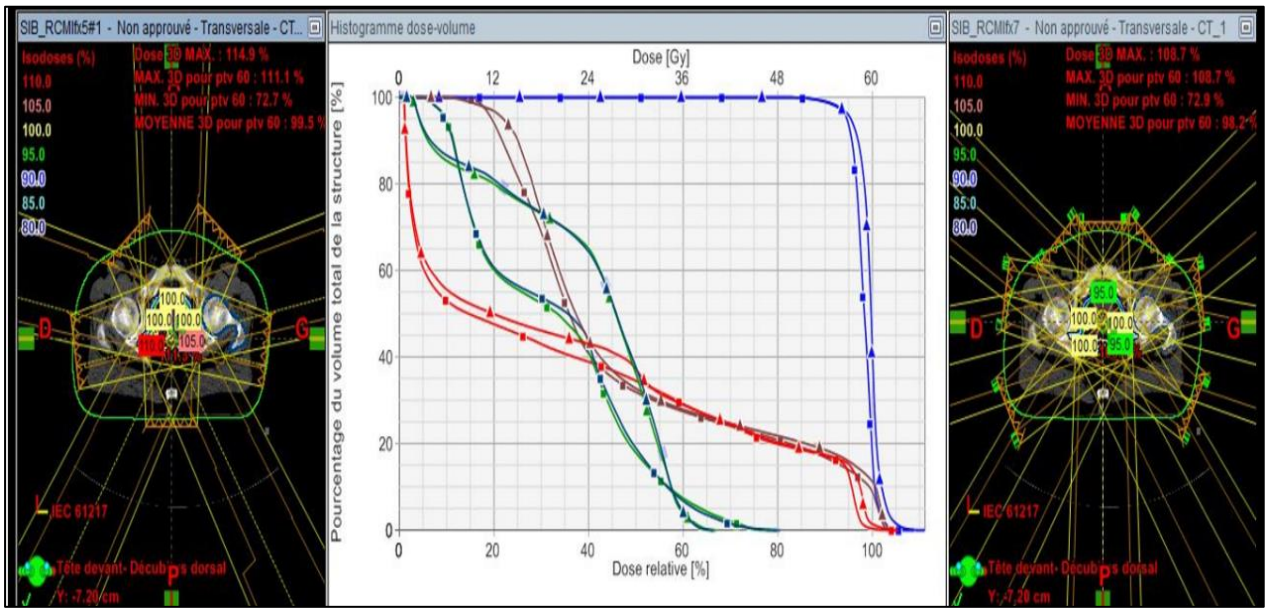

Figure II.9: Comparison between the 5 and 7 fields techniques on the TPS plan evaluation.

c. Materials and methods

- ***Materials***

Attracted DVHs from the TPS are transformed into (.Dat) cumulative format files where the dose is in (Gy) and volume in (%). We performed our calculations with the RadbioFor program using the identified parameters in the table below, where for the PTV60 we used the modified Poisson model (Marsden model) and for both rectum and bladder we used the LKB model.

Parameters	n	m	TD50	α	σα	ρcl	α/β
Rectum	0.12	0.15	80				3
Bladder	0.5	0.11	80				3
PTV60				0.155	0.058	1.00E+07	1.5

Table II.7: TCP and NTCP model parameters **(Kutcher et al. 1991, Uzan et al 2012, Podgorsak 2003)**.

- ***Analysis methods***

A non-Mann-Whitney parametric statistical test (Addinsoft XLStat 2020 software) was used in this work to select the best technique (5-field and 7-field) that

minimizes the complication on the organs at risk. The hypothesis is considered null when the two sets of results are equal. Conversely, if the results differ, the hypothesis is classified as a bilateral alternate, utilizing a 95% confidence interval within the framework of normal distribution.

After calculating the exact P-value, if this value is less than 0.05, the null hypothesis is rejected, indicating a statistically significant difference between the two data sets. If the P-value is greater than 0.05, then the bilateral alternative hypothesis is considered, and we include the absolute difference.

d. Results and discussion

- **NTCP Rectum**

Figures (10A) and (10B) depict the calculated NTCP and the absolute error, which is the difference between the 5-field and 7-field plans. No significant difference between the two techniques (P-value = 0.234).

In parallel, it should be noted that 15 patients had positive or zero errors. The difference between the two plans was evident in the calculated values for all patients. The mean calculated NTCP for five fields ranged from 1.9% to 14.5% with a mean value of 7.72%, while for seven fields, the range was 1.4% to 13.2% with a mean value of 3.79%. These findings suggest that the plan with seven fields is superior in preserving the rectum.

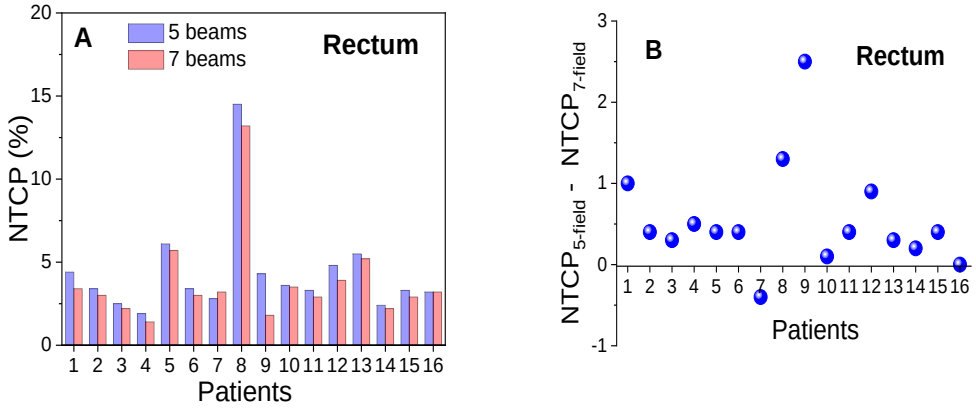

Figure II.10: A) Rectum wall NTCP of 5-field and 7-field, **B)** Rectum wall NTCP difference of 5-field and 7-field.

- **NTCP Bladder**

The absolute errors and NTCP calculated are shown in Figures (11A) and (11B) respectively. According to the statistical analysis, there is a significant difference between the two techniques (P-value = 0.045).

The mean calculated NTCP for 5-field was 0.22 % in the range of [0.07 % - 1.3 %] and 0.1 % in the range of [0.02 % - 0.37 %] for 7-field. The corresponding 7-field volume percentage is better than the 5-field in preserving the bladder.

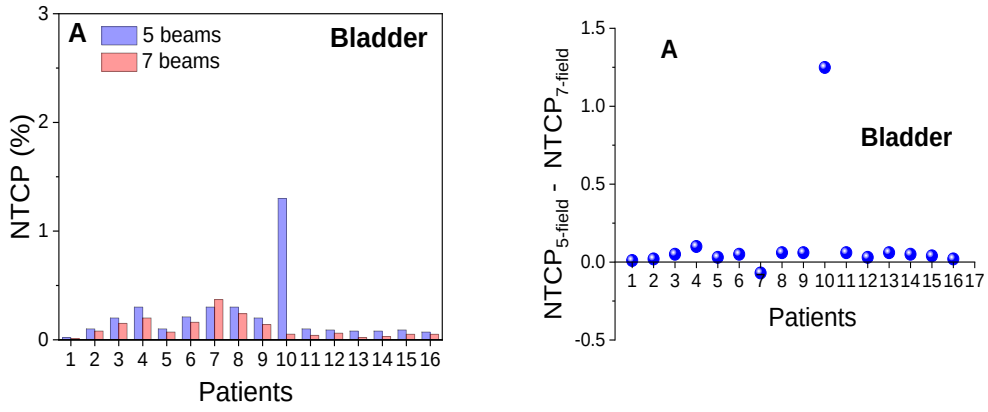

Figure II.11: A) Bladder wall NTCP of 5-field and 7-field, **B)** Bladder wall NTCP difference of 5-field and 7-field.

- **TCP PTV60**

Figure (12A) and (12B) shows the calculated TCP and absolute error. For PTV no significant differences suggest no statistically discernible distinction (P-value of 0.635).

The mean calculated TCP for 5 fields ranged from 51.5% to 79.9% with a value of 70.16%, while for 7 fields the calculated values ranged from 50.9% to 79.5% with a value of 69.77%. This comparison shows no significant differences between the two plans.

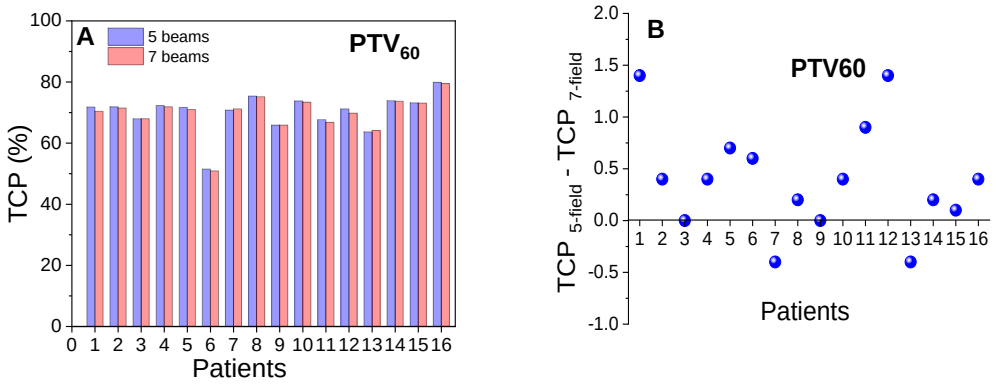

Figure II.12: A) TCP of 5-field and 7-field calculated for PTV60, **B)** TCP difference of 5-field and 7-field for PTV60.

The left and right femoral heads were analyzed but not shown, as their NTCP values for both techniques range from 10^{-5} % to 10^{-10} %, essentially zero.

Radiobiological and dosimetric comparison finding of the two plans (5 and 7 fields), based on ICRU 83 recommendations, IAEA requirements, and dose constraints for the hypofractionated protocol, leads to the conclusion that the 7-field plan is better than the 5-field plan for the treatment of early-stage cancer, giving the best results and better protection of organs at risk by calculating the probability of complications occurring in the rectum and the bladder.

These two examples of comparisons, as mentioned above, are carried out in the context of a calculation, this calculation enables us to choose between two techniques according to one or more criteria. In Chapter 3, we will explore the primary function of these indices: predicting toxicity and tumor control following treatment.

Chapter III: Analyzing the reliability of early and late complication predictions.

I. Classification of the toxicities

An objective standard description is necessary to assess the varying toxicity levels of different organs quantitatively. At least three rating scales have been proposed to measure radiation-induced complications. These scales are combined to provide an overall assessment of toxicity.

1. RTOG/EORTC

The RTOG scale was proposed by the Radiation Therapy Oncology Group for acute toxicities and after that, the European Organization for Research and Treatment of Cancer proposed another scale named EORTC, especially for late toxicities.

Most RTOG publications define "major" toxicities as combining Grades 3, 4, and 5. The details of Grade 4 and 5 toxicities have been presented. Cumulative probabilities of "major" or Grade 4 and 5 toxicities are given as risk estimates at specific intervals, such as 1 year, 2 years, etc. Late effects of radiation on normal tissues may increase with time, and interventions could reduce the risk or severity of these effects. More quantitative measures of severity are needed **(JD 1995, Cox 1986)**.

2. LENT/SOMA

Proposed in 1995. Correspond to the latest RTOG/EORTC scale for late toxicities and to replace the EORTC scale.

3. CTCAE

The abbreviation of the Common Terminology Criteria for Adverse Events, the National Cancer Institute has developed a standardized scale to evaluate the side effects of different cancer treatments, including radiotherapy and chemotherapy.

The scale has undergone several revisions over the years to provide an accurate and objective description of acute and delayed side effects. It aims to provide a reliable classification of side effects that can be used to assess the effectiveness of cancer treatments. The current version is V.5.0 dating from 2017 **(Shah 2022)**.

II. The endpoints used in the performed calculation.

Toxicity from cancer treatment is classified as acute or late depending on when it occurs with treatment. Each organ at risk has been evaluated according to one or more

endpoints (toxicity). This section will list the endpoints chosen and their definitions for each location.

1. Nasopharynx cancer

a. PTV: Advanced-stage UCNT cancer.

b. The brainstem: Necrosis/infarction

- Necrosis:

Radiation-induced brainstem necrosis (RIBN) is a life-threatening late complication that can occur after treatment in patients with nasopharyngeal carcinoma (NPC). However, the relationship between RIBN and radiation dose is unclear. Figure III.1 shows a typical appearance of brainstem necrosis on MRI in a 43-year-old man treated with IMRT. At 42 months of follow-up, the patient developed mild memory loss and swallowing dysfunction.

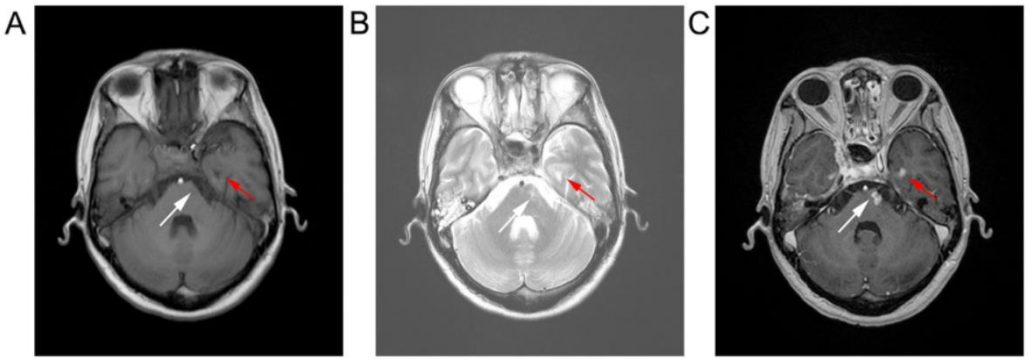

Figure III.1: Axial image shows marginal enhancement and surrounding edema in the pons (white arrow) and left temporal lobe (red arrow). T1-weighted image; (b) T2-weighted image; (c) Contrast-enhanced T1-weighted image **(Fan et al. 2022)**.

- Infraction:

A brainstem infarction is an area of tissue death due to a part of the brainstem not getting enough oxygen. Knowledge of anatomy, vascular supply, and physical examination can save lives and enable precise diagnosis and treatment during acute infarction **(Gowda et al. 2023)**.

c. The spinal cord: Myelitis/necrosis

- Myelitis:

An inflammation of the spinal cord disrupts the normal response of the brain to the rest of the body and the rest of the body to the brain. Inflammation of the spinal cord causes damage to myelin and axons, leading to symptoms such as paralysis and loss of sensation.

- Necrosis:

Defined as symptomatic toxicity. Is the most common late-delayed complication of RT and can occur a few months to as many as several decades after treatment **(Béhin et al. 2004)**.

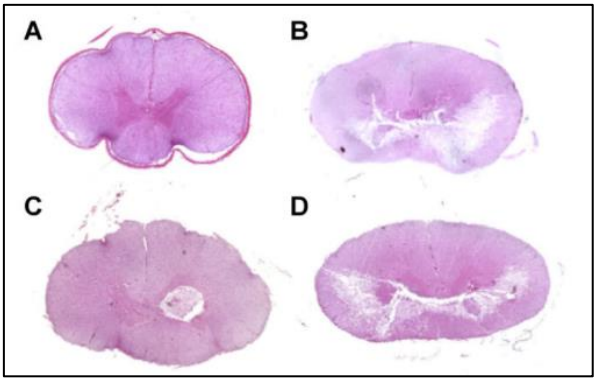

Figure III.2: Microscopic lateral view of the spinal cord. (A) Normal spinal cord. (B, D) Necrosis of the anterior horn, posterior horn, and white matter. (C) Central necrosis involves the dorsal and anterior horns and parts of the white matter **(Gaudry et al. 2018)**.

d. The optic chiasm: Blindness

Lesions with complete optic chiasm destroy axons in the nasal region of both eyes, resulting in vision loss in both the right and left halves of the right visual field.

e. Right and left optic nerves: Blindness

This complication is caused by radiation exposure to the optic nerve during radiation therapy for head and neck cancer. Their occurrence is associated with cumulative radiation doses exceeding 50 Gy, the presence of multiple diseases, and the presence of concurrent chemotherapy and radiotherapy. It presents with acute, painless, monocular vision loss that develops late after radiation exposure **(Ataídes et al. 2021)**.

f. Right and left middle ears: Two types of toxicities are being evaluated, namely:

- Acute serous otitis:

Acute otitis media (AOM) is a type of ear infection that causes inflammation of the middle ear's lining and the accumulation of infected fluid. The condition is characterized by a white, bulging tympanic membrane, which is shown in figure III.3 **(Meherali et al. 2019)**.

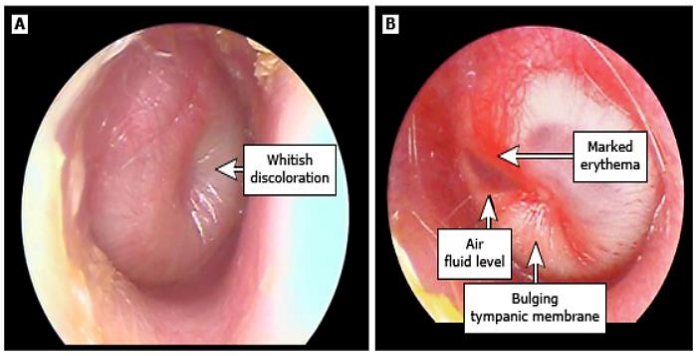

Figure III.3: (A) The tympanic membrane appears to be bulging with slight redness. (B) Tympanic membrane bulging with marked erythema and an air-fluid level **(Leskinen et al. 2005)**.

The most common cause of the infection is the dysfunction of the Eustachian tube, which leads to the accumulation and infection of retained secretions. A ruptured tympanic membrane can cause AOM along with purulent otorrhea. Antimicrobial therapy is usually effective in treating AOM promptly **(Leskinen et al. 2005)**. This toxicity usually develops during or shortly after treatment and is typically temporary.

- Chronic serous otitis:

COM is diagnosed when a chronic or recurrent ear infection causes a subacute or chronic tympanic membrane perforation. The substance being referred to is usually a consistent, pale-yellow color, similar to straw, and serous drainage through the perforated tympanic membrane **(Leskinen et al. 2005)**. Typically appears months to years after the end of treatment and is usually permanent.

g. Right and left parotids glands:

Xerostomia is a common side effect of radiotherapy (RT) that negatively impacts patient quality of life. Damage to the salivary glands is the most common long-

term complication of radiation therapy (RT) and chemoradiotherapy for head and neck cancer **(Galloway et al. 2012)**. Using both the salivary flow and the RTOG scale. The incidence of complications was modeled based on Grade 3 toxicity as the endpoint fits at 3, 6, and 12 months after RT for two models LKB and RS, and below 6 months for the Logit model **(Marzi et al. 2009)**.

Grade 3 of salivary gland toxicity is defined as complete dryness of mouth, and no response to stimulation. After moderate dryness of mouth, poor response to stimulation, and slight dryness of mouth, good response to stimulation of grade 2 and 1 respectively **(JD 1995)**.

Toxicity late RT	**Grade**				
	0	1	2	3	4
Salivary glands	No change from the baseline	Slight dryness of the mouth; good response to stimulation	Moderate dryness of mouth; poor response to stimulation	Complete dryness of the mouth; no response to stimulation	fibrosis

Table III.1: RTOG/EORTC late radiation morbidity scoring scheme including xerostomia occurring greater than 90 days after radiation therapy.

h. The right and left lens:

Cataracts cause part of the lens of the eye to be cloudy, caused by damaged cells that cover the back surface of the lens. Symptoms may appear as early as a year or two after exposure to high doses or many years after exposure to low doses. In this study, we examined the lens for cataracts requiring intervention **(Neriishi et al. 2007)**.

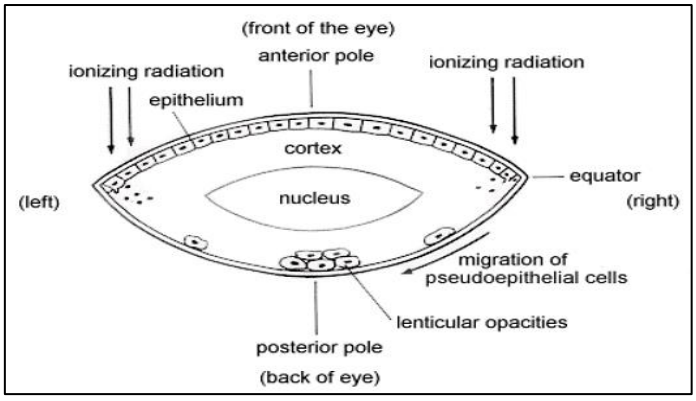

Figure III.4: Lens opacity at the posterior subcapsular region caused by radiation from Effects of A-bomb Radiation on the Human Body, ed by HICARE in 1991, courtesy of Bunkodo Co., Ltd., Tokyo **(Ardiet et al. 2007)**.

2. Prostate cancer

a. PTV:

- Early and intermediate-stage prostate adenocarcinoma treated with IMRT
- Early and intermediate-stage prostate adenocarcinoma treated with VMAT.

b. Rectum:

- Severe proctitis/necrosis/stenosis/fistula

CTCAE term	Grade 1	Grade 2	Grade 3	Grade 4	Grade 5
Proctitis	Rectal discomfort, intervention not indicated	Symptomatic (e.g., rectal discomfort, passing blood or mucus); medical intervention indicated; limiting instrumental ADL	Severe symptoms; fecal urgency or stool incontinence; limiting self care ADL	Life-threatening consequences; urgent intervention indicated	Death
Definition: A disorder characterized by inflammation of the rectum.					
Rectal necrosis	-	-	Tube feeding or TPN indicated; invasive intervention indicated	Life-threatening consequences; urgent operative intervention indicated	Death
Definition: A disorder characterized by a necrotic process occurring in the rectal wall.					
Rectal stenosis	Asymptomatic; clinical or diagnostic observations only; intervention not indicated	Symptomatic; altered GI function	Severely altered GI function; tube feeding or hospitalization indicated; elective operative intervention indicated	Life-threatening consequences; urgent operative intervention indicated	Death
Definition: A disorder characterized by a narrowing of the lumen of the rectum.					
Rectal fistula	Asymptomatic	Symptomatic, invasive intervention not indicated	Invasive intervention indicated	Life-threatening consequences; urgent intervention indicated	Death
Definition: A disorder characterized by an abnormal communication between the rectum and another organ or anatomic site.					

Table III.2: Late rectal complications scored according to CTCAE v 5.0 **(Shah 2022)**.

- Late rectal toxicity grade ≥ 2 RTOG 3-4 years

Is a consequence of ischemia and fibrosis of the rectal wall, according to the RTOG scale it was classified as none for grade 1. For grade 2 the toxicity includes moderate diarrhea and colic, bowel movement more than five times daily, excessive rectal mucus, or intermittent bleeding. Grade 3 consists of obstruction or bleeding requiring surgery. Grade 4 (necrosis /perforation fistula) is rarely encountered in current practice **(JD 1995)**.

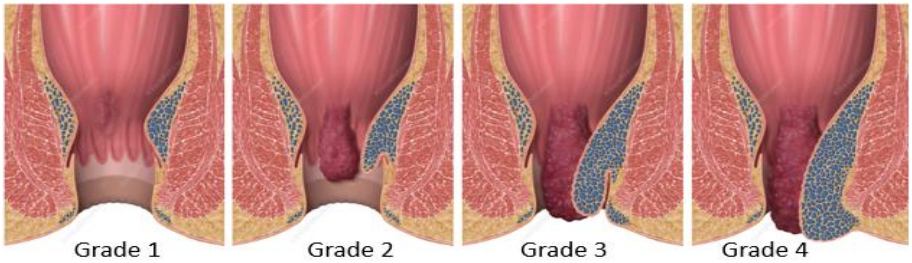

Figure III.5: Descriptive diagram of rectal bleeding according to RTOG scale.

- Mild RTOG rectum toxicity grade 2/3 (21 months)

The degree of radiation toxicity was documented using the RTOG grading system, where grade 2: symptoms responding to simple outpatient management, life style (performance status) not affected, and grade 3: distressing symptoms altering patients' lifestyle (performance status). Hospitalization for diagnosis or minor surgical intervention (such as urethal dilatation) may be required **(Lu et al. 1995, Jensen et al. 2011, Lawton et al. 1991)**.

- Rectal toxicity grade ≥ 2 LENT/SOMA 5 years

	Grade 2	**Grade 3**	**Grade 4**
S**bjective** **Tenesmus** **Mucosal loss,** **Sphyncter control** **Stool frequency** **Pain**	 Intermittent urgency Intermittent Intermittent 4 - 8 per day Intermittent & tolerable	 Persistent urgency Persistent Persistent >8perday Persistent & intense	 Refractory Refractory Refractory Uncontrolled diarrhea Refractory & excruciating
O**bjective** **Bleeding** **Ulceration** **Stricture**	 Occasionally > Uweek Superficial > 1 cm* l/3 - 2./3 normal diameter with dilatation	 Persistent/daily Deep ulcer c l/3 normal diameter	 Gross hemorrhage Perforation, Fistulae Complete obstruction
M**anagmentt** **Tenesmus & stool hequency**	 Regular, > 2 antidiarrheals/week	 Multiple, > 2 antidiarrhe&day	 Surgical intervention/ Permanent colostomy

Pain	Regular non-narcotic	Regular narcotic	Surgical intervention
bleeding	Occasional transfusion	Frequent transfusions	Surgical intervention I Permanent colostomy
Ulceration	Occasional steroids	Steroids per enema, hyperbaric oxygen	Surgical intervention/ Permanent colostomy
Stricture	Occasional dilatation	Regular dilatation	Surgical intervention/ Permanent colostomy
Sphincter control	Intermittent use of incontinence pads	Persistent use of incontinence pads	Surgical intervention/ Permanent colostomy
A**nalytic**			
Barium enema	Assessment of lumen and peristalsis		
Proctoscopy	Assessment of lumen and mucosal surface		
CT	Assessment of wall thickness, sinus and fistula formation		
MRI	Assessment of wall thickness, sinus and fistula formation		
Anal manometry	Assessment rectal compliance		
Ultrasound	Assessment of wall thickness. sinus and fistula formation		

Table III.3: Late rectal toxicities according to the LENT/SOMA scale.

c. Bladder:

- Symptomatic bladder contracture and volume loss

Bladder neck contracture (BNC) is a well-known complication that may occur after surgical treatment of benign and malignant prostate disease. Unfortunately, BNC recurrence after treatment is a common problem despite early success reported in many series **(Kostakopoulos et al. 2004, Brodak et al. 2010)**. The complexity of BNC ranges from simple, short annular contractures to occlusive strictures that do not respond to repeated treatments. Treatment of BNC requires a tailored approach, ranging from simple office procedures to complex surgical reconstruction **(Simhan et al. 2014)**.

- Acute genitourinary grade 2 RTOG

Acute genitourinary complications according to the modified RTOG/EORTC morbidity scale grade 2 were defined as the frequency of urination being less frequent than every hour (day: 12-16 times; nocturia 5-8 times)/ dysuria (difficult or painful urination. It is usually associated urgency and frequency of urination), urgency, bladder spasm requiring local anesthetic.

- Late bladder toxicity grade ≥ 2 LENT/SOMA (5 years)

	Grade 2	Grade 3	Grade 4
S**ubjective**			
Dysuria	Intermittent & tolerable	Persistent & intense	Refractory & excruciating
Frequency	2 - 3 hour intervals	1 - 2 hour intervals	Hourly
Hematuria	Intermittent	Persistent with clot	Refractory
Incontinence	< daily episodes	52padsJundergarmeWday	Refractory
Decreaseds tfeam	Intermittent	Persistent but incomplete obstruction	Complete obstruction
O**bjective**			
Hematuria	Intermittent macroscopic, c 10% decrease in hemoglobin	Persistent macroscopic, 10% - 20% decrease in hemoglobin	Refractory, > 20% decrease in hemoglobin
Endoscopy	Confluent atrophy or Telangiectasia with gross bleeding	Ulcerations into muscle	Perforation, fistula
Maximum volume	>2OOcc-3OOcc	> loocc-2oocc	<lOOcc
Residual volume	> 25 cc - 100 cc	> 1OOcc	
M**an agement**			
Dysuria	Regular non-narcotic	Regular narcotic	Surgical intervention
Frequency	Occasional anti-spasmodic	Regular narcotic	Cystectomy
Hematuria/ Telangiectasia	Occasional transfusion or single cauterization	Frequent transfusion or coagulation	Surgical intervention
Incontinence	Intermittent use of incontinence pads	Regular use of pad or selfcatheterization	Permanent catheter
Decreased stream	< Once-a-day selfcatheterization	Dilatation, > once-a-day self-catheterization	Permanent catheter, surgical intervention
A**nalytic**			
Cystography	Assessment of mucosal surface		
Volumetric analysis	Assessment of bladder capacity in milliliters		
Contrast radiography	Assessment for ulcers, capacity and contractility		
Ultrasound	Assessment of wall thickness, sinus and fistula formation		
Eleetromvomanhv	Assessment of sohincter activitv usine intralumenal pressure transducer. contraction pressure and volume curvea		

Table III.4: Late bladder toxicities according to the LENT/SOMA scale.

d. Femoral heads: necrosis

The necrosis occurs in grade 5 (bone death in the head of the femur) due to a defect in bone vascularization. This necrotic bone becomes more fragile than usual and more likely to fracture.

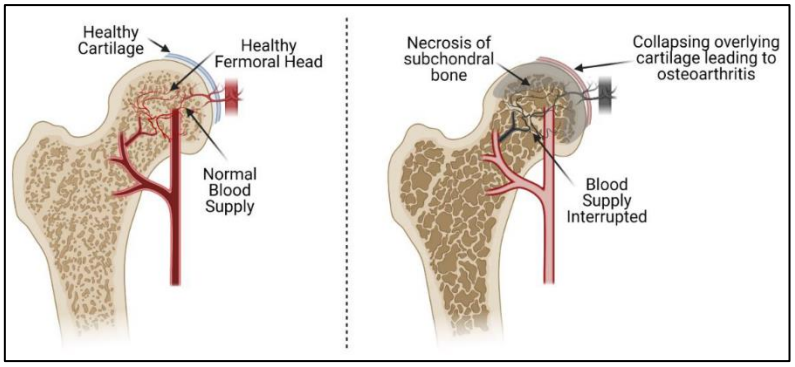

Figure III.6: Healthy femoral head versus femoral head with necrosis.

III. TCP and NTCP predictions.

The study included a group of 32 patients with nasopharyngeal and prostate cancers. Out of those, 10 had nasopharyngeal cancer and 22 had prostate cancer. The patients with advanced-stage nasopharyngeal cancer (T3-T4) were treated with a conventional regimen (70 Gy/2 Gy) in 35 sessions, using the IMRT technique. The mean tumor size was 380.1 cm^3, ranging from 225 cm^3 to 767.3 cm^3.

Out of the 12 patients with prostate cancer, some are low risk (PSA <10 ng/ml, Gleason score 6, and clinical stage T1-T2a) and some are intermediate risk (PSA between 10 and 20 ng/ml or Gleason score 7 or clinical stage T2b-T2c). They were treated by the VMAT technique. The remaining 10 prostate cancer patients were of intermediate and high risk (PSA >10 ng/ml or Gleason score >7 or clinical stage T2b-T4) and were treated with IMRT. All prostate cancer patients were treated with the conventional 76 Gy regimen in 2 Gy per fraction and 5 fractions per week.

In this study, we chose a single endpoint to represent toxicity or tumor control criteria for each organ at risk and PTV. We then computed the NTCP and TCP values for each endpoint. This allowed us to compare the outcomes of our radbio_for program to those from other sources in the literature (BioSuite, RADBIOMOD). By validating our computations, we proceeded with confidence in our research using the radbio_for program.

1. TCP prediction

The patients selected in this part are those with nasopharynx and prostate cancer treated with the IMRT and VMAT techniques, respectively. To calculate the TCP

values, we selected the radiobiological parameters appropriate to the stage of cancer and the treatment regimen in each localization.

1.1.Comparison between radiobiological programs.

1.1.1. Nasopharynx PTV

Using the identified parameters cited by Avanzo et al. **(2010)**, the calculation results are presented in figure III.7. The calculation was performed using the 3 radiobiological programs: BioSuite, RADBIOMOD, and Radbio-For. A set of radiobiological models was integrated into these three programs such as Marsden, fundamental Poisson, and logit models.

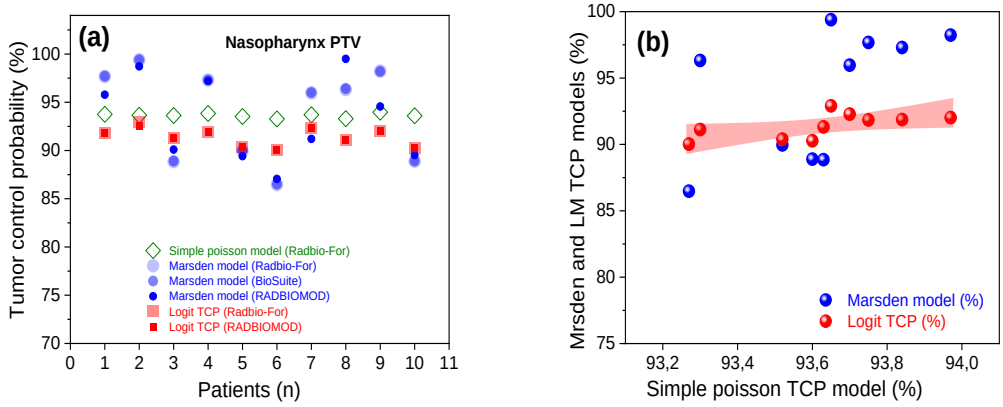

Figure III.7: a) comparison between radiobiological calculation programs of the nasopharynx PTV, b) comparison between radiobiological models.

Upon analyzing the calculation carried out by the Marsden model with three different programs, we have observed that the BioSuite and Radbio-for programs yield identical results. However, there exists a slight difference between the RADBIOMOD program and the other two. This difference was attributed to the number of iterations used to generate the calculation, as the RADBIOMOD program generates different results between two consecutive executions of the same calculation. Overall, this indicates that the choice of the program can significantly impact the results obtained from the calculation, and it is important to carefully evaluate the program iteration number being used to ensure the accuracy and reliability of the results. The results of the logit model of all patients are identical for both the RADBIOMOD and Radbio-for programs.

The comparison with the BioSuite program is irrelevant, as the model was not integrated into the program. Figure III.7 (b) shows a comparison of the last radiobiological models. The two models, Marsden and Logit, have been plotted against the fundamental simple Poisson model, the calculated TCP values with the Poisson model are different from the calculated TCP with the Marsden model (flat confidence band) and closer to the Logit model (linear confidence band) for all patients. The variation between the calculated values of TCP with the models is because of the parameters chosen in the literature, which were taken from the different patients, and the model's architecture (each model is based on a specific distribution and local control rate parameters): (D50, γ50, and a/ß) or (α, α-diffusion, ρ, and a/ß). The calculated TCP values by the Marsden model are based on different values of 'α' otherwise (various radio sensitivities) was the average of patient populations.

1.1.2. Prostate PTV

The calculation was performed using parameters identified by Okunieff et al. **(1995)** and Dearnaley et al. **(2007)**. Three radiobiological programs were used to perform this calculation, as shown in the figure III.8, the comparison yielded identical results of nasopharynx PTV. However, there was a discrepancy in the Marsden model's calculated result when compared to BioSuite and Radbio-for programs. Identical results were obtained with the logit model using RADBIOMOD and Radbio-For.

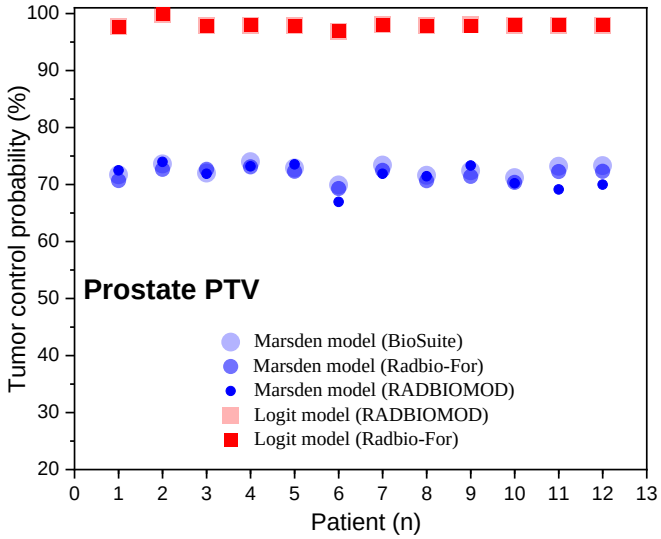

Figure III.8: Comparison between radiobiological calculation programs of the prostate PTV.

1.2. The effect of repopulation in TCP prediction

This part of the study is intended to compare the tumor control probabilities calculated by Radbio-for with and without accounting for the effect of repopulation for nasopharyngeal and adenocarcinoma of the prostate. The accuracy of biological modeling calculations in Radbio-For was validated by comparing them with the same calculations performed on other biological modeling programs (Biosuite and RADBIOMOD) for all clinical cases. This study used the Marsden model (see equation 31) and parameters identified in the literature **(Avanzo et al. 2010, Uzan et al. 2012, Fowler 2008, Pedicini et al. 2013).**

$$\mathrm{TCP} = \frac{1}{\sigma_\alpha\sqrt{2\pi}}\int_0^\infty exp\left\{-\rho_{clon}V\ exp\left[-\alpha D\left(1+\frac{\beta}{\alpha}d\right)\right]\right\} \times exp\left[\frac{-(\alpha-\alpha}{2{\sigma_\alpha}^2}\right] d\alpha + \ln(2)\frac{(T-T_k)}{T_{Pot}} \quad \ldots\ldots\ldots (31)$$

Where: **T:** Total treatment time.

T_{pot}: Potential doubling time

Tk: Kick-off or onset time

This study was based on sigmoid curve analysis of the TCP of treated PTVs.

1.2.1. <u>Nasopharynx PTV</u>

The obtained values are displayed in the table III.5 and graphical illustrations (Figure III.9) provided. This will facilitate the analysis of results for the nasopharyngeal.

Patients	**Volume (cm^3)**	**Radbio-For**	
TCP	PTV	TCP sans repopulation	TCP avec repopulation
Patient 1	298	95.99%	76.54%
Patient 2	316.4	95.59%	73.85%
Patient 3	315.1	87.99%	34.48%
Patient 4	351.2	95.58%	73.10%
Patient 5	373.2	88.60%	34.44%
Patient 6	767.3	85.20%	34.74%
Patient 7	407.5	94.33%	63.10%
Patient 8	225.74	94.74%	64.53%
Patient 9	225.75	96.52%	78.43%
Patient 10	522.3	87.53%	39.78%

Table III.5: The effect of repopulation on the TCP value of all nasopharyngeal patients.

The table indicates that for patients with a volume greater than nearly 315 cm^3, the TCP value with the effect of repopulation is less than 40%. This can be attributed to the effect of the total irradiated PTV volume, where a strong correlation between tumor size and the TCP is found. For patients with small PTV volumes (1, 8, and 9), when not accounting for the effect of repopulation, all calculated TCP values are above 94%. However, when the effect of repopulation was included in the TCP calculation, values dropped from 64% to 79%, still indicating the favorability of this treatment regimen for this stage of cancer.

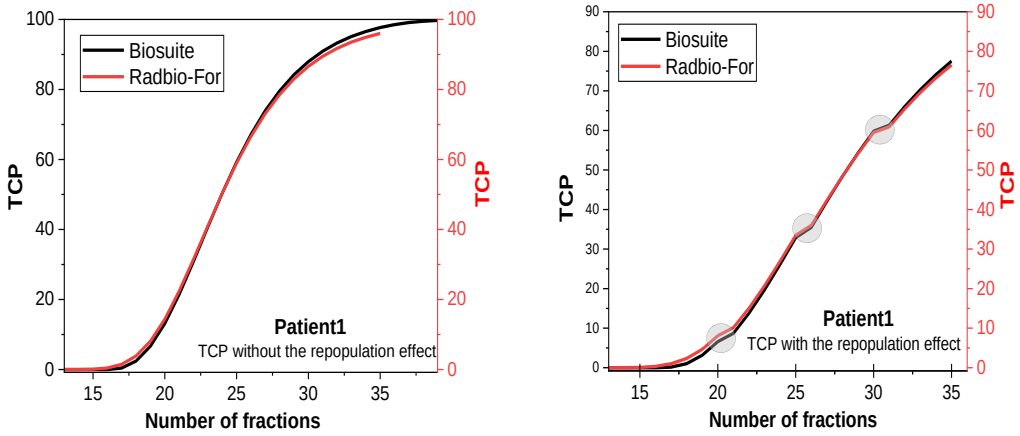

Figure III.9: Comparison of results obtained from the Biosuite and Radbio-For programs for nasopharyngeal cancer.

The TCP calculated using Radbio-For and Biosuite for two cases: with and without the effect of repopulation during treatment, shows identical curves.

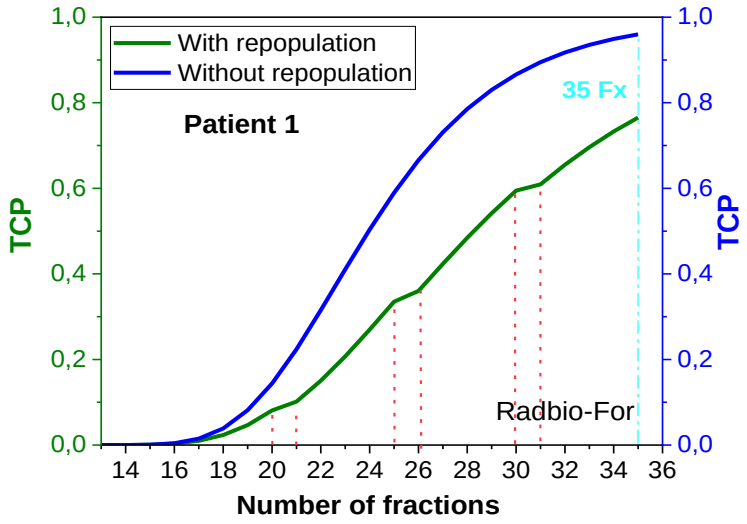

Figure III.10: The effect of repopulation for nasopharyngeal cancer patient 1.

The figure III.10 illustrates the impact of repopulation on the calculation of TCP using the Radbio-For program for patient 1. Without repopulation, we observed that the probability of tumor control starts to increase after the 15th fraction and follows a sigmoid shape (curve) as a function of dose until the 35th fraction (end of treatment), reaching a value of 95.99%. This indicates that the treatment scheme is favorable for this type of cancer and its stage of progression (TCP > 50%). However, when we factored in the effect of repopulation in the TCP calculation, we observed breaks in the TCP curve at the 20th, 25th, and 30th fractions, attributed to PTV repopulation during weekend breaks. In the final fraction (35th Fx), the TCP value decreased to 76.54%. Based on this observation, it is clear that the repopulation time of the PTV varies during radiotherapy.

Initially, the process is slow due to hypoxia, but after a certain period following the first fraction of radiotherapy and after 21 days, which is the time required for the tumor cells to start proliferating (Tk), repopulation accelerates, as shown in Figure III.10. This acceleration significantly impacts the TCP, leading to a decrease in the final results at the end of the treatment to 76.54%.

1.2.2. Prostate PTV

The obtained values are shown in the table III.6 and figure III.11.

Patients	Volume (cm^3)	Radbio-For	
TCP	PTV	TCP sans repopulation	TCP avec repopulation
Patient 1	96.69	69.62%	57.51%
Patient 2	74.12	71.65%	60.54%
Patient 3	97.15	70.04%	58.54%
Patient 4	65.63	72.09%	61.05%
Patient 5	78.91	70.85%	59.24%
Patient 6	138.71	61.18%	51.48%
Patient 7	91.21	71.44%	60.30%
Patient 8	125.66	69.59%	57.95%
Patient 9	99.65	70.38%	58.85%
Patient 10	126.68	69.29%	57.89%
Patient 11	74.90	71.25%	60.02%
Patient 12	76.64	71.28%	60.16%

Table III.6: The effect of repopulation on the TCP value of all prostate patients.

The results summarized in the table indicate that the volume effect plays an important role in tumor repopulation for patients with prostate cancer. We estimated a high TCP value (61.05 %) after integrating the effect of repopulation for patient 4, who had a small volume (65.63 cm^3) implying fewer proliferating cells and more dead cells after radiotherapy, and the opposite for patient 6 which had an important volume (138.71 cm^3), and less value of calculated TCP (51.48 %).

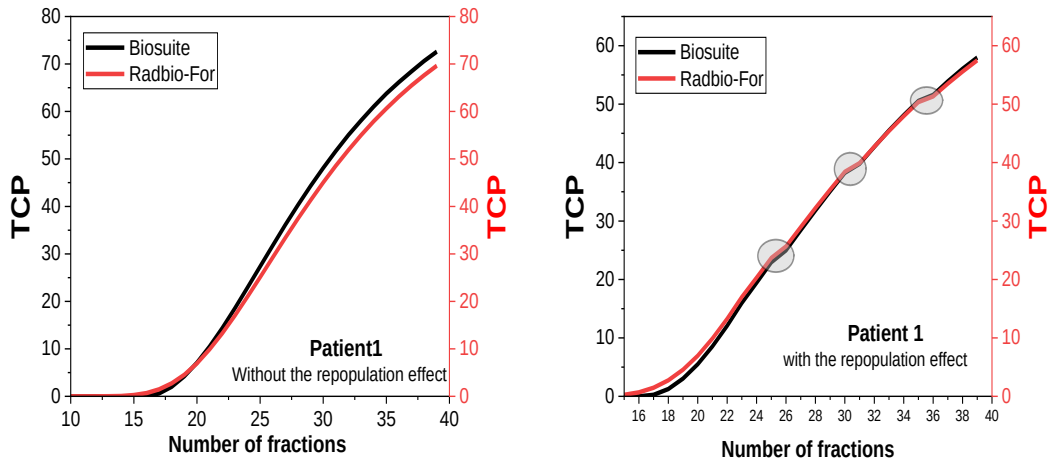

Figure III.11: Comparison of results obtained from the Biosuite and Radbio-For programs for prostate cancer.

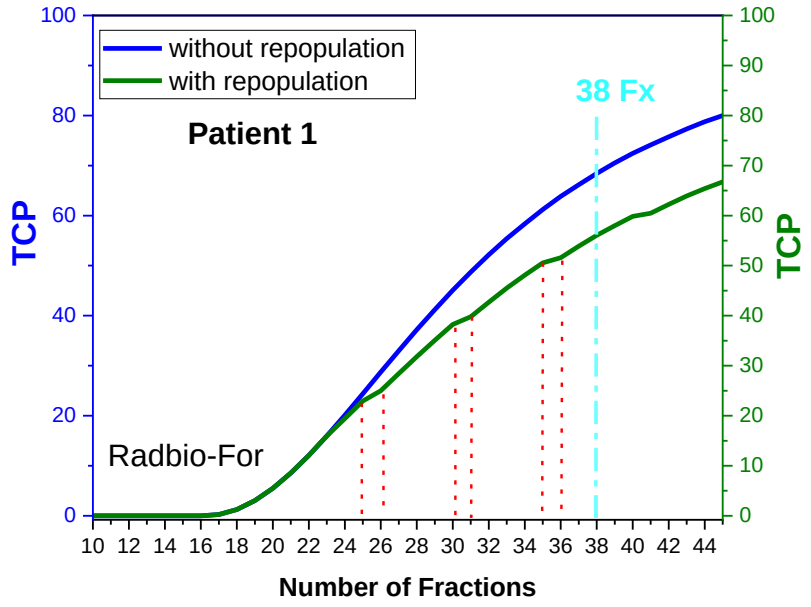

Figure III.12: The effect of repopulation for prostate cancer patient 1.

The figure III.12 illustrates the impact of repopulation on the calculation of TCP using the Radbio-For program for a prostate cancer case of patient 1. Without considering the repopulation effect, the TCP begins to increase after the 17th fraction and reaches 69.62% by the end of the 38th fraction, indicating a favorable treatment regimen for this type of cancer. However, when factoring in the effect of repopulation in the TCP calculation, we observe breaks in the TCP curve at the 25th, 30th, and 35th fractions due to PTV repopulation during weekend breaks.

In the final fraction (38th), the TCP value drops to 57.51%. Based on this observation, it is evident that the repopulation time of all PTVs (prostate tumor cells) varies during radiotherapy. Initially, the repopulation is slow, following the first fraction of radiotherapy, and around 25 days later, repopulation accelerates (see Figure III.12). The repopulation process began before the tumor reached the period of rapid growth, or the time required for the tumor cells to start multiplying (Tk=31 days).

This analysis shows that the very low value of the α/β ratio (1.5 Gy) makes the tumor cells more sensitive to the dose per fraction, which in turn makes the tumor resistant to the conventional treatment (very low percentages of proliferating cells). As a result, there is an increased chance of surviving cancer cells multiplying rapidly after radiation treatment.

2. NTCP prediction.

This section involves validating of our program by comparing it with other available programs. Furthermore, comparing the integrated models and assessing their predictive accuracy. To perform the calculation, we have selected radiobiological parameters that are fitted to specific toxicity (endpoint) for each organ at risk. These parameters are presented according to their architecture: serial, parallel, and serial-parallel. It is important to note that the choice of parameters must be made carefully, taking into account the patient group chosen for the study, as well as the definition of volumes, organs, and appropriate fractionation regimens.

2.1 Comparison between radiobiological programs.

a. Serial organs

For this type of architecture, five organs at risk namely the brainstem, spinal cord, optical chiasm, optic nerves, and middle ears, were selected to perform our study. We factored in various toxicities, including necrosis/infarction, myelitis/necrosis, blindness, acute and chronic serous otitis, to conduct our calculation. Figure III.13 below presents the calculation results obtained using RS, LKB, and Logit models integrated into Radbio-For, BioSuite, and RADBIOMOD. The calculation results of NTCP and the comparison with other programs are presented in the form of scatter points, using identified parameters of corresponding toxicities **(Burman et al. 1991, Semenenko et al. 2008, Kan et al. 2014, Oinam et al. 2011, Hamatani et al. 2017)**. The difference between the results obtained and calculated by the NTCP models depends on the different architecture of the mathematical models, radiobiological parameters, also on characteristics, and inter-patient variation. However, for the three NTCP models, we used the parameters adjusted for the 5% in the interval of (2-8 %) complications grade 1 or higher. In parallel, we note that the values produced by Radbio-For are identical to the results produced by BioSuite and RADBIOMOD.

As shown in figure III.13 (a) of the brainstem, all the results are less than 2% and in good agreement with the results obtained in the clinic (no necrosis and infarction were observed in the brainstem which was considered as endpoints in our study) for the three models RS, LKB, and Logit. The complication chosen for the evaluation of the spinal cord was myelitis/necrosis. According to the results found, all the patients show no probability of a complication greater than or equal to grade 1 toxicity see figure

III.13 (b), the calculated NTCP values are less than 1%, these results confirm that the plan chosen to treat the patients presents no danger to the quality of treatment. Another evaluation was made on the optical chiasm to study the probability of predicting blindness. Ninety percent of the cases are in good agreement with the acceptable threshold and perfectly reflect the dosimetric indices see figure III.13 (c). The calculated NTCP values of the right and left optical nerve (blindness) are shown in figure III.13 (d-e) the only NTCP value that exceeds the acceptable threshold is of patient 6 calculated with the RS model (right and left), and for the other patients, the NTCP values are lower than the ideal threshold recommended by the ICRU **(Grégoire et al. 2011, Podgorsak 2005)**. Following the order of priority, figure III.13 (f-g) represents the NTCP values calculated of the right middle ear for acute and chronic serous otitis, successively **(Limb et al. 2017, Lustig et al. 2018)**, we notice that the values are very high for the acute toxicity calculated with the three models of all the patients. On the other hand, the chronic serous otitis NTCP is significantly lower (less than 5%) except for two patients who are excluded from the discussion since the dose constraints were not respected. In figure III.13 (h-i) same observation for the left middle ear, three patients exceeded the threshold of NTCP for the chronic complication and they did not show a significant difference in acute toxicity.

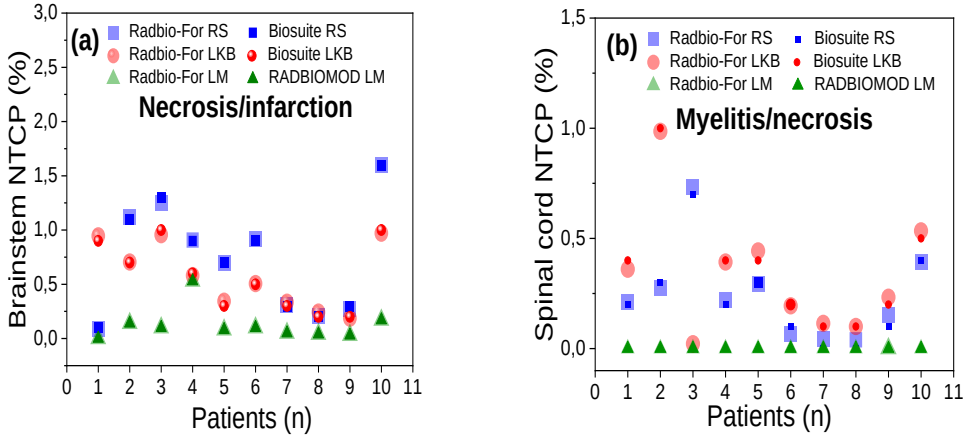

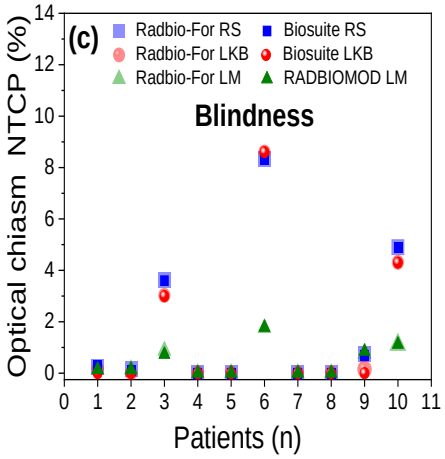
(c)
Radbio-For RS
Biosuite RS
Radbio-For LKB
Biosuite LKB
Radbio-For LM
RADBIOMOD LM
Blindness
Optical chiasm NTCP (%)
Patients (n)

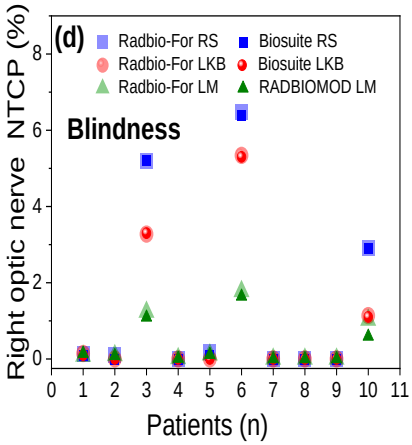
(d)
Radbio-For RS
Biosuite RS
Radbio-For LKB
Biosuite LKB
Radbio-For LM
RADBIOMOD LM
Blindness
Right optic nerve NTCP (%)
Patients (n)

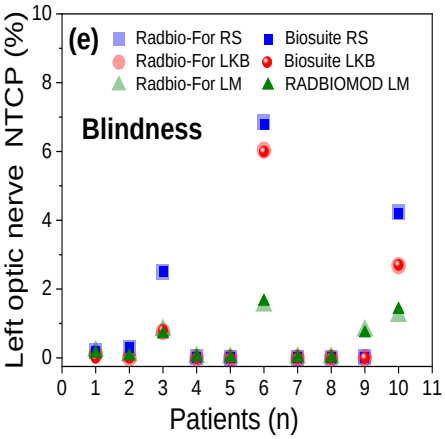
(e)
Radbio-For RS
Biosuite RS
Radbio-For LKB
Biosuite LKB
Radbio-For LM
RADBIOMOD LM
Blindness
Left optic nerve NTCP (%)
Patients (n)

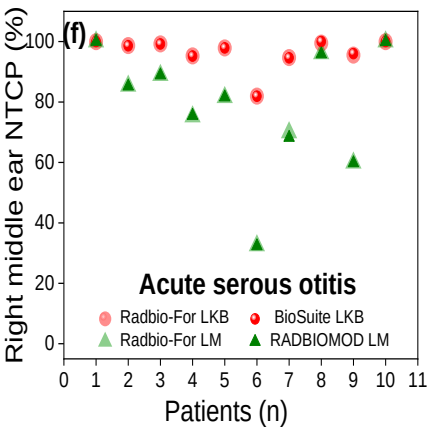
(f)
Acute serous otitis
Radbio-For LKB
BioSuite LKB
Radbio-For LM
RADBIOMOD LM
Right middle ear NTCP (%)
Patients (n)

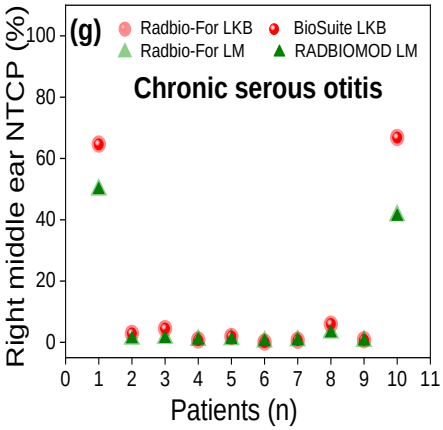
(g)
Radbio-For LKB
BioSuite LKB
Radbio-For LM
RADBIOMOD LM
Chronic serous otitis
Right middle ear NTCP (%)
Patients (n)

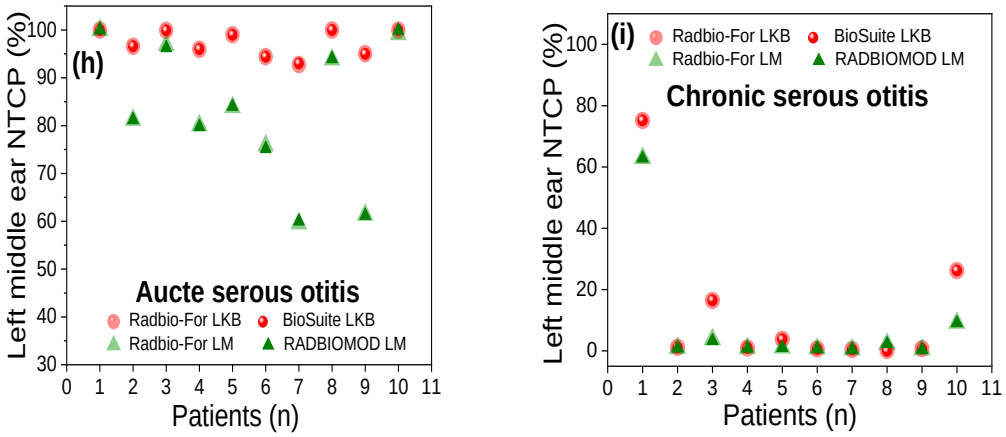

Figure III.13: Comparison of calculation programs for serial organs and validation of our Radbio-For program.

b. Parallel organs.

In this study, only the parotid glands, which are organized in a parallel architecture, were evaluated for xerostomia (grade ≥ 3) using RS and LKB models **(Marzi et al. 2009)**. For the Logit model, we used the identified parameters 6 months after radiotherapy **(Semenenko et al. 2008)**. The results are shown in figure III.14 (a-b) for the right and left parotids, respectively. All the NTCP values calculated with RS and LKB are greater than 20%, indicating that the prediction of this complication can occur 12 months after radiotherapy. The NTCP values calculated with the Logit model are greater than 15% and, in most cases, greater than those calculated with the LKB and RS models.

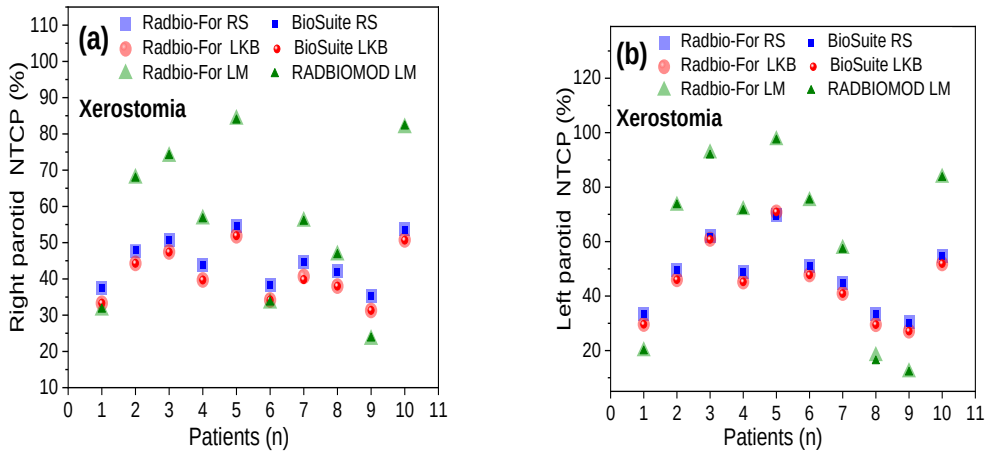

Figure III.14: Comparison of calculation programs for parallel organs and validation of our Radbio-For program.

c. Serial-parallel organs.

The lens, rectum, and bladder are classified as serial-parallel organs. Figure III.15 displays the calculated NTCP of the lens using identified parameters of cataract requiring intervention complication **(Burman et al. 1991, Kan et al. 2014, Oinam et al. 2011)**. The results indicate that the NTCP values of both the right and left lens are not significant see figure III.15 (a-b), with only two patients exceeding the acceptable threshold (> 5%) compared to the other cases.

Figure III.15 (c) shows the NTCP calculated for the rectum using identified parameters of (severe proctitis/necrosis/stenosis/fistula) as an endpoint, and the results are below 5% **[Burman et al. 1991, Jameson et al. 2015, Kang et al. 2017, Rana et al. 2014)**. The calculated NTCP of the bladder using identified parameters of bladder contracture and volume loss are presented in figure III.15 (d) **(Burman et al. 1991, Jameson et al. 2015, Kang et al. 2017)**. The calculation results using LKB and LM were below 1%, and below 6% using the RS model.

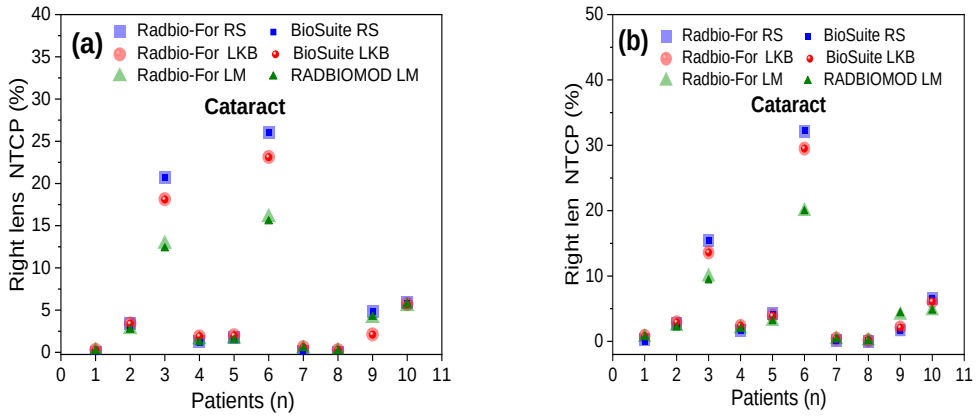

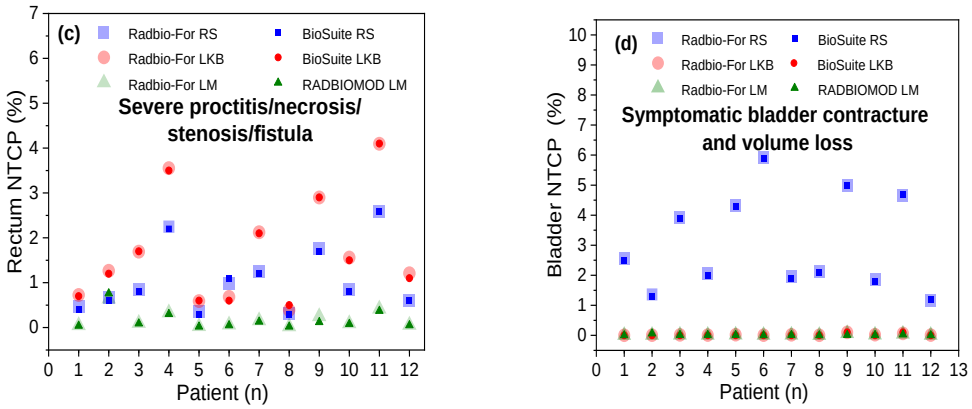

Figure III.15: Comparison of calculation programs for serial-parallel organs and validation of our Radbio-For program.

3. The significance of dose constraints in predicting early and late radiation-induced complications based on NTCP.

The calculated NTCP allowed us to predict the complications of normal tissues after external radiotherapy of advanced-stage nasopharyngeal and prostate cancer. On the other hand, the question asked was about the most appropriate predictive model of the reliable NTCP value. To find it, we compared the three radiobiological models and the dose constraints to fix this or those that follow well and reflect the dose constraints, which, in turn, can influence the value of the NTCP.

We have compared the calculated NTCP value for an organ at risk for all patients by each model with the specific constraint of this organ in the three cases when the constraint is respected, at the limit of the constraint, and when the constraint exceeds the threshold required to validate a treatment plan. The optimum choice of radiation dose delivery technique in the plan's treatment is to minimize the NTCP because the NTCP value should be less than or equal to 0.05 for a typical radiotherapy treatment.

3.1.Nasopharyngeal

- **Brainstem**

The table presented below indicates that for all patients, the NTCP values are below 5%, and the D2% dose constraint is below 54 Gy. It is notable that NTCP values follow the D2% dose constraint, as demonstrated by patients 2 and 10, where the NTCP increases as the constraint approaches the limit.

Brainstem	NTCP		
	RS	LKB	Logit
Patient 1	$9.17*10^{-1}$	$9.46 * 10^{-1}$	$1.59 * 10^{-1}$
Patient 2	1.12	$7.05*10^{-1}$	$1.43*10^{-1}$
Patient 3	1.25	$9.57*10^{-1}$	$1.78*10^{-1}$
Patient 4	$9.07*10^{-1}$	$5.8*10^{-1}$	$1.15*10^{-1}$
Patient 5	$7.69*10^{-1}$	$3.43*10^{-1}$	$3.8*10^{-5}$
Patient 6	$9.92*10^{-1}$	$5.06*10^{-1}$	$9.95*10^{-3}$
Patient 7	$3.11*10^{-1}$	$3.34*10^{-1}$	$5.31*10^{-2}$
Patient 8	$2.03*10^{-1}$	$2.43*10^{-1}$	$3.71*10^{-2}$
Patient 9	$2.72*10^{-1}$	$1.87*10^{-1}$	$3.35*10^{-2}$
Patient 10	1.69	$9.71*10^{-1}$	$2.10*10^{-1}$

Table III.7: Calculated dose constraints and NTCP for the brainstem of all patients

- **Spinal cord**

For all patients, the NTCP value is very low < 1%. We note here that for the spinal cord, the D2% constraint is very low and well respected (order of priority in the TPS template).

Spinal cord	NTCP		
	RS	LKB	Logit
Patient 1	$2.11*10^{-1}$	$3.60 * 10^{-1}$	$1.54 * 10^{-5}$
Patient 2	$2.73*10^{-1}$	$9.86*10^{-1}$	$2.89*10^{-5}$
Patient 3	$7.33*10^{-1}$	$2.17*10^{-2}$	$9.81*10^{-5}$
Patient 4	$2.20*10^{-1}$	$3.926*10^{-1}$	$2.45*10^{-5}$
Patient 5	$2.94*10^{-1}$	$4.43*10^{-1}$	$3.8*10^{-5}$
Patient 6	$6.50*10^{-2}$	$1.94*10^{-1}$	$6.61*10^{-6}$
Patient 7	$4.46*10^{-2}$	$1.14*10^{-1}$	$2.92*10^{-6}$
Patient 8	$3.93*10^{-2}$	$1.66*10^{-1}$	$2.05*10^{-6}$
Patient 9	$1.52*10^{-1}$	$2.33*10^{-1}$	$1.36*10^{-5}$
Patient 10	$3.94*10^{-1}$	$5.34*10^{-1}$	$7.62*10^{-6}$

Table III.8: Calculated dose constraints and NTCP for the spinal cord of all patient

- **Optical chiasm**

Based on the table provided, it can be observed that both the RS and LKB models follow the D2% constraint as a percentage compared to the logit model, which is farther away. The constraint in the case of patient 3 is well respected, the NTCP value calculated with RS and LKB is <5%, while the value in the case of patient 10 is increased, and the NTCP value is increased but still following D2%. In the case of

patient 6, the constraint is beyond the limit threshold, with an NTCP value greater than 5%.

Optical Chiasm	NTCP		
	RS	LKB	Logit
Patient 1	$2.53*10^{-1}$	$1.81 * 10^{-1}$	$1.32 * 10^{-1}$
Patient 2	$1.48*10^{-1}$	$3.34*10^{-3}$	$1.55*10^{-1}$
Patient 3	3.61	3.024	$8.75*10^{-1}$
Patient 4	0	$6.55*10^{-8}$	$4.23*10^{-9}$
Patient 5	$1.17*10^{-7}$	$2.33*10^{-6}$	$7.52*10^{-2}$
Patient 6	8.35	8.60	1.76
Patient 7	0	$4.76*10^{-6}$	$3.84*10^{-9}$
Patient 8	$1.26*10^{-8}$	$2.60*10^{-4}$	$1.15*10^{-4}$
Patient 9	$7.60*10^{-1}$	$1.47*10^{-1}$	$7.55*10^{-1}$
Patient 10	4.90	4.312	1.10

Table III.9: Calculated dose constraints and NTCP for the optical chiasm of all patients

- **Right and left optical nerves.**

In the case of optical nerve, the LKB and RS models continue to prove that the D2% constraint dominates the NTCP value (the NTCP value increases with increasing D2%) for both sides (right and left) as shown in the following table. Inversely with logit model which found far.

Right optical nerve	NTCP			Left optical nerve			
	RS	LKB	Logit		RS	LKB	Logit
Patient 1	0.12	0.14	0.07	**Patient 1**	0.18	0.11	0.18
Patient 2	0.09	0.001	0.09	**Patient 2**	0.02	0	0.06
Patient 3	5.19	3.273	1.23	**Patient 3**	2.50	0.71	0.80
Patient 4	0.003	0.001	0.01	**Patient 4**	0.009	0.003	0.01
Patient 5	0.16	0.03	0.10	**Patient 5**	0	0	0
Patient 6	6.47	5.34	1.77	**Patient 6**	6.87	6.0354	1.51
Patient 7	0	0	0	**Patient 7**	0	0	0
Patient 8	0	0	0.03	**Patient 8**	0	0	0
Patient 9	0	0	0	**Patient 9**	0.01	0	0.02
Patient 10	2.92	1.134	1.02	**Patient 10**	4.25	2.67	1.21

Table III.10: Calculated dose constraints and NTCP for the right and left optical nerves of all patients.

The figure III.16 illustrates how the calculated NTCP value aligns with the dose constraint. In this case, the delivered dose to 2% of the total optic nerve volume was 47.3 Gy, which is well respected, and the calculated NTCP value was 0.16%. This

indicates a very low probability of complications. When the dose constraint was increased to 53.98 Gy (near the limit), the calculated NTCP value increased to 2.92%. In another case where the dose deposited in 2% of the total volume was 54.41 Gy (beyond the limit) and the maximum dose was 60.415 Gy, the calculated NTCP value was 6.47%. These analyses demonstrate that the RS model accurately complies with the constraint in percentage terms. Moreover, it indicates a high degree of accuracy in predicting the reliable values for the endpoint of blindness.

These findings are consistent with the results of Noël et al. **(2022)** study, which showed that the risk of blindness over five years is between 0-5% if the maximum dose to the optic nerve is within 50-60 Gy. However, the risk increases to 50% if the maximum dose reaches 65 Gy.

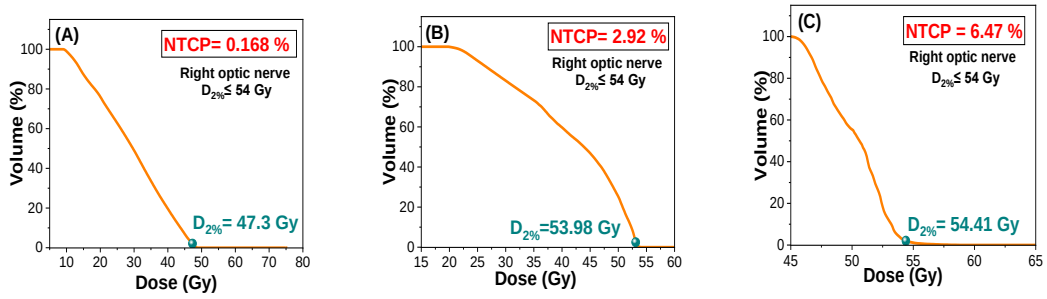

Figure III.16: The dose constraint imposed on the calculation of NTCP for the optic nerve (serial organ): **A)** the dose constraint is well respected, **B)** the dose constraint is near the limit required, and **C)** the dose constraint is beyond the limit.

- **Right and left middle ears**

Regarding acute toxicity (acute serous otitis), the D2% constraint does not have an impact on the calculated NTCP value. From the table below, it is apparent that all the values are greater than 90%. However, in cases of late toxicity (chronic serous otitis), the NTCP value is affected by the constraint D2%. For example, when the dose is well-respected (D2 = 53.06 Gy) for patient 2, the NTCP value is less than 5%. On the other hand, for patient 8, when D2% is exceeded the calculated (D2 = 56.5 Gy), the calculated NTCP is 5.91%. If the dose constraint exceeds the threshold limit (D2= 68.8 Gy), the calculated NTCP value is much higher as shown in the case of patient 1 (64.68%). The LKB model follows the dose constraint compared with the logit model.

Right middle ear	NTCP				Left middle ear	NTCP			
	LKB		Logit			LKB		Logit	
	AG	CH	AG	CH		AG	CH	AG	CH
Patient 1	99.99	64.68	99.95	49.75	**Patient 1**	99.99	75.18	99.97	62.85
Patient 2	98.67	2.91	85.28	1.08	**Patient 2**	96.60	1.144	81.19	0.87
Patient 3	99.22	4.46	88.85	1.37	**Patient 3**	99.92	16.46	96.83	3.69
Patient 4	95.25	0.76	75.13	0.67	**Patient 4**	95.95	0.93	80.02	0.828
Patient 5	97.90	1.91	81.52	0.89	**Patient 5**	99.02	3.75	83.83	1.003
Patient 6	81.94	0.07	32.46	0.16	**Patient 6**	94.42	0.61	75.82	0.69
Patient 7	94.69	0.6	69.85	0.55	**Patient 7**	92.78	0.42	59.52	0.39
Patient 8	99.47	5.91	96.04	3.12	**Patient 8**	99.98	0	93.81	2.21
Patient 9	95.52	0.82	59.85	0.39	**Patient 9**	95.04	0.72	61.33	0.41
Patient 10	99.99	66.84	99.93	41.31	**Patient 10**	99.97	26.19	99.09	9.10

Table III.11: Calculated dose constraints and NTCP for the right and left middle ears of all patients.

- **Right and left parotid glands**

The treatment plans for the parotid case were validated based on two constraints mean dose and V30 Gy. However, as shown in the table below, these two constraints exceeded the recommended thresholds for all patients. As a result, the calculated NTCP values were very high. It is important to note that the NTCP is more influenced by the mean dose than by V30 Gy. This is demonstrated by the cases of patients 3 and 5.

Right parotid	NTCP			Left parotid	NTCP		
	RS	LKB	Logit		RS	LKB	Logit
Patient 1	37.37	33.27	31.3	**Patient 1**	33.45	29.56	19.73
Patient 2	47.66	44.26	67.72	**Patient 2**	49.58	46.019	73.17
Patient 3	50.79	47.41	73.71	**Patient 3**	61.90	60.816	92.39
Patient 4	43.75	39.69	56.45	**Patient 4**	48.82	45.16	71.56
Patient 5	54.67	51.89	83.96	**Patient 5**	69.59	70.86	97.24
Patient 6	38.29	34.15	33.25	**Patient 6**	51.11	47.78	74.85
Patient 7	44.65	40.66	55.83	**Patient 7**	44.91	40.94	57.29
Patient 8	42.08	37.99	46.53	**Patient 8**	33.39	29.52	17.95
Patient 9	35.29	31.27	23.24	**Patient 9**	30.37	27.10	11.98
Patient 10	53.69	50.75	81.61	**Patient 10**	54.62	51.85	83.42

Table III.12: Calculated dose constraints and NTCP for the right and left parotids glands of all patients.

The usual dose constraints recommended in the literature are the V30 and the D_{mean}. We evaluated two cases that have no significant difference in volume received a dose of 30 Gy, 48.17% and 48.98%, of the first and second case respectively see figure

III.17 (A-B), and the associated mean dose varies between 33.50 Gy and 36.70 Gy, the calculated NTCP was 37.37% and 43.75%. In figure III.17 (C-D) the volumes received 30 Gy in the two cases were 61.5% and 55.5% (important difference) and there was a slight difference in dose mean (42.49 Gy and 41.95 Gy), the NTCP calculated with the RS model is 54.67% and 53.69%.

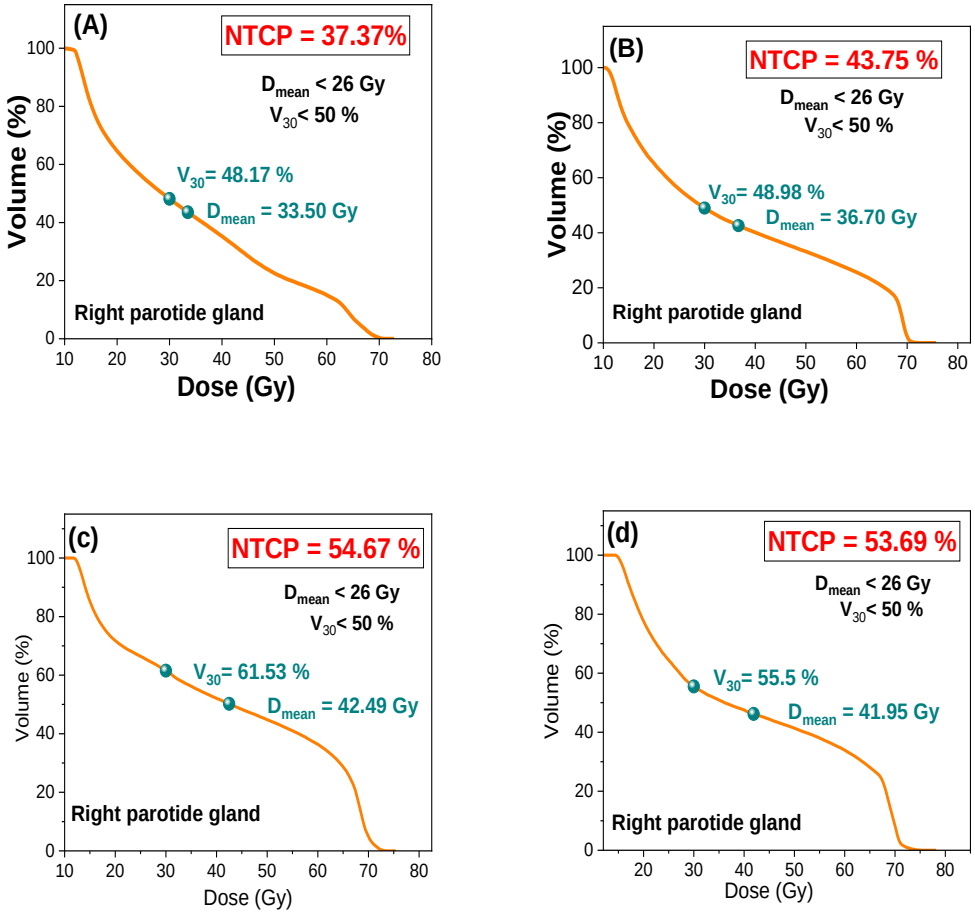

Figure III.17: The dose constraint imposed on the NTCP calculation for the parotid (parallel organ).

- **Right and left lens**

The NTCP values calculated for both the left and right lens are affected by the mean dose more than the D2%, and this is demonstrated by the results obtained in the following table. Both LKB and RS models model well the does constraints.

Right lens	NTCP	Left lens	NTCP

	RS	LKB	Logit		RS	LKB	Logit
Patient 1	0.029	0.29	0.17	**Patient 1**	0.34	0.83	0.62
Patient 2	3.36	3.41	2.70	**Patient 2**	2.67	2.9151	2.31
Patient 3	20.68	18.14	12.81	**Patient 3**	15.45	13.60	9.87
Patient 4	1.25	1.88	1.51	**Patient 4**	1.70	2.37	1.9
Patient 5	1.74	2.02	1.6	**Patient 5**	4.22	3.93	3.08
Patient 6	26.04	23.14	15.97	**Patient 6**	32.17	29.50	19.90
Patient 7	0.14	0.60	0.42	**Patient 7**	0.06	0.43	0.28
Patient 8	0.01	0.25	0.14	**Patient 8**	0.006	0.16	0.07
Patient 9	4.89	2.13	4.02	**Patient 9**	4.89	5.12	4.02
Patient 10	5.85	5.710	5.44	**Patient 10**	6.63	6.093	4.7

Table III.13: Calculated dose constraints and NTCP for the right and left lens of all patients

We chose cases with the same D2% but different Dmean as shown in figures III.21 (A-B-C) to compare the variation of calculated NTCP for Dmean and D2% with the RS model. This was done to confirm whether the reliable values of NTCP calculated would be exactly correct or just assumptions. The mean doses in these cases were 8.95 Gy, 10.17 Gy, and 12.67 Gy, while the deposited doses in 2% of the total volume were 13.2 Gy, 13.2 Gy, and 13.44 Gy. The calculated NTCP values were 4.22%, 6.63%, and 15.45%, respectively. The results show that RS follows Dmean in percentage well. However, the NTCP value increases exactly with the increase of Dmean. In the other three cases as shown in figure III.18 (D-E-F) the mean dose is fixed at the same value (8.26 Gy, 8.47 Gy, 8.95 Gy), while the dose deposited in 2% of the volume varies (9.2 Gy, 11.48 Gy, 13.2 Gy). A good correlation was observed between the calculated NTCP and the dose constraint D2%, but not with good precision as Dmean, because there was a slight difference in the mean dose and was not fixed exactly to the same number. Overall reliable NTCP value for the lens followed the dose constraints of D_{mean} and D2%, but it was slightly higher for the mean dose (in percentage) than D2%.

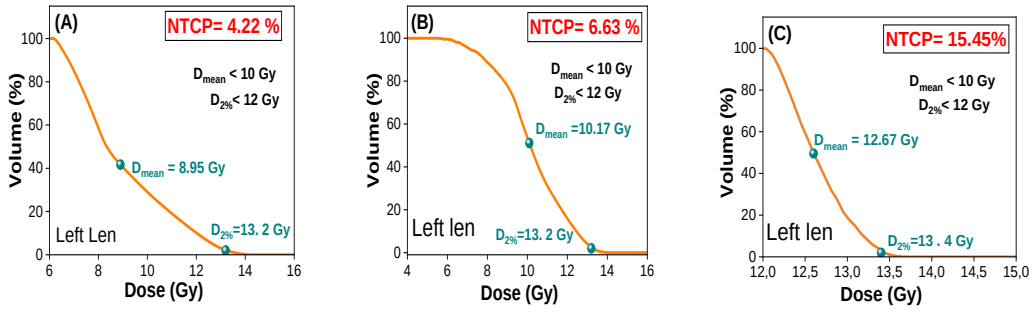

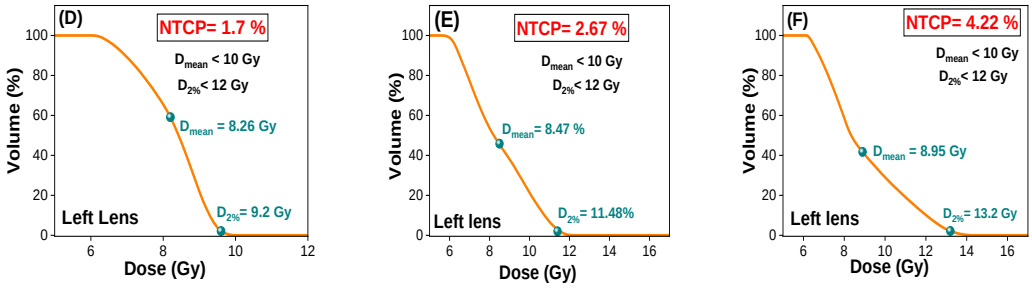

Figure III.18: The dose constraint imposed on the NTCP calculation for the lens (serial-parallel organ).

3.2.Prostate

The organs analyzed for prostate cancer are the rectum and bladder, both of which are organized in a serial-parallel architecture.

- **Rectum**

In this case, we illustrated two examples in which the dose deposited in 2% of the rectal volume is the same (71.5 Gy), and a slight difference in the dose constraints V70, with values of 14.31 Gy and 15.98 Gy. The figure III.19 (C-D) shows that there is a difference in the V60 values between the two cases. However, the difference in the calculated NTCP value is non-significant, only around ±0.02%. This difference is due to the V60 and V70 constraints. The results confirm the serial-parallel architecture of the rectum.

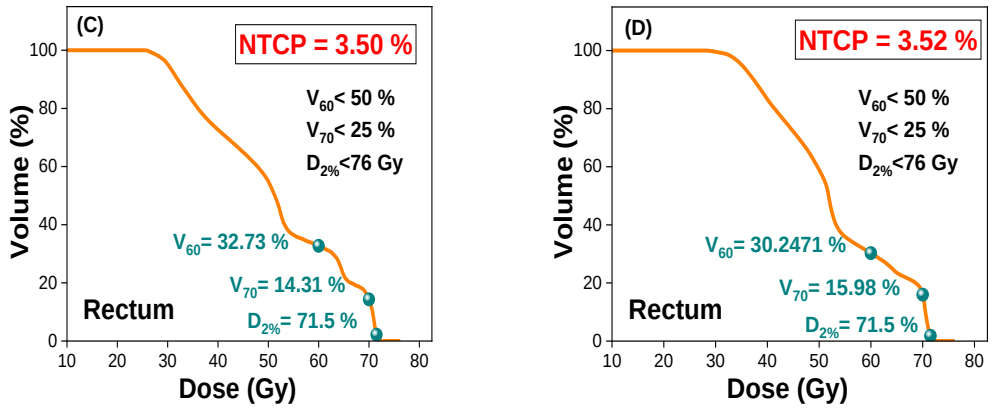

Figure III.19: The dose constraint imposed on the NTCP calculation for the rectum.

- **Bladder**

In both cases, the dose received in 2% of the total bladder volume is the same, which is 72.5 Gy. However, the values of the two constraints V60 and V70 differ, as shown in figures III.23 (A-B). Case 1 presented in figure III.20 (A) has a V60 value of 33.57 Gy and a V70 value of 23.29 Gy, while case 2 figure III.20 (B) has a V60 value of 29.94 Gy and a V70 value of 21.18 Gy. The difference in V60 and V70 values between the two patients has a minor impact on the calculated NTCP values, with a variation of only ± 0.39%.

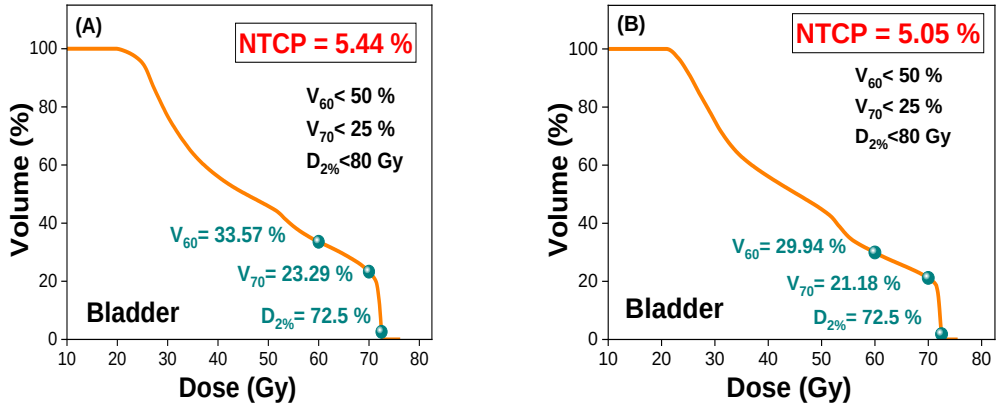

Figure III.20: The dose constraint imposed on the NTCP calculation for the bladder.

The figure III.21 shows three different patients for which the D2% dose constraint value is different. In both figures III.21 (A-B), the 70 Gy dose is deposited almost in the same bladder volume, and in both figures III.21 (A-C), the 60 Gy dose is almost set to the same number. A slight difference in the NTCP values was calculated for the slight difference in V70 Gy received by the patient, and a slight difference in the large difference of V60 Gy. Furthermore, the two constraints V70 play a very important role in the calculation of the NTCP than V60 which slightly affects the NTCP value. The finding results confirm the serial-parallel architecture of the rectum and bladder **(Zhu 2013, Zhu et al. 2016, Harsolia et al. 2007, Baradaran-Ghahfarokhi 2014)**, and do not support serial architecture **(Cahlon et al. 2008, Thor et al. 2016, Zelefsky et al. 2008)**.

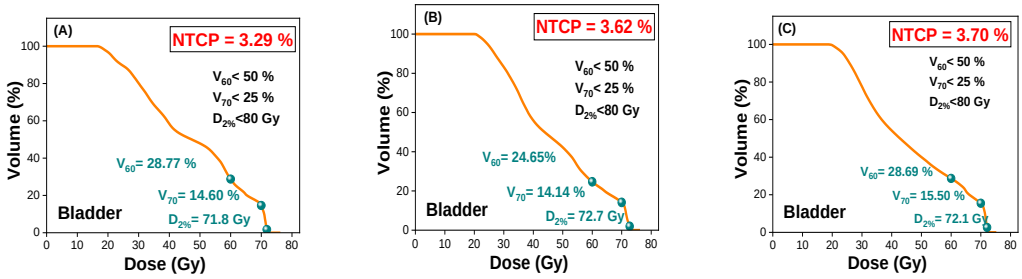

Figure III.21: A), **B)**, and **C)** The dose constraint imposed on the NTCP calculation for the bladder (serial-parallel organ) of three different cases of patients.

When the 2% dose is increased in the example cited in figure III.21 (B) (72.7 %) compared to that of figure III.21 (A) (71.8%), and the V60 and V70 are decreased the value of NTCP was 3.62%. On the other hand, this value of NTCP (3.62%) is decreased compared to that calculated in the case illustrated in figure III.21 (C) (3.70%), even the value of D2% is decreased but the values of V60 and V70 are increased. From this study, it appears that the value of the NTCP is slightly influenced by the V60 and V70 and predominantly influenced by the D2% or the maximum dose received for the organ at risk. The RS model gives reliable NTCP values for late toxicities where the NTCP values follow exactly the dose constraints, particularly at the constraint limit.

After analyzing the data, we can conclude that the constraint that has the most impact on the NTCP for organs that are organized in series is D2%, while for organs that are organized in parallel, it is the mean dose. For serial-parallel organs, both the mean dose and D2% affect the NTCP value, but the mean dose is the primary dominant in most cases.

IV. TCP and NTCP correlation to dose constraints predictions.

This part of the study aims to assess the models' capability to accurately predict various types of toxicity and the reliability of expected radiation-induced early and late complication calculations. To facilitate a more detailed analysis, we have classified the different types of toxicity according to the responses of organs at risk and their structural characteristics. The document provides clear analytical expressions of expected late complications specifically tailored to TPS_D (calculated dose from the

TPS). It includes three illustrative examples for each architectural type, ensuring comprehensive understanding and application.

1. Serial organs architecture.

Our observations show that the accuracy of the LKB model degrades considerably for small values of NTCP, as observed in some patients with both the brainstem and spinal cord examples. In contrast, the RS model reproduces the same examples with great accuracy.

The LKB and RS models provide reliable NTCP values for the two cases involving optical nerves and chiasm, making them the preferred choice for predicting toxicity outcomes. The logit model, on the other hand, does not reflect the dose constraint as accurately. Regarding middle ears, the LKB model shows a strong correlation with chronic rectal toxicity and dose constraint, thereby providing highly accurate predictive values.

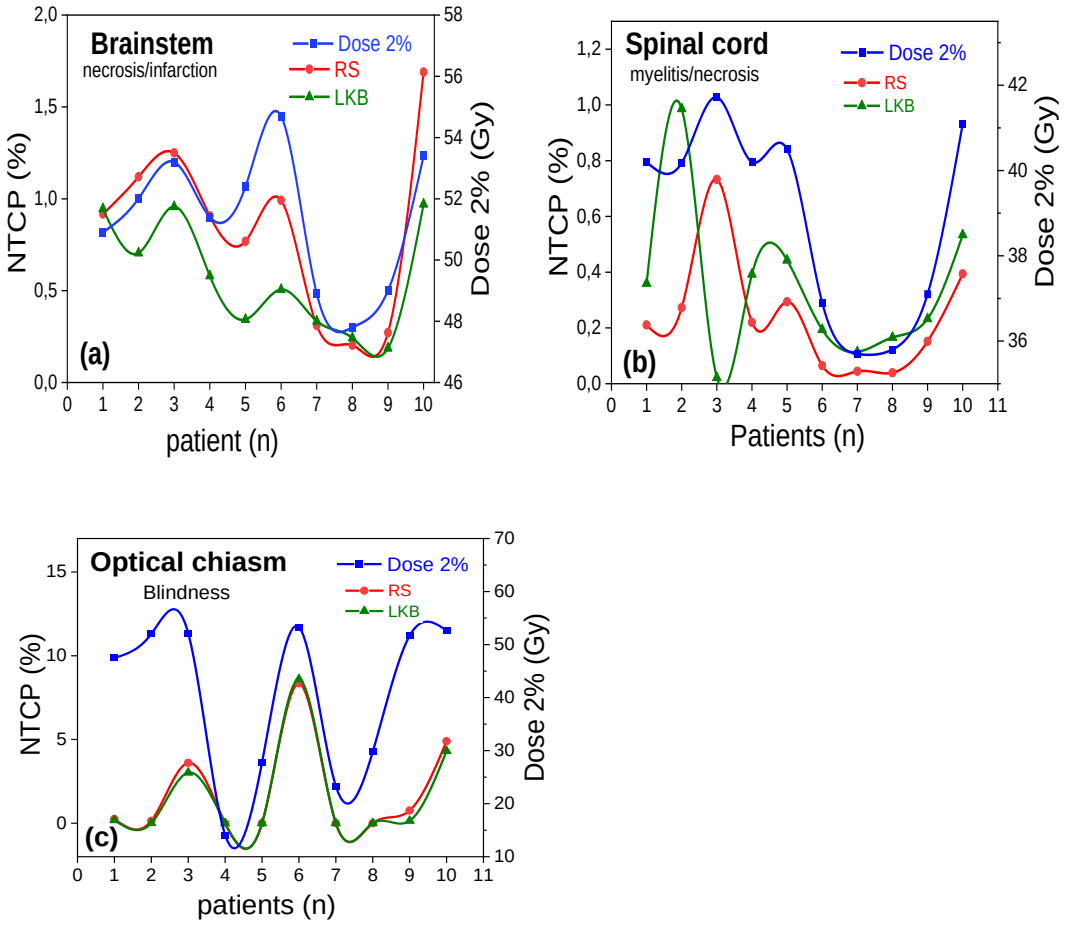

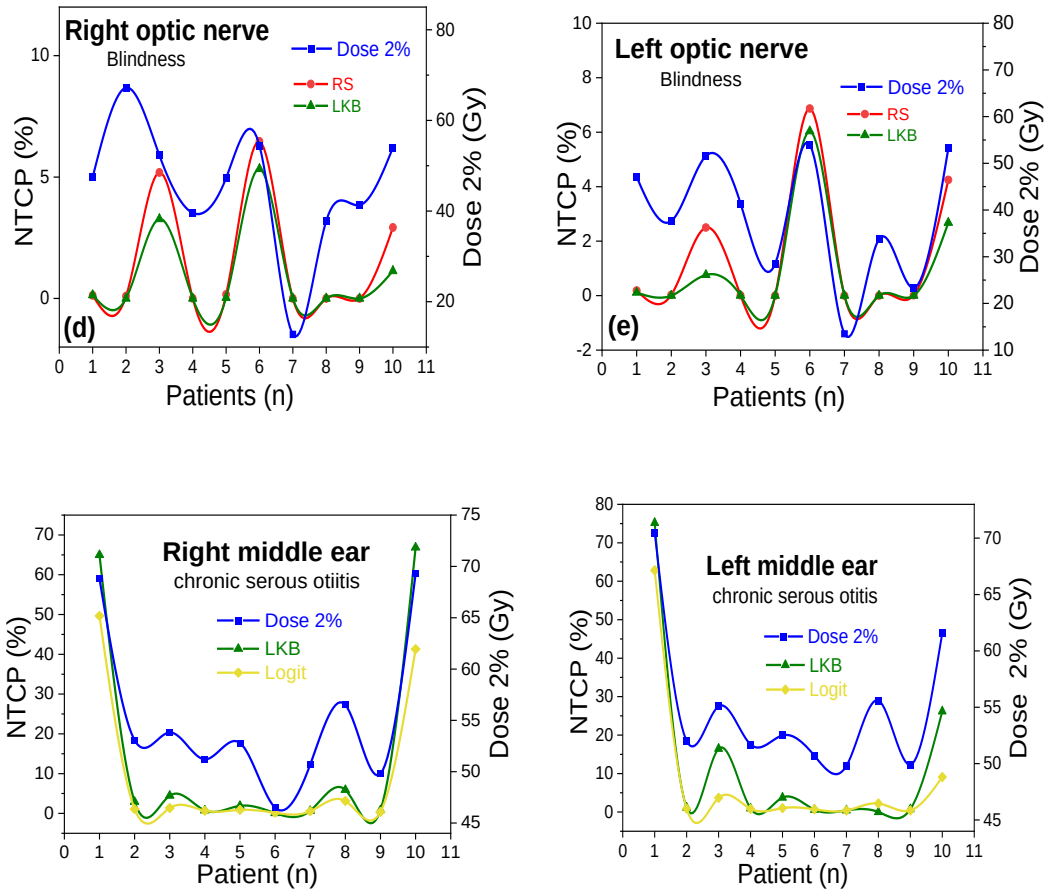

Figure III. 22: Reliable NTCP prediction and dominant dose constraints for organs organized in a serial structure.

The figure III.23 presents an analytical fitting (on a logarithmic scale) of the expected probabilities derived from the RS model of blindness for both the left and right optic nerves, correlated with the TPS_D2% values. The TPS_D2% represents the dose calculated based on the TPS within 2% of the target volume. The resulting expression for NTCP is defined as NTCP (%) = 10^{Y}, where Y is determined by the equation $Y = -2.55 - 0.046 \times TPS\_D2\% + 0.0019 \times (TPS\_D2\ \%)^2$.

This equation highlights the intricate interplay between the delivered radiation dose and the probability of developing blindness, offering critical insights for radiotherapy treatment planning.

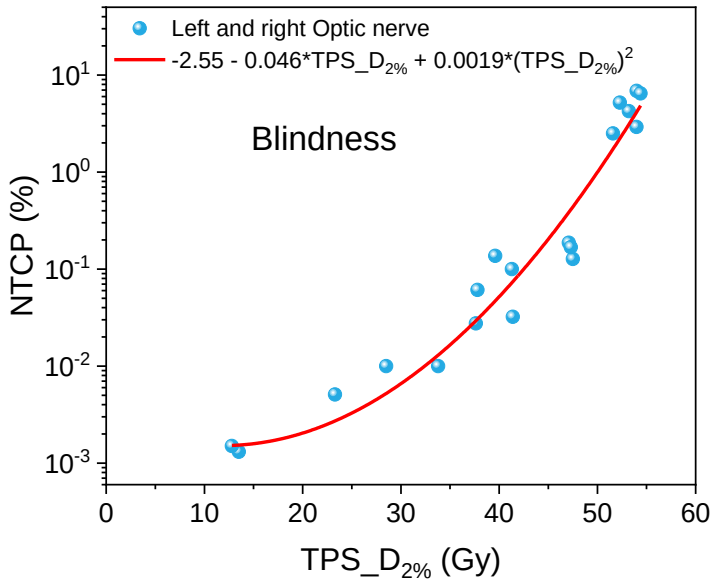

Figure III.23: Analytic fitting (log scale) of expected probabilities of blindness for left and right optic nerve.

2. Parallel organs architecture.

For parotids, the two RS and LKB models produce different results for the same endpoint, and the logit model is excluded from consideration due to a different endpoint.

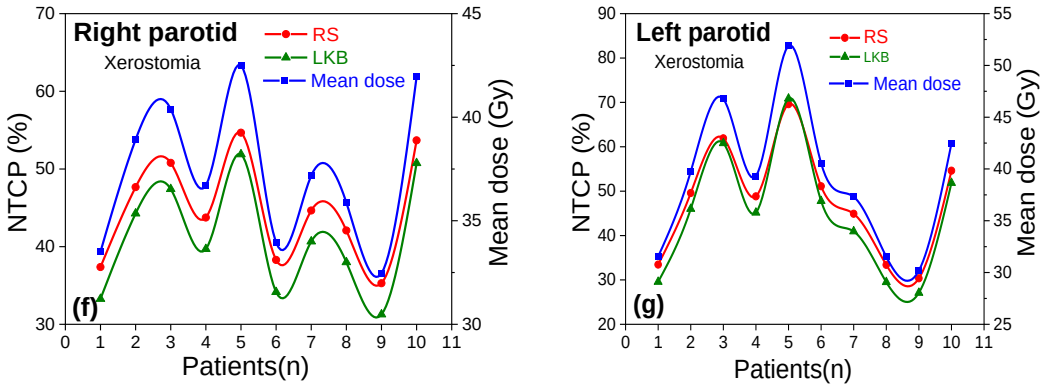

Figure III.24: Reliable NTCP prediction and dominant dose constraints for organs organized in a parallel structure.

In this analysis, we observed a notable linear relationship when plotting NTCP predictions against TPS_D_{mean} for both the left and right parotid glands (figure III.24).

The relationship is represented by the equation NTCP (%) = -23.7 + 1.8 × TPS_D_{mean}. This finding enhances the reliability of our predictions regarding the incidence of xerostomia following radiotherapy.

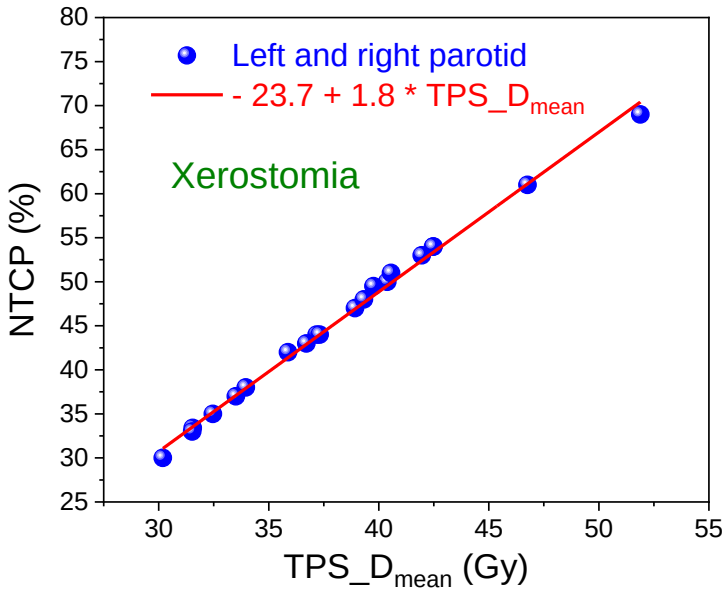

Figure III.25: Analytic fitting of expected probabilities of xerostomia for left and right parotid gland.

3. Serial-parallel organs architecture.

In the case of the lens, all three models offer acceptable predictive results in comparison with the dose constraint. However, at the constraint limit, the RS and LKB models follow the constraint more closely.

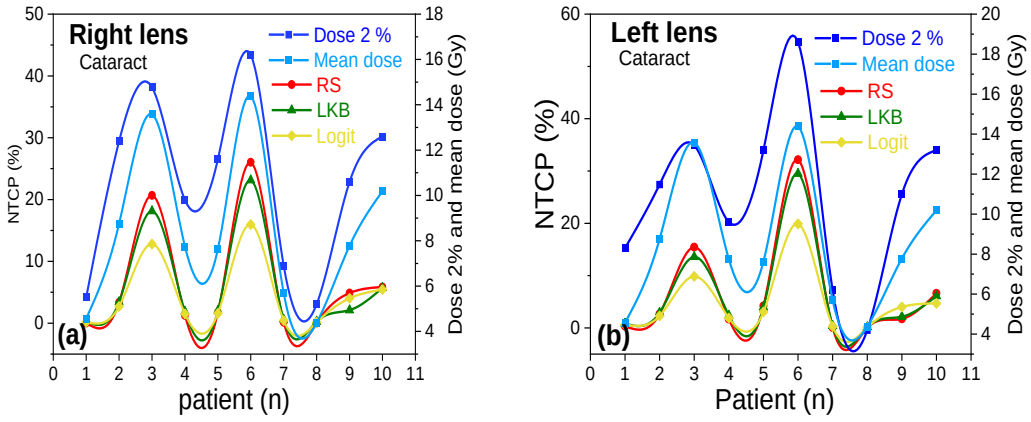

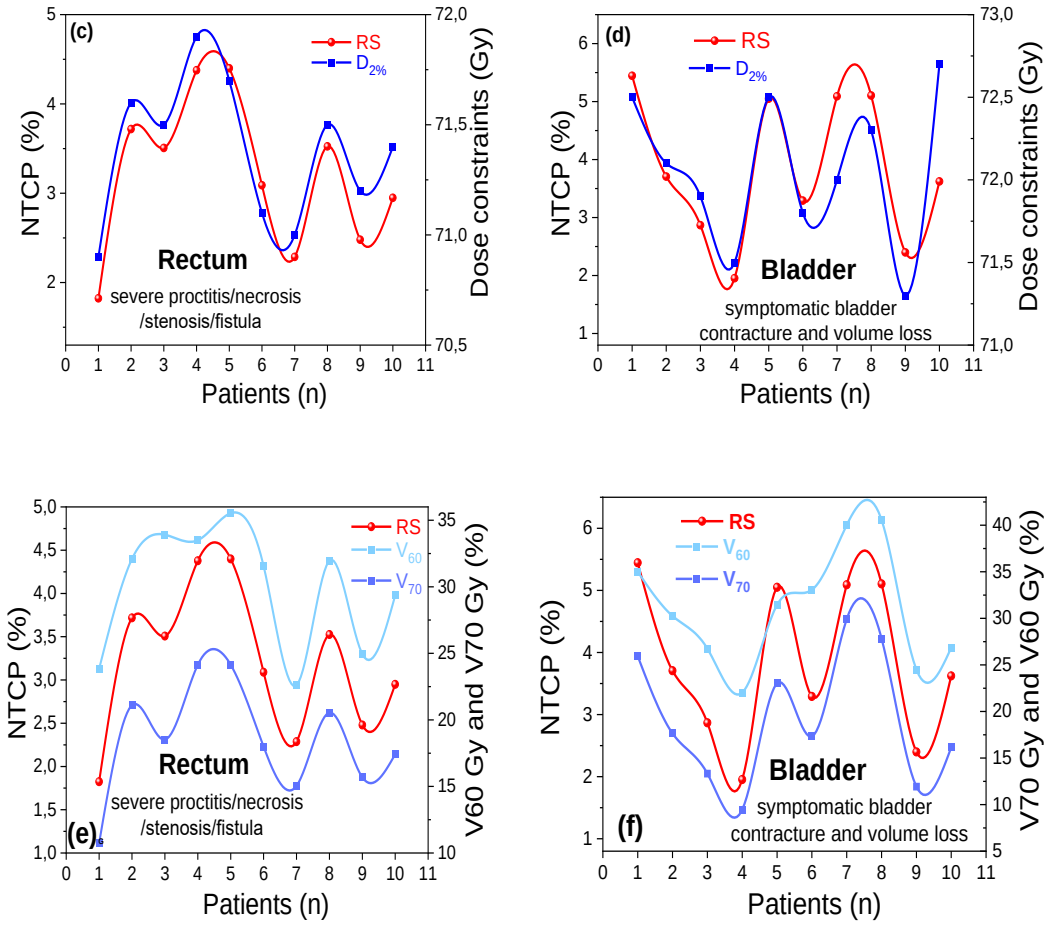

Figure III.26: Reliable NTCP prediction and dominant dose constraints for organs organized in a serial-parallel structure.

In the example of rectal and bladder, the low NTCP values suggest negligible long-term risk for the planning technique described in this work, consistent with other studies in the literature **(Shimizuguchi et al. 2017, Viani et al. 2019, Poncyljusz et al. 2016)**. Our findings indicate that low NTCP was achieved for all patients in rectal calculations, as shown in Figure III.26 (c). In contrast, for the bladder, 60% of patients had an overall NTCP of less than 5% see figure III.26 (d). the same figures show that the RS model fits well the dose constraints of D2% even for the 40 % of the patients that have NTCP > 5 % in bladder cases.

The expressions for expected probabilities of developing cataracts associated with the functioning of the left and right parotid glands, based on TPS_Dmean and TPS_D2%, are shown in Figure III.27. The area between the two curves provides the

best fit for the predicted cataract values, which can be expressed as 10Y1 < NTCP (%) < 10Y2. The equations are: Y1 = -0.018 × (TPS_D2%)² + 0.66 × TPS_D2% - 4.6 and Y2 = -0.03 × (TPS_Dmean)² + 0.9 × TPS_Dmean - 5.

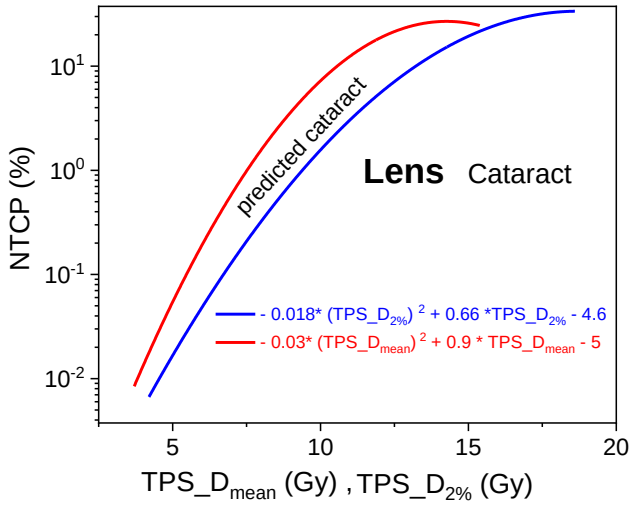

Figure III.27: Fitting expressions of expected probabilities of cataract for left and right parotid gland function of *TPS_D*$_{mean}$ (red) and *TPS_D*$_{2\%}$ (blue); The region between the two curves best fits the predicted cataract values.

It is important to note that all models possess a highly and unevenly accurate predictive capacity for chronic toxicity, especially when compared to the most critical constraints involved in the planning of treatment plans. However, at the limit or when the constraints are well respected, the two models LKB and RS are the preferred options for generating a value that can be utilized to compare different plans or to validate toxicity predictions.

The predictive performance of the LKB and RS models was very similar, suggesting that they can equally be used to estimate the probability of complication. The choice of the NTCP model does not appreciably influence the estimation of the complication incidence.

Chapter IV: Optimising the prescription dose and fractionation regimens.

I. Predicting NTCP as a function of time

After analyzing the nasopharyngeal treatment plan, we noted that the parotids are the first organs at risk of developing a major late complication for an advanced stage, due to their priority order in the planning template, which increases the difficulty of tightening the two-dose constraints V30 and mean dose. Internal ear chronic serous otitis can also occur if the D2% constraint is not respected, as in the case of patients 1 and 10.

In this section, we will focus on these 2 complications as a function of time and the possibility of functional recovery over time, to make the points underlining the treatment plan optimization using the UTCP index and dose fractionation including BED tools using the LKB and Marsden models.

a) Parotids glands

In chapter 3, we established a strong relationship between the amount of radiation delivered to the parotid glands and the incidence of toxicity. In this section, we precisely evaluated the response of the parotid function over time. We calculated the incidence of xerostomia at 3, 6, and 12 months after the end of radiotherapy. As shown in the figure IV.1, the incidence of xerostomia is very high at 3 months and gradually decreases over time. Salivary function mostly starts to recover within 1 year after radiotherapy.

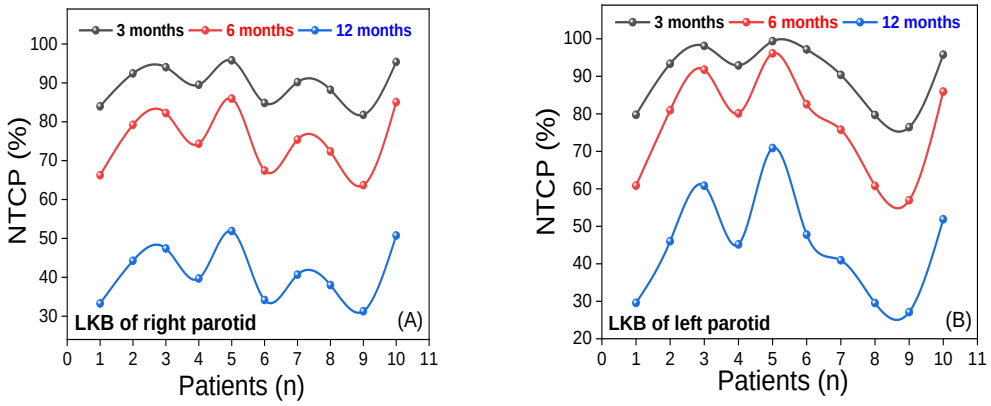

Figure IV.1: A and B) Modeling the incidence of grade 3 xerostomia complications at 3, 6, and 12 months after RT of right and left parotids glans calculated with LKB model.

We have conducted a recalculation of NTCP using the RS model. The results we obtained from these calculations were non-significant, ultimately leading us to the same conclusion as we had arrived at with the LKB model see figure IV.2.

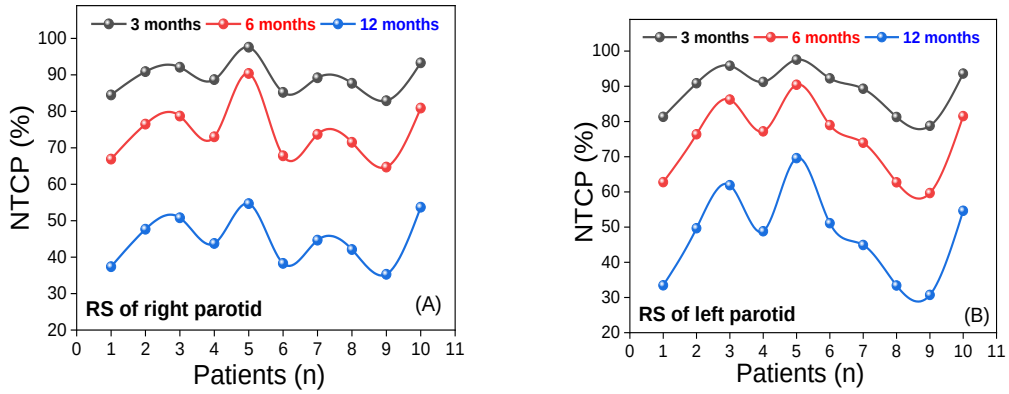

Figure IV.2: A and B) Modeling the incidence of grade 3 xerostomia complications at 3, 6, and 12 months after RT of right and left parotids glans calculated with RS model.

b) Middle ears

Acute toxicity typically occurs within the first three months of starting radiotherapy, whereas chronic toxicity can occur beyond three months after radiotherapy has ended. The relationship between acute toxicity and compliance with the constrained dose is less important. However, in cases where D2% is well respected, the acute toxicity value is very high (> 90%). In contrast, the relationship between constraint and late toxicity is substantial. Based on the figure IV.3, it is evident that as long as the D2% constrained dose is respected, the late complication is less than 5%. However, if the limited threshold for this constraint is exceeded (≥ 54%), then the delayed complication exceeds 5%, as illustrated in the cases of patients 1 and 10.

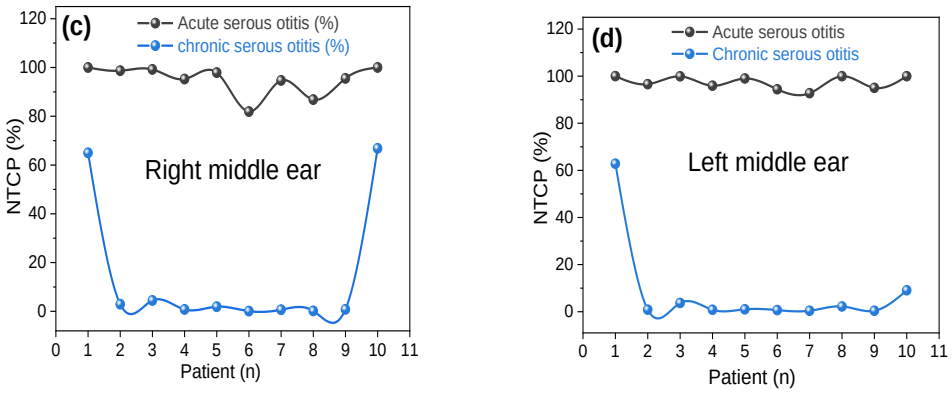

Figure IV.3: (a, b) The incidence of serous otitis toxicity over time.

In the same figure, we can conclude that the serous otitis complication has decreased over time. This implies that time is a very important factor in the appearance of the complication.

II. UTCP calculation

The time criterion employed in assessing the two toxicities has significantly impacted the selection of potential toxicities that may affect the optimization quality. It provides a reliable foundation to ensure better optimization of treatment plans for this particular cancer case. In this section, we analyzed the plan treatments using the UTCP index over time.

1. Calculation method and results

1.1.Method

The method described to calculate the UTCP of each treatment plan is based on the calculation of the two quantities P(I) and P(B) cited below:

$$P(B) = TCP = \frac{TCP}{100} \quad \text{.....(32)}$$

$$P(I) = 1 - NTCP = \frac{100 - NTCP}{100} \quad \text{.....(33)}$$

$$UTCP = [P(I) * P(B)] \quad \text{.....(34)}$$

In situations where an organ at risk is exposed to multiple toxicities or when we assess multiple organs at risk in a single treatment plan, we conduct the calculation of P(I) and other related parameters as shown below:

$$P(I) = \left[\left(1 - NTCP_{Toxicity1}^{OAR1}\right)\left(1 - NTCP_{Toxicity2}^{OAR2}\right) \dots \left(1 - NTCP_{Toxicityn}^{OARn}\right)\right] \quad (35)$$

$$UTCP = [P(I)^1 * P(I)^2 * P(I)^n * P(B)] \quad (36)$$

1.2. Nasopharyngeal results

Initially, we assessed the UTCP value using the TCP value of the PTV and the NTCP of all organs at risk, excluding the middle ears and parotids (left and right). However, as these two organs are essential in evaluating treatment plans for all patients, we have deemed it necessary to incorporate their assessment in our evaluations over time. To ensure a detailed study of treatment plans. Secondly, to show that we can make an evolution and a prediction of toxicities over time i.e. we can follow the toxicities during each period after the treatment.

Table IV.1 shows the UTCP values of all patients without taking into account the parotids and middle ears. The calculated UTCP values are greater than 50% except for patient 6, due to the increased NTCP values of both lenses.

	P(B) PTV_{70}	P(I) BS	P(I) SC	P(I) OC	P(I) RON	P(I) LON	P(I) RP	P(I) LP	UTCP
Patient 1	0.977	0.990	0.996	0.998	0.998	0.998	0.997	0.991	94.60
Patient 2	0.994	0.992	0.990	1	1	1	0.965	0.970	91.37
Patient 3	0.889	0.990	0.999	0.969	0.967	0.992	0.818	0.864	57.75
Patient 4	0.973	0.994	0.996	1	1	1	0.981	0.976	92.22
Patient 5	0.90	0.996	0.995	1	1	1	0.979	0.960	83.82
Patient 6	0.865	0.994	0.998	0.914	0.946	0.939	0.768	0.705	37.71
Patient 7	0.96	0.996	0.998	1	1	1	0.993	0.995	94.27
Patient 8	0.964	0.997	0.998	1	1	1	0.997	0.998	97.75
Patient 9	0.982	0.998	0.997	0.998	1	1	0.978	0.978	92.63
Patient 10	0.889	0.990	0.994	0.956	0.988	0.973	0.942	0.939	71.01

Table IV.1: Calculated UTCP values for all planes excluding parotids and middle ears.

Subsequently, we incorporated the parotid glands into our assessment of UTCP, specifically calculating the probability of xerostomia (dry mouth) occurring 6 months after radiotherapy. Adding the parotid glands led to a significant reduction in the UTCP

values (Table IV.2). This clearly resulted from a substantial increase in the NTCP values of the parotid glands during this period.

Patients	P(B) PTV_{70}	P(I) BS	P(I) SC	P(I) OC	P(I) RON	P(I) LON	P(I) RP	P(I) LP	P(I) RL	P(I) LL	UTCP
Patient 1	0.977	0.990	0.996	0.998	0.998	0.998	0.338	0.392	0.997	0.991	12.3
Patient 2	0.994	0.992	0.990	1	1	1	0.208	0.197	0.965	0.970	3.75
Patient 3	0.889	0.990	0.999	0.969	0.967	0.992	0.178	0.082	0.818	0.864	0.84
Patient 4	0.973	0.994	0.996	1	1	1	0.257	0.199	0.981	0.976	4.71
Patient 5	0.90	0.996	0.995	1	1	1	0.141	0.038	0.979	0.960	0.49
Patient 6	0.865	0.994	0.998	0.914	0.946	0.939	0.326	0.174	0.768	0.705	2.13
Patient 7	0.96	0.996	0.998	1	1	1	0.246	0.242	0.993	0.995	5.61
Patient 8	0.964	0.997	0.998	1	1	1	0.277	0.392	0.997	0.998	10.36
Patient 9	0.982	0.998	0.997	0.998	1	1	0.363	0.431	0.978	0.978	14.59
Patient 10	0.889	0.990	0.994	0.956	0.988	0.973	0.149	0.141	0.942	0.939	1.49

Table IV.2: Calculated UTCP values for all planes excluding middle ears at 6 months after radiotherapy.

In Table IV.3, we have modified the endpoint for the parotid gland and recalculated the UTCP values of the radiotherapy plans for all patients, using the parameters associated with xerostomia 12 months after completing radiotherapy. We observed an increase in the UTCP value, which is attributed to a reduction in the NTCP values of the parotid glands at the 12-month. This implies that the parotid glands continue to recover over time.

Patients	P(B) PTV_{70}	P(I) BS	P(I) SC	P(I) OC	P(I) RON	P(I) LON	P(I) RP	P(I) LP	P(I) RL	P(I) LL	UTCP
Patient 1	0.977	0.990	0.996	0.998	0.998	0.998	0.668	0.704	0.997	0.991	44.47
Patient 2	0.994	0.992	0.990	1	1	1	0.55	0.244	0.965	0.970	12.26
Patient 3	0.889	0.990	0.999	0.969	0.967	0.992	0.527	0.391	0.818	0.864	11.90
Patient 4	0.973	0.994	0.996	1	1	1	0.603	0.548	0.981	0.976	30.47
Patient 5	0.90	0.996	0.995	1	1	1	0.481	0.291	0.979	0.960	11.73
Patient 6	0.865	0.994	0.998	0.914	0.946	0.939	0.658	0.522	0.768	0.705	12.96
Patient 7	0.96	0.996	0.998	1	1	1	0.593	0.590	0.993	0.995	32.98

Patient 8	0.964	0.997	0.998	1	1	1	0.620	0.704	0.997	0.998	41.65
Patient 9	0.982	0.998	0.997	0.998	1	1	0.687	0.729	0.978	0.978	46.71
Patient 10	0.889	0.990	0.994	0.956	0.988	0.973	0.492	0.481	0.942	0.939	16.82

Table IV.3: Calculated UTCP values for all planes excluding middle ears at 12 months after radiotherapy.

The results obtained when the middle ears were included in the UTCP calculation at 6 and 12 moths after radiotherapy are presented in tables IV.4 and IV.5, respectively.

Patients	P(B) PTV_{70}	P(I) BS	P(I) SC	P(I) OC	P(I) RON	P(I) LON	P(I) RME	P(I) LME	P(I) RP	P(I) LP	P(I) RL	P(I) LL	UTCP
Patient 1	0.97	0.99	0.99	0.99	0.99	0.99	0.35	0.24	0.33	0.39	0.99	0.99	1.06
Patient 2	0.99	0.99	0.99	1	1	1	0.97	0.98	0.20	0.19	0.96	0.97	3.59
Patient 3	0.88	0.99	0.99	0.96	0.96	0.99	0.95	0.83	0.17	0.08	0.81	0.86	0.67
Patient 4	0.97	0.99	0.99	1	1	1	0.99	0.99	0.25	0.19	0.98	0.97	4.62
Patient 5	0.90	0.99	0.99	1	1	1	0.98	0.96	0.14	0.03	0.97	0.96	0.46
Patient 6	0.86	0.99	0.99	0.91	0.94	0.93	0.99	0.99	0.32	0.17	0.76	0.70	2.11
Patient 7	0.96	0.99	0.99	1	1	1	0.99	0.99	0.24	0.24	0.99	0.99	5.54
Patient 8	0.96	0.99	0.99	1	1	1	0.99	1	0.27	0.39	0.99	0.99	10.34
Patient 9	0.98	0.99	0.99	0.99	1	1	0.99	0.99	0.36	0.43	0.97	0.97	14.35
Patient 10	0.88	0.99	0.99	0.95	0.98	0.97	0.33	0.73	0.14	0.14	0.94	0.93	0.36

Table IV.4: Calculated UTCP values for all planes including middle ears at 6 months after radiotherapy.

Patients	P(B) PTV_{70}	P(I) BS	P(I) SC	P(I) OC	P(I) RON	P(I) LON	P(I) RME	P(I) LME	P(I) RP	P(I) LP	P(I) RL	P(I) LL	UTCP
Patient 1	0.97	0.99	0.99	0.99	0.99	0.99	0.35	0.24	0.66	0.70	0.99	0.99	3.86
Patient 2	0.99	0.99	0.99	1	1	1	0.97	0.98	0.55	0.24	0.96	0.97	11.75
Patient 3	0.88	0.99	0.99	0.96	0.96	0.99	0.95	0.83	0.52	0.39	0.81	0.86	9.49
Patient 4	0.97	0.99	0.99	1	1	1	0.99	0.99	0.60	0.54	0.98	0.97	29.95
Patient 5	0.90	0.99	0.99	1	1	1	0.98	0.96	0.48	0.29	0.97	0.96	11.07
Patient 6	0.86	0.99	0.99	0.91	0.94	0.93	0.99	0.99	0.65	0.52	0.76	0.70	12.86
Patient 7	0.96	0.99	0.99	1	1	1	0.99	0.99	0.59	0.59	0.99	0.99	32.62
Patient 8	0.96	0.99	0.99	1	1	1	0.99	1	0.62	0.70	0.99	0.99	41.58

Patient 9	0.98	0.99	0.99	0.99	1	1	0.99	0.99	0.68	0.72	0.97	0.97	45.95
Patient 10	0.88	0.99	0.99	0.95	0.98	0.97	0.33	0.73	0.49	0.48	0.94	0.93	4.12

Table IV.5: Calculated UTCP values for all planes including middle ears at 12 months after radiotherapy.

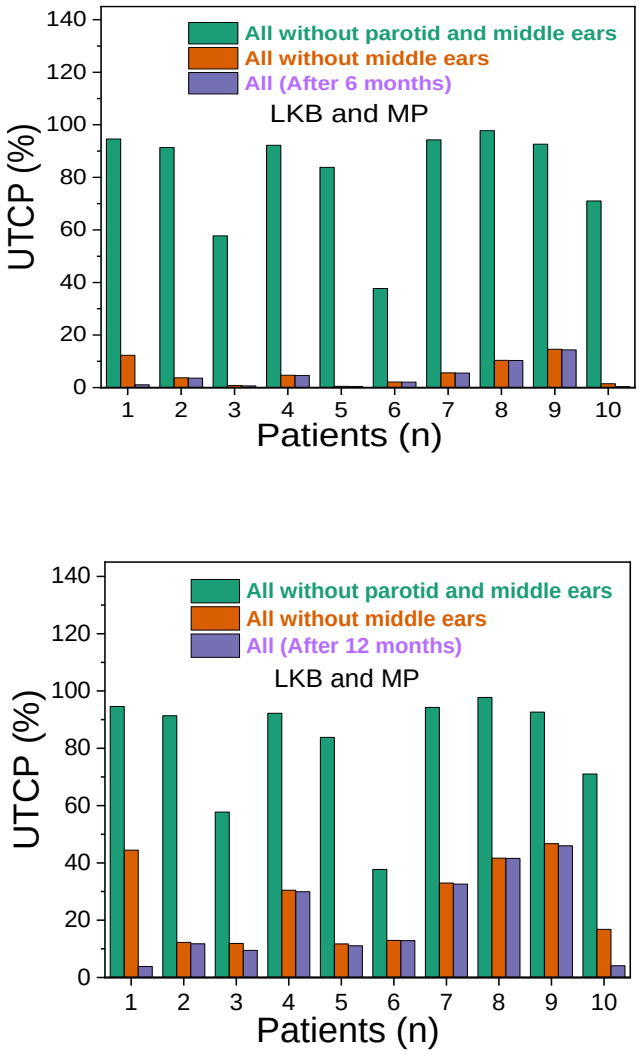

Figure IV.4: UTCP evaluation of the treatment plans at (a) 6 and (b) 12 months after radiotherapy.

No significant difference was observed in the UTCP values calculated (figure IV.4) for all patients, except for patients 1, 3, and 10. This was due to the very low NTCP value calculated for serous chronic otitis, which was less than 4%. However, the NTCP value for patients 1, 3, and 10 was very high, more than 5%. This was because the dose constraints were not respected due to the large tumor size. As a result, UTCP values have decreased significantly.

It is important to emphasize that, when the dose constraint is thoroughly met in the middle ears, the parotid gland becomes the most critical organ in validating treatment plans.

1.3. Prostate results

The evaluation of radiotherapeutic plans in prostate cancer with the UTCP index was based on a set of late and acute toxicities in the rectum and bladder described in table IV.6 using the LKB model and the Marsden model.

Models	OAR	Type de toxicité	Grade	Classification scale	Folow up
LKB	Rectum	Late rectal toxicity P_r (1) **(Jensen et al. 2011, Brenner 2004)**	Grade ≥ 2	RTOG	3-4 years
		Mild RTOG rectal toxicity P_r (2) **(Lu et al. 1995)**	Grade 2/3	RTOG	21 months
	Bladder	Acute genitourinary P_b (1) **(Dai et al. 2020)**	Grade 2	RTOG	/
		Late bladder toxicity P_b (2) **(Zhu et al. 2016)**	≥ grade 2	LENT/ SOMA	5 years
Marsden	PTV_{76}	Tumor control P(B) **(Walsh et al. 2016)**			5 years

Table IV.6: The included endpoints in the UTCP calculation of prostate treatment plans.

As part of the evaluation process, we have computed the NTCP values for each organ at risk including late and acute toxicities, and the TCP value of the PTV76 Gy, as mentioned in table IV.7. The selection of the late rectal toxicity P_r (1) and Mild rectal toxicity RTOG P_r (2) for the LKB model used in calculating UTCP was achieved through extensive research into the definition of toxicities.

OAR	PTV76 TCP	Rectum NTCP		Bladder NTCP	
Patients	Tumor control	Late rectal toxicity	Mild RTOG rectal toxicity	Acute genitourinary	Late bladder toxicity
Patient 1	99.89	1.439	7.276	23.530	5.263
Patient 2	99.93	1.763	1.432	19.255	4.893
Patient 3	99.90	2.3011	6.3356	28.877	9.604
Patient 4	99.94	4.924	29.149	22.958	6.718
Patient 5	99.91	0.941	1.158	30.0683	10.3284
Patient 6	99.77	1.726	8.786	33.419	11.651
Patient 7	99.93	3.105	6.712	22.422	6.458
Patient 8	99.89	0	0	21.942	5.161
Patient 9	99.91	4.112	20.758	32.310	12.538
Patient 10	99.88	2.166	4.168	22.903	7.152
Patient 11	99.92	5.619	44.880	31.023	11.380
Patient 12	99.92	1.599	1.566	18.528	4.760

Table IV.7: TCP and NTCP values calculated for all the endpoints.

The same table indicates that the NTCP values for late rectal toxicity are either equal to or less than 5 for all patients, which is expected at this stage of cancer as this complication can be severe. However, for mild rectal RTOG toxicity, the calculated NTCP values are higher. If we look at the definition of toxicity, we can see that grade 3 of mild RTOG rectal toxicity is similar to grade 2 of late rectal toxicity. This suggests that the latter is slightly less severe, which justifies the increased probability of complication in the second toxicity (as indicated by the increased values). NTCP values are increased in acute genitourinary toxicity (maximum 6 months after radiotherapy) even if here the probability of complication is generally accepted because grade 2 of any toxicity is clinically accepted. For TCP, good expected tumor control was achieved.

To calculate the UTCP, we adopted a method that involved taking into account one of the two late rectal toxicities along with the late bladder toxicity. This was followed by integrating the acute bladder toxicity in the two previous calculations. Our approach involved carefully analyzing the late toxicities of both the rectum and bladder and factoring them into our calculations. We also ensured that the acute bladder toxicity

was incorporated in a way that was consistent with our methodology. The resulting UTCP value is presented in tables IV.8 and IV.9.

Patients	Marsden	LKB			
	PTV_{76}	Rectum		Bladder	
	P (B)	P_r (1)	P_r(2)	P_b(1)	P_b(2)
Patient 1	0.9989	0.98561	0.92724	0.7647	0.94737
Patient 2	0.9993	0.98237	0.98568	0.80745	0.95107
Patient 3	0.9990	0.97699	0.93664	0.71123	0.90396
Patient 4	0.9994	0.95076	0.70851	0.77042	0.93282
Patient 5	0.9991	0.99059	0.98842	0.69932	0.89672
Patient 6	0.9977	0.98274	0.91214	0.66581	0.88349
Patient 7	0.9993	0.96895	0.93288	0.77578	0.93542
Patient 8	0.9989	1	1	0.78058	0.94839
Patient 9	0.9991	0.95888	0.79242	0.6769	0.87462
Patient 10	0.9988	0.97834	0.95832	0.77097	0.92848
Patient 11	0.9992	0.94381	0.5512	0.68977	0.8862
Patient 12	0.9992	0.98401	0.98434	0.81472	0.9524

Table IV.8: P(B) and P(I) quantities for PTV 76 and organs at risk for all patients.

Index	UTCP (%)			
Patients	**Late (1)**	**Acute (1)**	**Late (2)**	**Acute (2)**
Patient 1	93.27	71.32	87.74	67.10
Patient 2	93.36	75.38	93.67	75.64
Patient 3	88.20	62.73	84.58	60.15
Patient 4	88.63	68.28	66.05	50.88
Patient 5	88.74	62.06	88.55	61.92
Patient 6	87.03	57.95	80.40	53.53
Patient 7	90.57	70.26	87.20	67.64
Patient 8	94.73	73.94	94.73	73.94
Patient 9	83.79	56.71	69.24	46.87
Patient 10	90.72	69.94	88.96	68.58
Patient 11	83.57	57.64	48.80	33.66
Patient 12	93.64	76.29	93.67	76.31

Table IV.9: Calculated UTCP values for all treatment plans.

In Figure IV.5 (a), the calculation of UTCP has been carried out based on late rectal and bladder toxicity grade ≥ 2 for the rectum and bladder, respectively. Furthermore, acute genitourinary grade 2 for the bladder has also been included. In

Figure IV.5 (b), we replaced the late rectal toxicity of the rectum with the mild RTOG rectal toxicity.

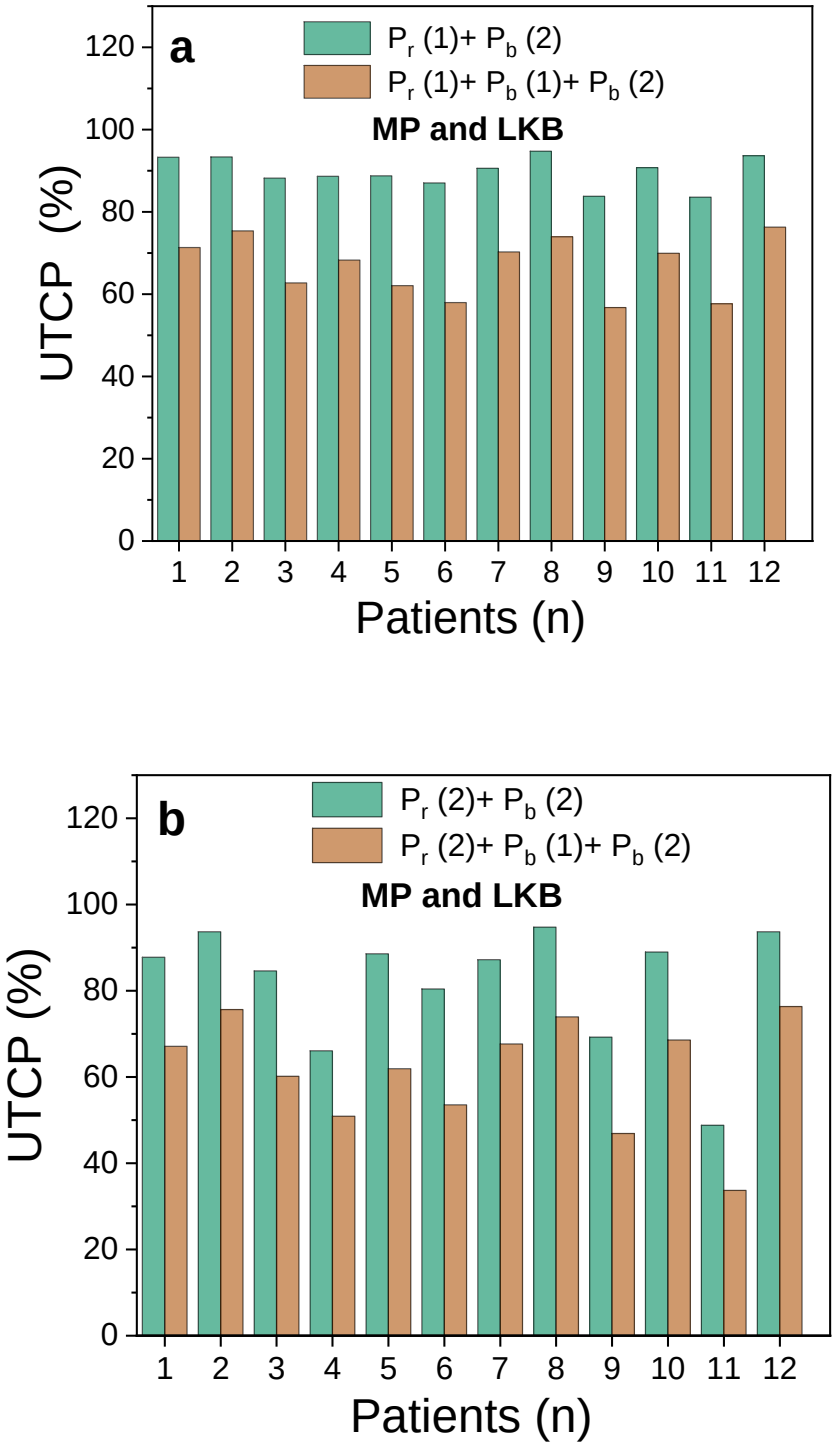

Figure IV.5: Calculated UTCP by considering: a) rectal toxicity grade ≥ 2 and b) Mild RTOG rectal toxicity.

As per the analysis of Figure IV.5 (a), it is apparent that the UTCP values calculated without considering the acute genitourinary toxicity are relatively high. This is primarily because the NTCP values calculated for late rectal and bladder toxicities are low. However, the UTCP values decreased significantly after incorporating the high NTCP values calculated for acute genitourinary toxicity. The acute genitourinary toxicity directly impacts UTCP, influencing calculated values.

Figure IV.5 (b) shows that the UTCP values have decreased. It's important to note that the two toxicities have different definitions. However, the second toxicity (Mild RTOG grade 2/3) excludes necrosis, fistula, and perforation. This decrease in toxicity grade has an impact on the NTCP calculated for all patients. Additionally, this decrease has an impact on the UTCP calculated taking into account the acute genitourinary toxicity.

III. Improvement using UTCP

The UTCP values assessed for each patient treated for nasopharyngeal cancer showed significant variability, although individuals were classified at the same advanced stage. In this part we conducted a comprehensive exploration of strategies aimed at personalizing and optimizing treatment plans. From a radiobiological standpoint, we have proposed a solution aimed at reducing toxicities and enhancing treatment quality, particularly for patients with a calculated UTCP of less than 50%.

We suggested prioritizing the TPS template order of the parotid and middle ears. Reducing the dose to the parotids can reduce the prevalence and severity of xerostomia while maintaining the same or even improved efficacy for the brainstem, spinal cord, optical chiasm, and optical nerves see Figure IV.6. As a numerical example, we have redone the planning of patient 10 according to our proposal which makes us gain 4.85% in the value of UTCP. This solution allowed us to increase the expected benefit of treatment. Whereas the probability of complication decreased by 17.77 % for parotids, Additionally, in the middle ears the late effect probability decreased by 21.36 % for the middle ear. On the other hand, we noticed an increase in the complication probability of the lens by 12.13%.

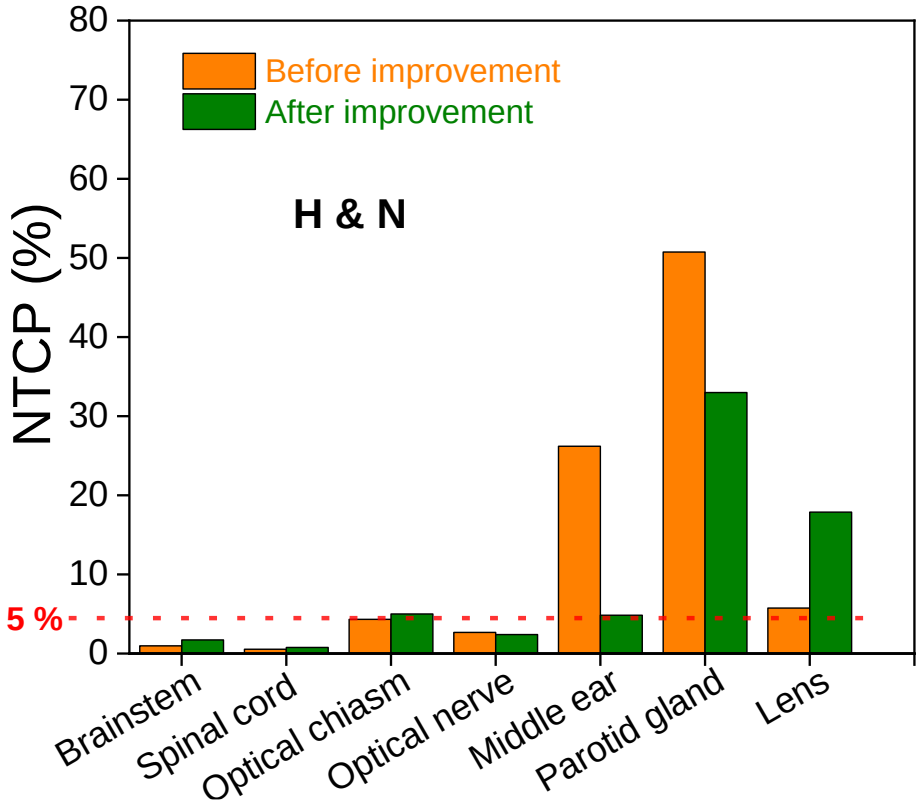

Figure IV.6: Improving treatment plans by increasing the TPS template order of parotid and middle ears.

IV. Improvement using Dose fractionation including BED

1. Improving the nasopharyngeal treatment plan.

In this part of our work, we implemented a method for optimizing and individualizing radiotherapy treatments. However, Fowler **(2006)** was the first to introduce the idea of optimization plans using the biologically effective dose tool, the important factor was the relative increase in tumor BED versus acute mucosal BED with increasing fraction and total time. After that, Uzan et al. **(2012)** gave an overview of dose optimization in radiation therapy planning based on radiobiological models. Additionally, they introduced different levels of dose optimization.

In our study, we implemented these two optimization concepts based on dose fractionation using BED for patient 9 using the Radbio-For program. The results are presented in plots (TCP vs. NTCP curves) as a function of the number see figure IV.7.

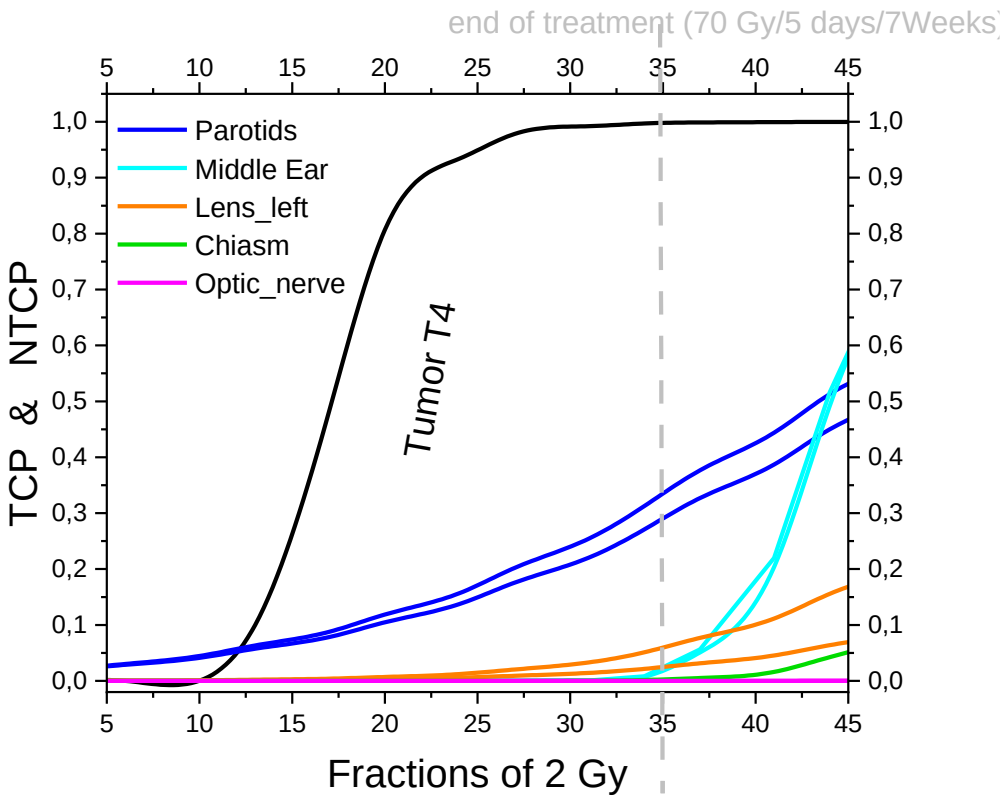

Figure IV.7: Plotted TCP and NTCP of UCNT tumor and organs at risk of patient 9 using the presented program Radbio-For in function of fraction number.

In examining the treatment duration until its completion, it is noted that the NTCP values for all organs tend to approach 0%. Nonetheless, an increase in these values is observed as the number of treatment sessions rises. This situation contrasts with the findings related to patient 10, as illustrated in figure IV.8, where the NTCP values of the parotid glands and ears are increased, nearing 100% at the end of the treatment. This significant increase complicates the improvement and optimization of the treatment plan because of its potential impact on tumor control outcomes.

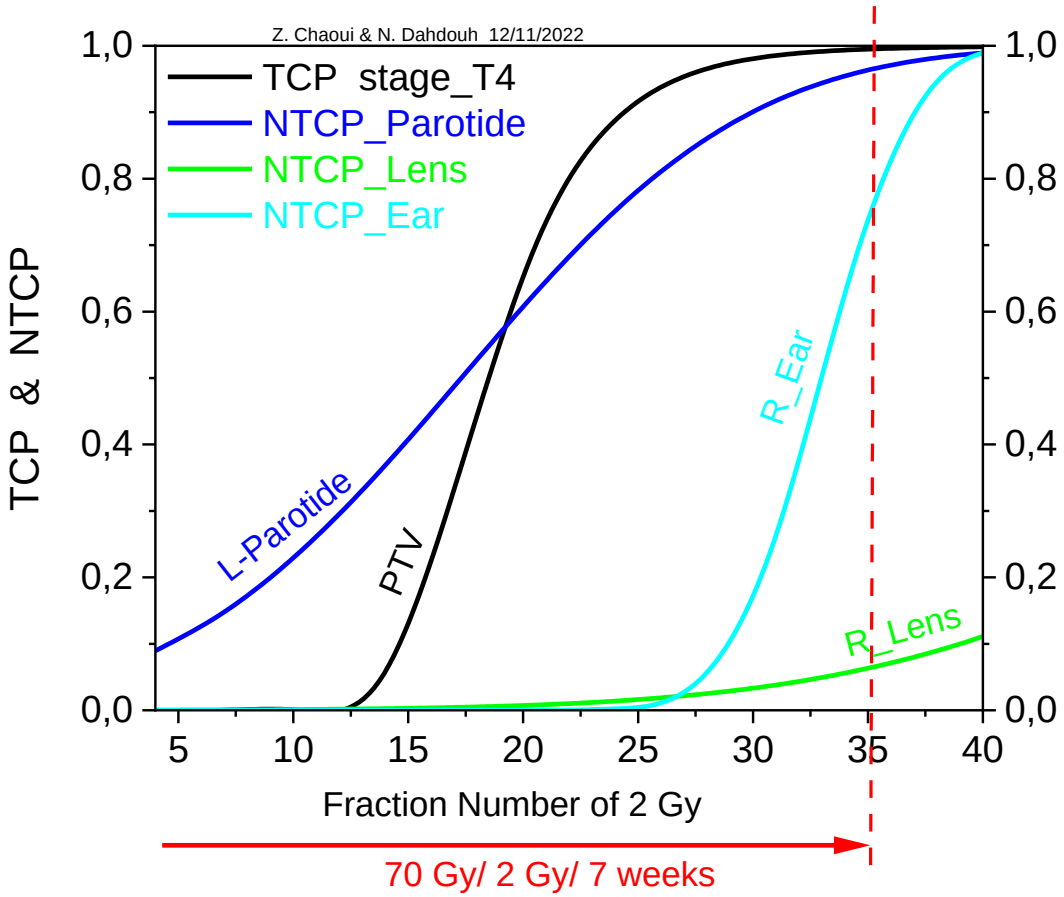

Figure IV.8: Plotted TCP and NTCP of left parotide, right ear and lens of patient 10 using the presented program Radbio-For in function of fraction number.

In Figure IV.9, we have concentrated on the organs that exhibit increased NTCP levels, specifically the parotid gland and the middle ear. Our observations indicate that tumor control reaches its optimal level of 100% after the 28th session, which aligns with the radiobiological objective of radiotherapy. Thus, we have the option to conclude treatment at this point while maintaining low NTCP levels, thereby ensuring the well-being of these two organs at risk. However, we recommend confirming the absence of recurrence or secondary cancers post-treatment and verifying that the dose administered

to the tumor is adequate

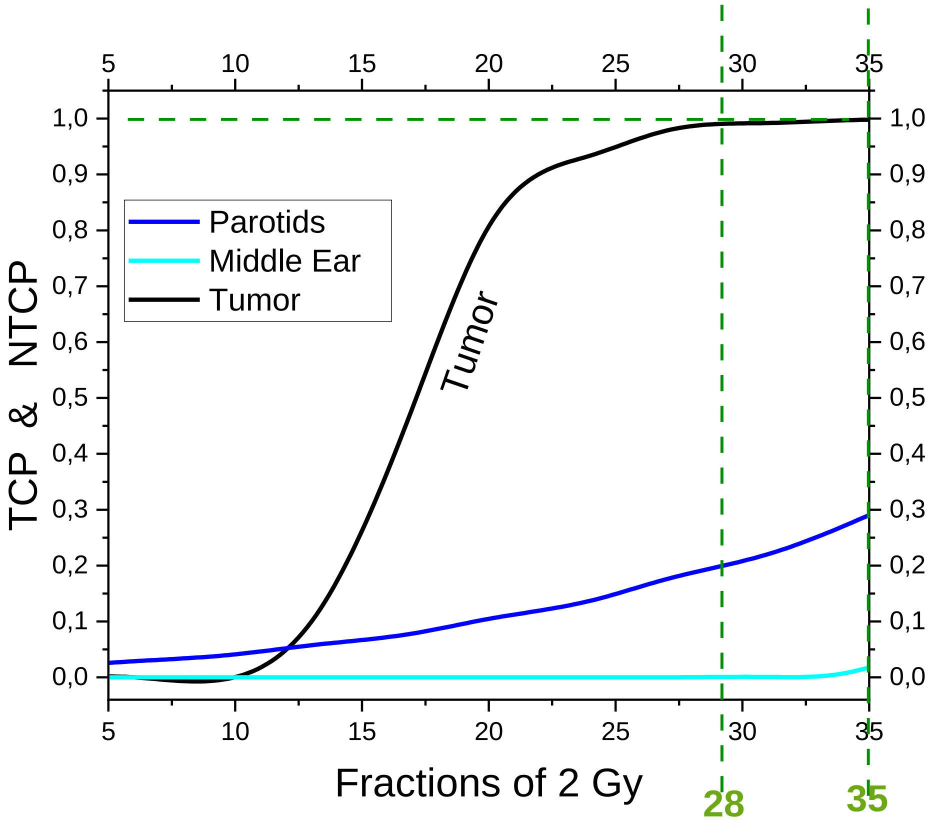

Figure IV.9: Plotted TCP and NTCP of parotide and middel ear of patient 9 using the presented program Radbio-For in function of fraction number.

When transferring parameters between two or more BED-based treatment protocols, it's important to consider that this process involves converting the dose scale deposited in each PTV subvolume in the DVH using the EQD2 formula. It's crucial to note that this conversion is a linear correction to the treatment plan and does not account for volume effects that can contribute to organs at risk complications. For that reason, to take into account the number of fractionations inside each volume fraction v_i of the organs at risk, a correction should be performed to D_i, before calculating the radiobiological models, by using an associated α/β ratio of organs at risk.

$$D_i = D_i \frac{\alpha/\beta + D_i/n_{fr}}{\alpha/\beta + 2} \qquad \text{(37)}$$

In this section, the correction was made using (equation 37) above where n_{fr} is the number of the fraction. D_i is the physical dose in each volume fraction v_i converted to the total equivalent biological dose normalized to a nominal standard fraction of 2 Gy. Our results show that for advanced-stage nasopharyngeal cancer, the NTCP rate

value of the parotid and middle ear increases as the dose per fraction increases (hypofractionation) and equals or decreases as the dose per fraction decreases (hyperfractionation) without loss of tumor control, see figure IV.10.

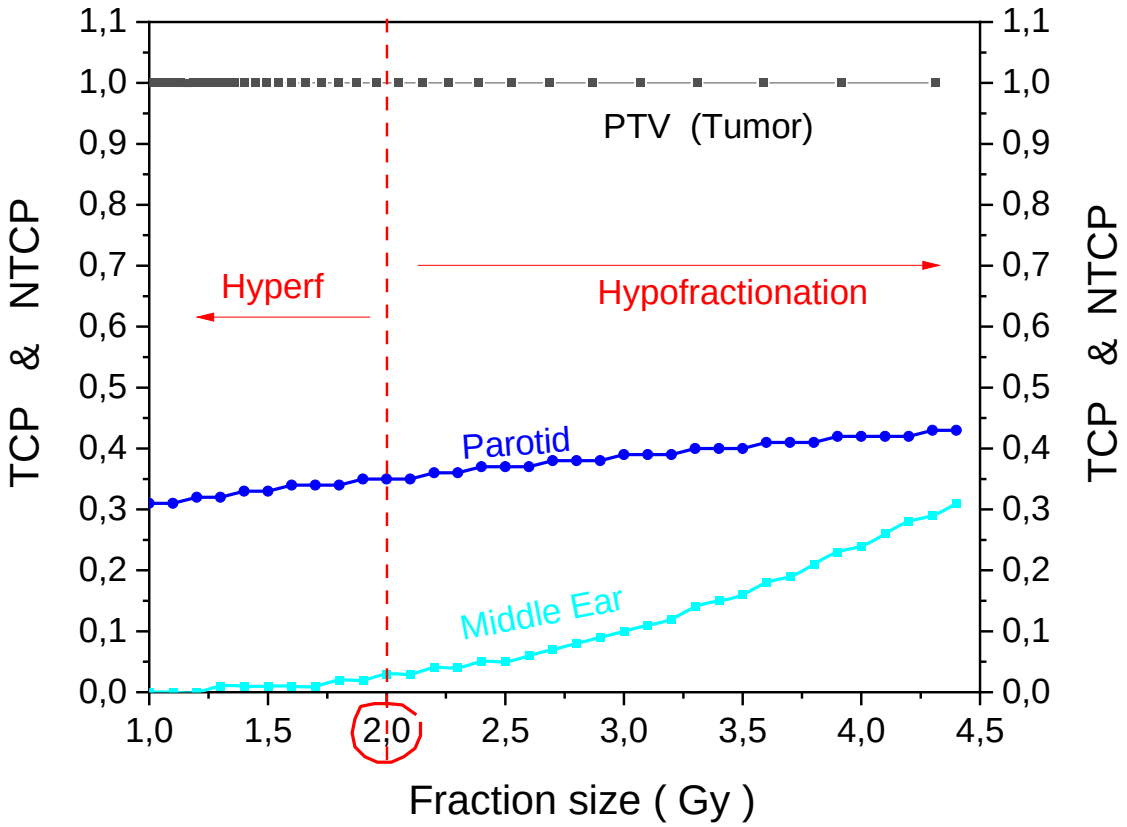

Figure IV.10: Optimization of the treatment plan of patient 9 using the presented program Radbio-For in function of fraction size.

According to figure IV.11 and 12, the late complication probability rate of the parotid and middle ear is increased by 0.08% and 0.05 %, respectively for the 3 Gy/21Fx scheme (hypofractionation), and no significant difference for the 1.5 Gy/48Fx scheme (hyperfractionation) compared to the standard regimen.

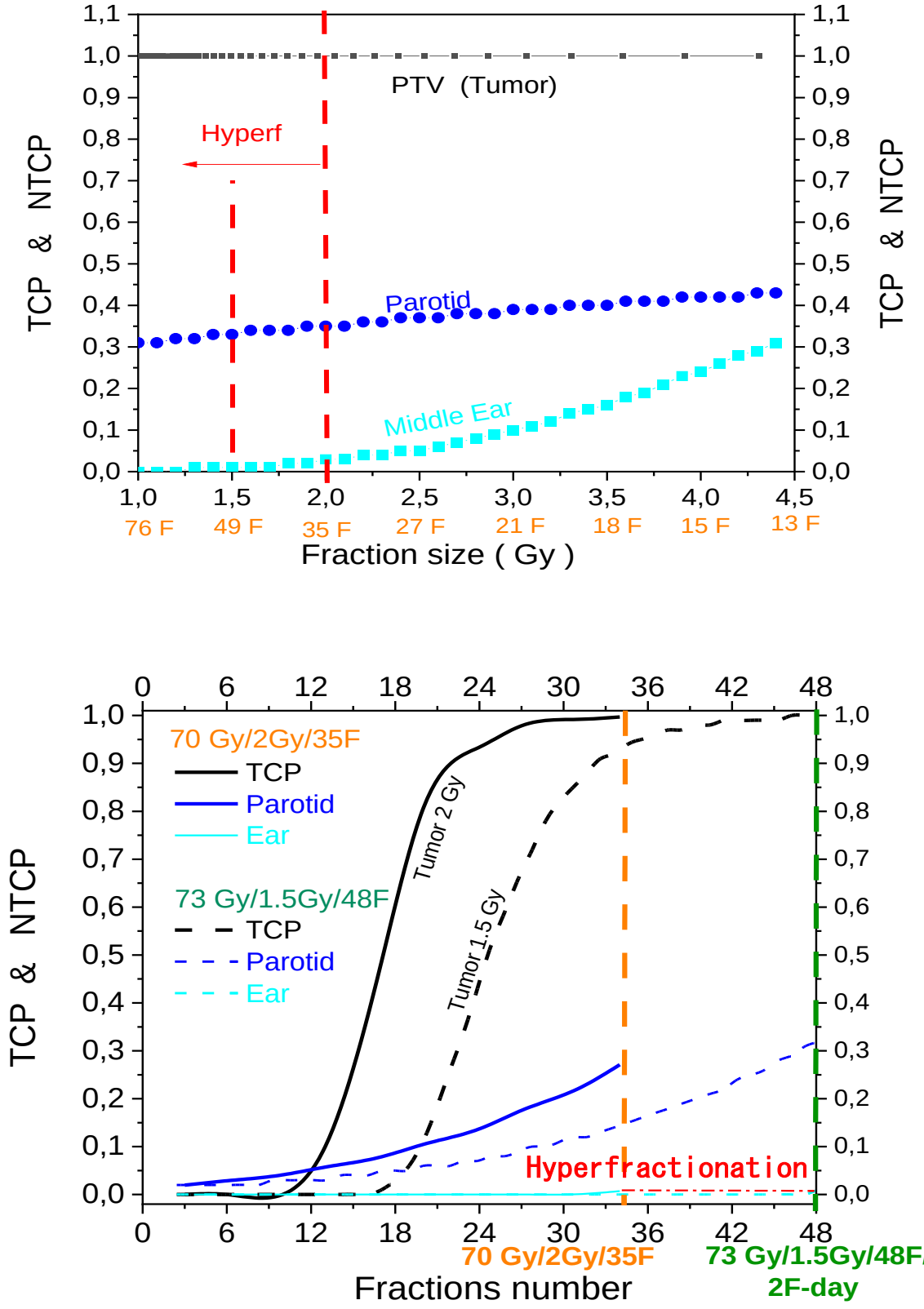

Figure IV.10: Improved prediction of tumor control and normal tissue complication probability to hyperfractionation using dose fractionation and biological equivalent dose (BED).

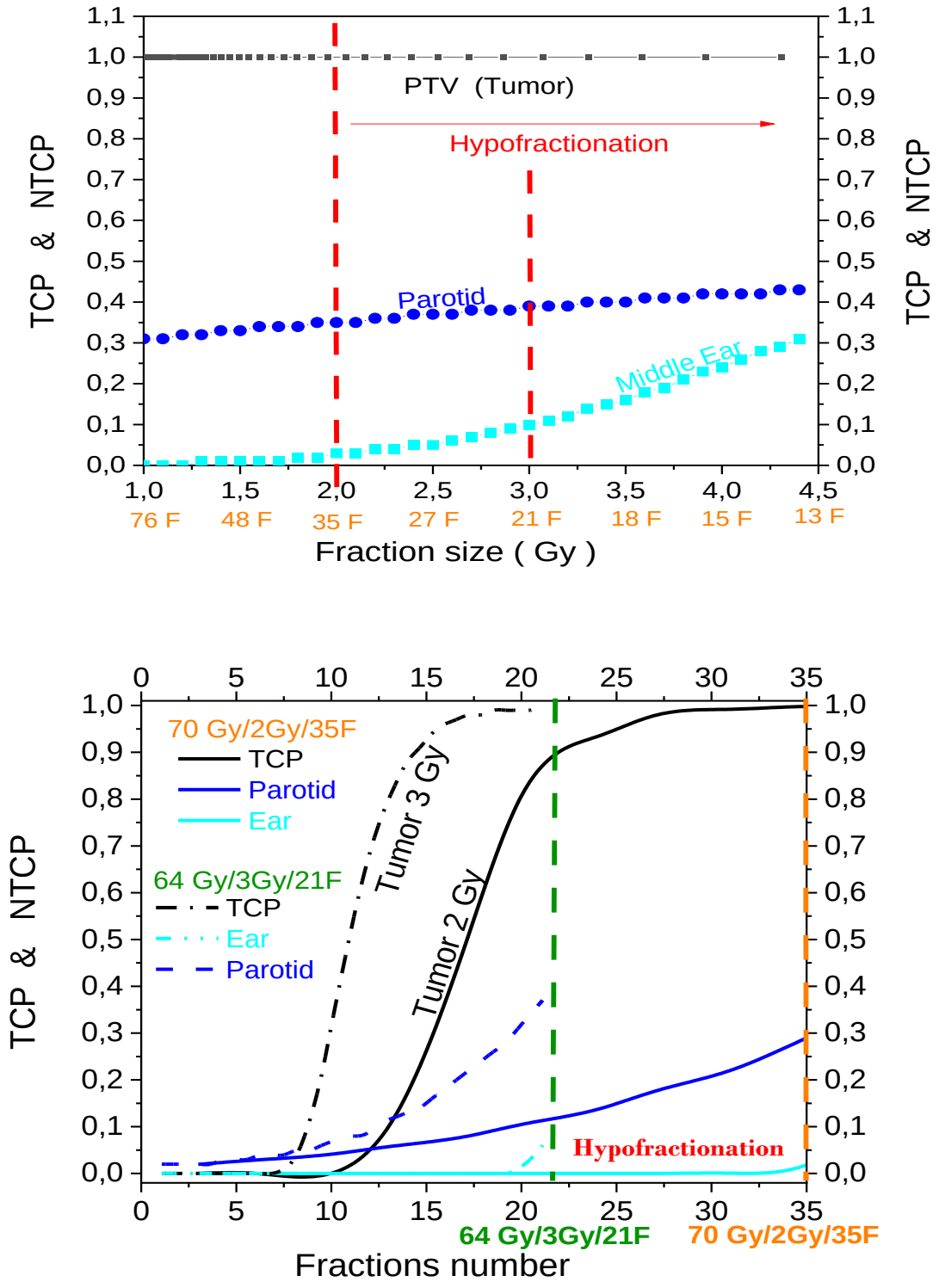

Figure IV.11: Improved prediction of tumor control and normal tissue complication probability to hypofractionation using dose fractionation and biological equivalent dose (BED).

The doses are increased since we have divided BED on (1+d/α/β) which implies the increase of BED and the NTCP value. Therefore, it is found that Fowler **(2008)** has proposed other treatment regimens where the dose per fraction is greater than 2 Gy but for early-stage UCNT cancer (late toxicities can be kept low). Thus, we have found that the hypofractionated regimen is not suitable for treating patients at an advanced stage of cancer.

2. Improving the prostate treatment plan.

The optimization of the head and neck treatment plan shows that cancer staging is a crucial factor in optimizing the treatment plan. Additionally, the value of alpha over beta significantly impacts BED conversion. In this section, we outline a method for optimizing the treatment plan for patient number 9 of prostate cancer.

After calculating the TCP values of the PTV and the NTCP of the rectum and bladder (toxicities cited in table IV.6), the total NTCP of both organs at risk is presented in figure IV.12 as a function of the number of fractions. Figure IV.13 shows the calculated value of the UTCP using the TCP and total NTCP.

It is evident from this figure that the TCP and NTCP curves are well separated, creating a wide window therapeutic range. Therefore, the UTCP curve reaches its maximum value towards the end of treatment, exceeding 80%.

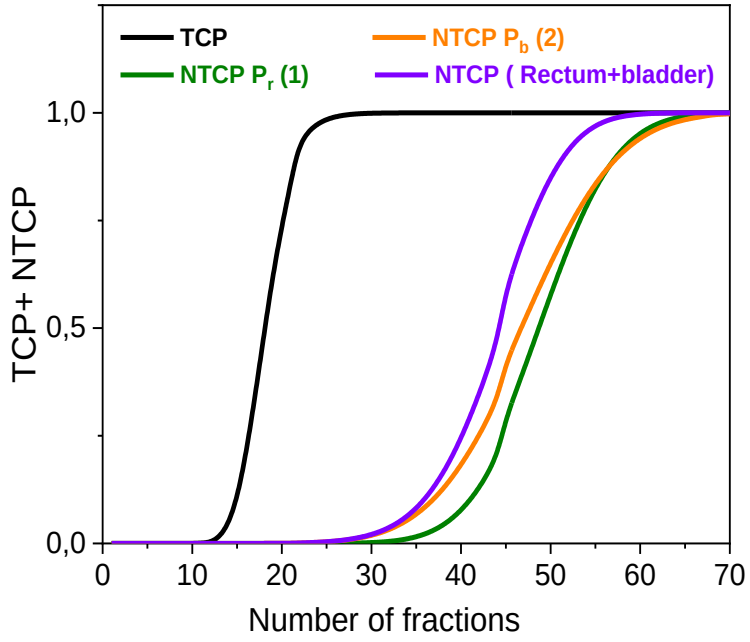

Figure IV.12: The curves of TCP and total NTCP of rectum and bladder for patient 9.

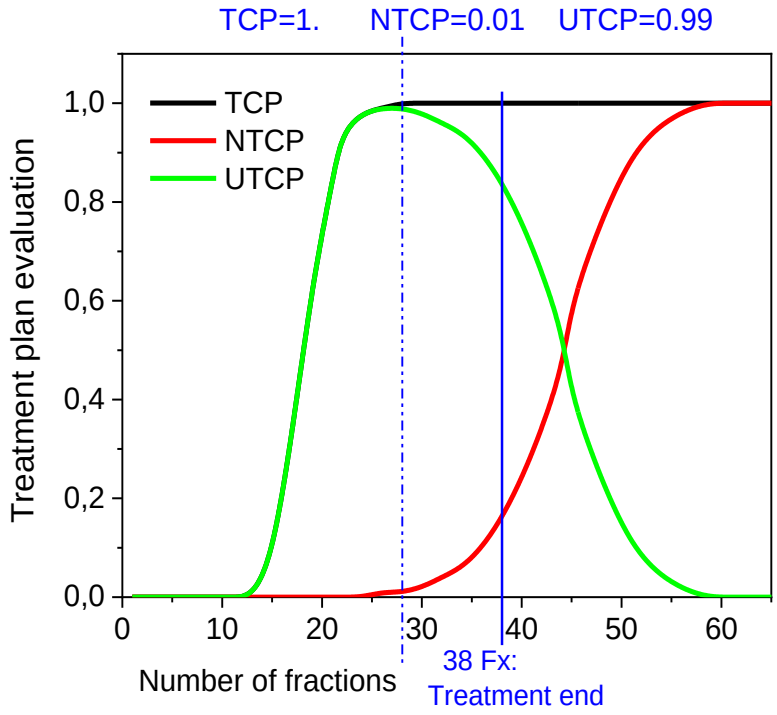

Figure IV.13: UTCP curve calculated from TCP and total NTCP of rectum and bladder.

After integrating the mild RTOG (Grade 2/3) complication into the total NTCP calculation, the gap between the TCP and NTCP curves narrows and the radiotherapeutic gap becomes less wide, affecting the decreasing UTCP value (<70%) towards the end of treatment 38 fractions figure IV.14.

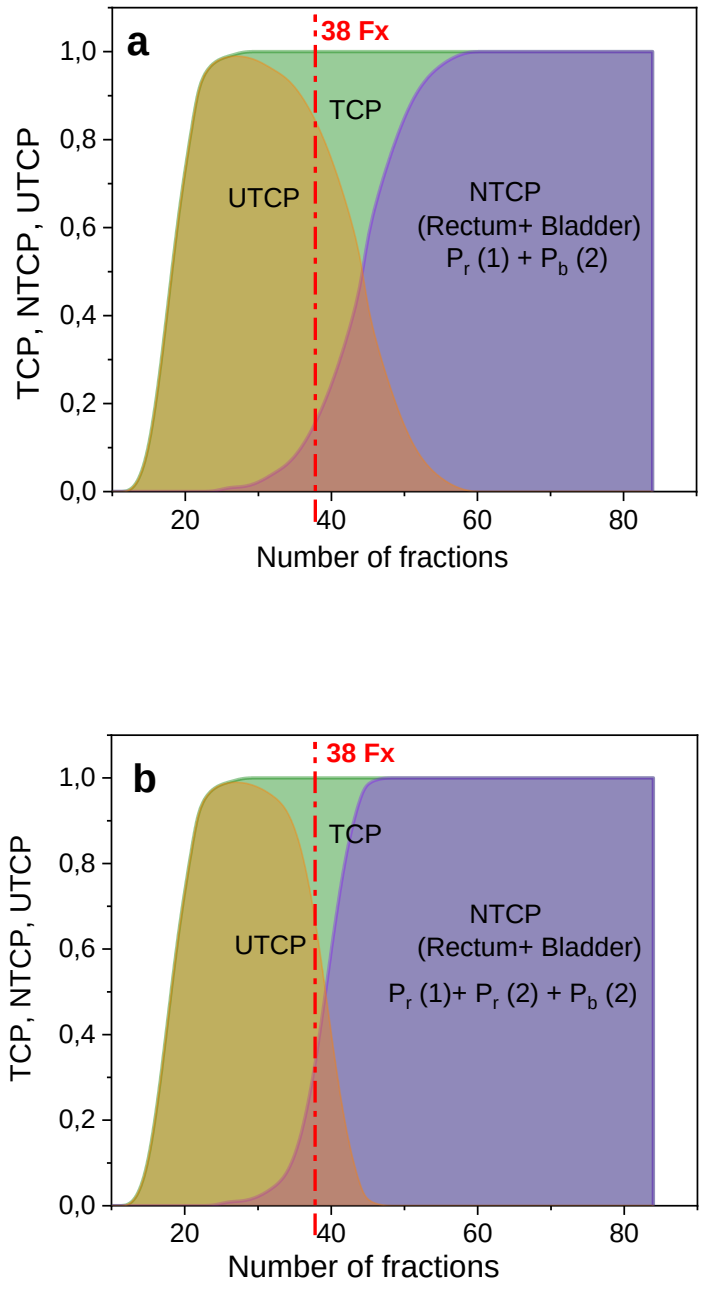

Figure IV.14: Comparison between calculated UTCP **a)** before integrating the mild RTOG complication, **b)** after integrating the mild RTOG complication in the treatment plan evaluation.

Figure IV.15 shows the evaluation of patient 9's treatment plan, where even here the UTCP value was decreased after the introduction of mild RTOG toxicity. However, it's important to note that this toxicity is relatively mild for the patient. Thus, the UTCP value is still above 60%, which defines the dose level and guarantees good tumor control while effectively protecting organs at risk.

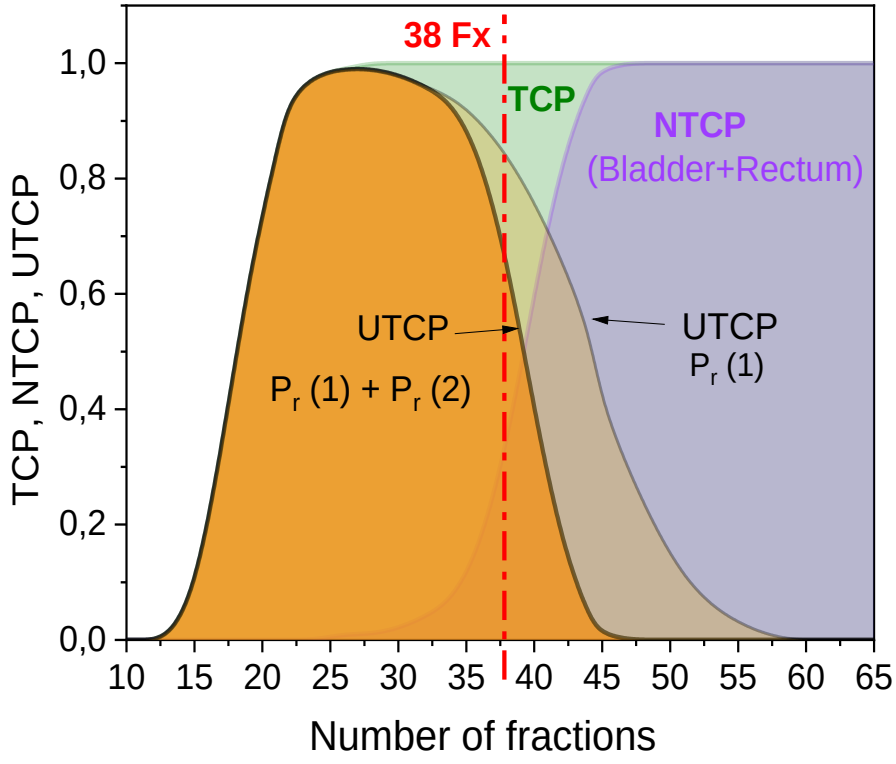

Figure IV.15: Treatment plan optimization of prostate cancer.

From the same figure we observe that by switching to the hypofractionated regimen while maintaining a TCP rate of 100%, we can reduce the number of treatment sessions to 25. This will keep the uncomplicated tumor control probability (UTCP) at a high level, helping to minimize side effects on organs at risk (resulting in a total NTCP, trending towards 0%). Conversely, switching to the hyperfractionated regimen will increase the risk of complications in organs at risk, leading to a decrease in UTCP, which is not desirable.

The results of this section of work demonstrate that the hypofractionated regimen is well-suited for addressing the staging of this specific type of prostate cancer.

Conclusion

The research findings detailed in Chapters 2, 3, and 4 provide a comprehensive understanding of how many factors shape the utilization of radiobiological tools. Key among these factors is the tumor's anatomical location, which can significantly affect the treatment approach and outcomes; the stage of cancer, indicating the extent of the disease and its progression; and the inherent radiosensitivity of the tumor, which refers to how susceptible the tumor cells are to radiation damage.

A notable advantage of radiobiological tools is their capacity to monitor treatment-related toxicity continuously. This monitoring capability is essential, as it allows for the assessment of adverse effects at any point: whether they emerge in the short term, weeks or months after treatment, or even years later, ensuring patient safety and treatment effectiveness. This becomes particularly important during and after radiotherapy treatment, provided there is access to the necessary radiobiological parameters that can inform clinicians about the patient's response to the therapy.

In addition, the sensitivity of tumors to radiation, often referred to as α-sensitivity, is typically assessed within a designated confidence interval. This statistical approach enables to predict the likelihood of toxicity occurring within this specific α-interval [...,...]. Drawing from the principles outlined in Chapter 1, which provides a detailed understanding of modern radiobiology, particularly relating to the concepts of the intrinsic α/β ratio and α radiosensitivity, it is important to recognize that each patient presents with a unique α-value. This individualized characteristic is crucial, as it allows for a more tailored prediction of radiation-induced toxicity based on the specific sensitivities exhibited by the tumor in question. Consequently, such an approach enhances our ability to approximate potential toxicity on a patient-by-patient basis, thereby optimizing treatment plans and improving patient outcomes.

The TCP values calculated with the three models MP, SP, and LM predicted a commendable level of local tumor control post-treatment planning, achieving rates exceeding 90%.

This study allows us to determine that the NTCP accurately models the differences between the dose constraints for the three radiobiological models RS, LKB, and LM. The RS model is particularly effective in capturing and characterizing late and

early tissue effects resulting from radiation, suggesting its superior applicability in clinical.

The reliability of calculating expected late complications has been confirmed by correlating NTCP with TPS dose constraints and using relevant clinical criteria along with the OAR's tissue structure. This work demonstrates NTCP's effectiveness as a radiobiological index in the TPS for predicting long-term complications, such as radiation-induced necrosis, myelitis, blindness, high-grade xerostomia, and cataracts in high-grade NPC treated with IMRT. Other endpoints cited in chapter 3 of rectum, bladder, and femoral heads in prostate cancer treated with IMRT and VMAT. It also suggests incorporating NTCP in automated treatment planning based on artificial intelligence and radiobiological tools to optimize treatment.

Based on alternate fractionation and isotopic plans developed in this study, the presented optimization tool has effectively applied and reduced late effects. This innovative method stands out for its dual focus on maximizing treatment efficacy and reducing the risk of long-term complications for patients.

Current radiobiological calculations clearly identify which organs are particularly sensitive and critical in the validation of treatment plans, unlike dosimetric indices. Our optimization tool for isotoxic plans has proven to be highly effective and can be utilized as a personalized radiotherapy tool to predict alternative fractionation schedules and reduce the total number of fractions.

The main findings of this study suggest that multiple factors can influence the prediction of toxicity, such as:

1. The effect of tumor staging.
2. The impact of treatment modality and technique.
3. The influence of the chosen radiobiological model.
4. The radiobiological parameters (endpoints).
5. The effect of treatment regimens, including standard, hypofractionated, and hyperfractionated approaches.
6. The consideration of time elapsed following treatment.

References

Ågren, A., Brahme, A., & Turesson, I. (1990). Optimization of uncomplicated control for head and neck tumors. *International Journal of Radiation Oncology* Biology* Physics*, *19*(4), 1077-1085.

Altun, M., Fandi, A., Dupuis, O., Cvitkovic, E., Krajina, Z., & Eschwege, F. (1995). Undifferentiated nasopharyngeal cancer (UCNT): current diagnostic and therapeutic aspects. *International Journal of Radiation Oncology* Biology* Physics*, *32*(3), 859-877.

Andrea, P., & Nahum, A. (2007). Supplementary details on codes of practice for absolute dose determination. *Handbook of Radiotherapy Physics: Theory and Practice*, 385-427.

Ardiet, J. M., Bourhis, J., Eschwege, F., Gerard, J. P., Martin, P., Mazeron, J. J., ... & Claude, L. (2007). Guide for External Beam Radiotherapy. Procedures 2007; Guide des procedures de radiotherapie externe.

Astudillo V, A., Paredes G, L., Resendiz G, G., Posadas V, A., Mitsoura, E., Rodriguez L, A., & Flores C, J. M. (2015). TCP and NTCP radiobiological models: conventional and hypo fractionated treatments in radiotherapy.

Ataídes, F. G., Silva, S. F. B. R., & Baldin, J. J. C. M. D. C. (2021). Radiation-Induced optic neuropathy: literature review. *Neuro-Ophthalmology*, *45*(3), 172-180.

Avanzo, M., Stancanello, J., Franchin, G., Sartor, G., Jena, R., Drigo, A., ... & Capra, E. (2010). Correlation of a hypoxia based tumor control model with observed local control rates in nasopharyngeal carcinoma treated with chemoradiotherapy. *Medical physics*, *37*(4), 1533-1544.

Banaei, A., Hashemi, B., & Bakhshandeh, M. (2015). Comparing the monoisocentric and dual isocentric techniques in chest wall radiotherapy of mastectomy patients. Journal of applied clinical medical physics, *16(1)*, 130-138.

Baradaran-Ghahfarokhi, M. (2014). Normal tissue complication probability modeling of radiation-induced bladder complications. *J Radiobiol*, *1*(1), 19-20.

Béhin, A., & Delattre, J. Y. (2004, December). Complications of radiation therapy on the brain and spinal cord. In *Seminars in neurology* (Vol. 24, No. 04, pp. 405-417). Copyright© 2004 by Thieme Medical Publishers, Inc., 333 Seventh Avenue, New York, NY 10001, USA.

Bentzen, S. M. (2018). Radiation dose-response relationships. In *Basic clinical radiobiology* (pp. 44-53). CRC press.

Bray, F., Ferlay, J., Soerjomataram, I., Siegel, R. L., Torre, L. A., & Jemal, A. (2018). Global cancer statistics 2018: GLOBOCAN estimates of incidence and mortality worldwide for 36 cancers in 185 countries. *CA: a cancer journal for clinicians*, *68*(6), 394-424.

Bedford, J. L., & Warrington, A. P. (2009). Commissioning of volumetric modulated arc therapy (VMAT). International Journal of Radiation Oncology* Biology* Physics, 73(2), 537-545.

Boyer, A. L., Goitein, M., Lomax, A. J., & Pedroni, E. S. (2002). Radiation in the treatment of cancer. *Physics Today*, *55*(9), 34-36.

Brenner, D. J., & Hall, E. J. (1999). Fractionation and protraction for radiotherapy of prostate carcinoma. *International Journal of Radiation Oncology* Biology* Physics*, *43*(5), 1095-1101.

Brenner, D. J. (2004). Fractionation and late rectal toxicity. *International journal of radiation oncology, biology, physics*, *60*(4), 1013-1015.

Brenner, D. J., & Hall, E. J. (2018). Hypofractionation in prostate cancer radiotherapy. *Transl Cancer Res*, *7*(Suppl 6), S632-9.

Brodak, M., Kosina, J., Pacovsky, J., Navratil, P., & Holub, L. (2010). Bipolar transurethral resection of anastomotic strictures after radical prostatectomy. *Journal of endourology*, *24*(9), 1477-1481.

Burman, C., Kutcher, G. J., Emami, B., & Goitein, M. (1991). Fitting of normal tissue tolerance data to an analytic function. International Journal of Radiation Oncology* Biology* Physics, 21(1), 123-135.

Burnet, N.G., Thomas, S.J., Burton, K.E. and Jefferies, S.J., 2004. Defining the tumour and target volumes for radiotherapy. Cancer Imaging, 4(2), p.153.

Cahlon, O., Zelefsky, M. J., Shippy, A., Chan, H., Fuks, Z., Yamada, Y., ... & Amols, H. (2008). Ultra-high dose (86.4 Gy) IMRT for localized prostate cancer: toxicity and biochemical outcomes. *International Journal of Radiation Oncology* Biology* Physics*, *71*(2), 330-337.

Chaikh, A. (2012). Méthodologie d'évaluation des impacts cliniques et dosimétriques d'un changement de procédure en radiothérapie: Aspect-Radio physique et médical (Doctoral dissertation, Grenoble).

Chaikh, A., Thariat, J., Thureau, S., Tessonnier, T., Kammerer, E., Fontbonne, C., Dubray, B., Balosso, J. and Fontbonne, J.M., 2020. Construction des modèles radiobiologiques de type TCP (tumor control probability) et NTCP (normal tissue complication probability): de la dose à la prédiction des effets cliniques. Cancer/Radiothérapie, 24(3), pp.247-257.

Chang, J. H., Gehrke, C., Prabhakar, R., Gill, S., Wada, M., Joon, D. L., & Khoo, V. (2016). RADBIOMOD: a simple program for utilising biological modelling in radiotherapy plan evaluation. *Physica Medica*, *32*(1), 248-254.

Chapman JD. Single-hit mechanism of cell killing by radiation. Int J Radiat Biol 2003;79:71–81.

Chapman, J. D., & Nahum, A. E. (2016). Radiotherapy treatment planning: linear-quadratic radiobiology. CRC Press.

Cody, W. J. (1969). Rational Chebyshev approximations for the error function. *Mathematics of computation*, *23*(107), 631-637.

Compton, C. C., Byrd, D. R., Garcia-Aguilar, J., Kurtzman, S. H., Olawaiye, A., & Washington, M. K. (Eds.). (2012). AJCC cancer staging atlas: a companion to the seventh editions of the AJCC cancer staging manual and handbook. Springer Science & Business Media.

Cooper, A. P. (1840). On the Anatomy of the Breast (Vol. 1). Longman.

Cox, J. D. (1986). Fractionation—A paradigm for clinical research in radiation oncology. *International Journal of Radiation Oncology* Biology* Physics*, *12*, 88.

Dai, Z., Zhu, L., Cao, T., Wang, A., Guo, X., Wang, Z., ... & Xiang, Z. (2020). Dosimetric and biological comparison of treatment plans between EDGE and CyberKnife systems in stereotactic body radiation therapy for localized prostate cancer.

Dale, R. G., & Jones, B. (Eds.). (2007). *Radiobiological modelling in radiation oncology*. British Inst of Radiology.

Dearnaley, D. P., Sydes, M. R., Graham, J. D., Aird, E. G., Bottomley, D., Cowan, R. A., ... & Parmar, M. K. (2007). Escalated-dose versus standard-dose conformal radiotherapy in prostate cancer: first results from the MRC RT01 randomised controlled trial. *The lancet oncology*, *8*(6), 475-487.

Doerr, W., Herrmann, T., & Baumann, M. (2014). Application of organ tolerance dose-constraints in clinical studies in radiation oncology. *Strahlentherapie und Onkologie*, *190*.

Doerr, W., 2009a. Time factors in normal tissue responses to irradiation. In: Joiner, M., Van der Kogel, A. (Eds.), Basic Clinical Radiobiology. 4th ed. Hodder Arnold, London, pp. 149–157.

Doerr, W., 2009b. Pathogenesis of normal tissue side effects. In: Joiner, M., Van der Kogel, A. (Eds.), Basic Clinical Radiobiology. 4th edn. Hodder Arnold, London, pp. 169–190.

Doerr, W., 2009c. Biological response modifiers: normal tissues. In: Joiner, M., Van der Kogel, A. (Eds.), Basic Clinical Radiobiology. 4th edn. Hodder Arnold, London, pp. 301–315.

Duchesne, G. M., & Peters, L. J. (1999). What is the alpha/beta ratio for prostate cancer? Rationale for hypofractionated high-dose-rate brachytherapy. *International journal of radiation oncology, biology, physics*, *44*(4), 747-748.

Ellis, H., & Mahadevan, V. (2013). Anatomy and physiology of the breast. *Surgery (Oxford)*, *31*(1), 11-14.

Emami, B., Lyman, J., Brown, A., Cola, L., Goitein, M., Munzenrider, J. E., ... & Wesson, M. (1991). Tolerance of normal tissue to therapeutic irradiation. International Journal of Radiation Oncology* Biology* Physics, 21(1), 109-122.

Emami, B. (2013). Tolerance of normal tissue to therapeutic radiation. *Reports of radiotherapy and Oncology*, *1*(1), 123-7.

Fan, X., Huang, Y., Xu, P., Min, Y., Li, J., Feng, M., ... & Lang, J. (2022). Dosimetric analysis of radiation-induced brainstem necrosis for nasopharyngeal carcinoma treated with IMRT. *BMC cancer*, *22*(1), 178.

Fine, S. W., & Reuter, V. E. (2011). Anatomy of the prostate revisited: implications for prostate biopsy and zonal origins of prostate cancer. Histopathology, 60(1), 142–152.

Fleet, A. (2006). Radiobiology for the Radiologist: Eric J. Hall, Amato J. Giaccia.

Fowler, J. F. (1989). The linear-quadratic formula and progress in fractionated radiotherapy. *The British journal of radiology*, *62*(740), 679-694.

Fowler, J. F. (2006). Development of radiobiology for oncology—a personal view. *Physics in Medicine & Biology*, *51*(13), R263.

Fowler, J. F. (2008). Optimum overall times II: Extended modelling for head and neck radiotherapy. *Clinical oncology*, *20*(2), 113-126.

Frometa-Castillo, T., Pyakuryal, A., Wals-Zurita, A., & Mesbahi, A. (2020). Proposals of models for new formulations of the current complication-free cure (P+) and uncomplicated tumor control probability (UTCP) concepts, and total normal tissue complication probability of late complications. *International Journal of Radiation Biology*, *96*(7), 847-850.

Fwu, P. T., Chen, J. H., Li, Y., Chan, S., & Su, M. Y. (2015). Quantification of regional breast density in four quadrants using 3d mri—a pilot study. *Translational oncology*, *8*(4), 250-257.

Galloway, T., Amdur, R. J., Brizel, D. M., Brockstein, B. E., Deschler, D. G., & Ganz, P. A. (2012). Management of late complications of head and neck cancer and its treatment. *Retrieved December*, *18*, 2012.

Gaudry, M., Lagier, D., Brige, P., Frandon, J., Rolland, P. H., Barral, P. A., ... & Vidal, V. (2018). Onyx migration into the anterior spinal artery during lumbar artery embolisation: an adverse event. *EJVES Short Reports*, *39*, 20-23.

Gay, H. A., & Niemierko, A. (2007). A free program for calculating EUD-based NTCP and TCP in external beam radiotherapy. *Physica Medica*, *23*(3-4), 115-125.

Gray, L. H., & Scholes, M. E. (1951). The Effect of Ionizing Radiations on the Broad Bean Root Part VIII. The British journal of radiology, 24(278), 82-92.

Grégoire, V., & Mackie, T. R. (2011). State of the art on dose prescription, reporting and recording in Intensity-Modulated Radiation Therapy (ICRU report No. 83). *Cancer/Radiothérapie*, *15*(6-7), 555-559.

Greene, F. L., Compton, C. C., Fritz, A. G., Shah, J. P., & Winchester, D. P. (Eds.). (2006). AJCC cancer staging atlas. New York, NY: Springer New York.

Gowda, S. N., Munakomi, S., & De Jesus, O. (2023). Brainstem Stroke. *StatPearls [Internet]*.

Guilbert, P., Gaillot-Petit, N., Vieren, L., & Nguyen, T. D. (2012). Conventional 2D and monoisocentric 3D techniques in breast and lymphatic irradiation: a dosimetric comparison. *Cancer Radiotherapie: Journal de la Societe Francaise de Radiotherapie Oncologique*, *16*(5-6), 473-478.

Hamatani, N., Sumida, I., Takahashi, Y., Oda, M., Seo, Y., Isohashi, F., ... & Ogawa, K. (2017). Three-dimensional dose prediction and validation with the radiobiological gamma index based on a relative seriality model for head-and-neck IMRT. *Journal of Radiation Research*, *58*(5), 701-709.

Harsolia, A., Vargas, C., Yan, D., Brabbins, D., Lockman, D., Liang, J., ... & Kestin, L. L. (2007). Predictors for chronic urinary toxicity after the treatment of prostate cancer with adaptive three-dimensional conformal radiotherapy: dose–volume analysis of a phase II dose-escalation study. *International Journal of Radiation Oncology* Biology* Physics*, *69*(4), 1100-1109.

Jackson, A., Kutcher, G. J., & Yorke, E. D. (1993). Probability of radiation-induced complications for normal tissues with parallel architecture subject to non-uniform irradiation. *Medical physics*, *20*(3), 613-625.

Jameson, M. G., Ohanessian, L., Batumalai, V., Patel, V., & Holloway, L. C. (2015). Comparison of Oncentra® Brachy IPSA and graphical optimisation techniques: a case study of HDR brachytherapy head and neck and prostate plans. *Journal of Medical Radiation Sciences*, *62*(2), 168-174.

JD, C. (1995). Toxicity criteria of the Radiation Therapy Oncology Group (RTOG) and the European Organization for Research and Treatment of Cancer (EORTC) 92-04. *Int J Radiat Oncol Biol Phys*, *31*, 134-136.

Jensen, I., Carl, J., Lund, B., Larsen, E. H., & Nielsen, J. (2011). Radiobiological impact of reduced margins and treatment technique for prostate cancer in terms of tumor control probability (TCP) and normal tissue complication probability (NTCP). *Medical Dosimetry*, *36*(2), 130-137.

Källman, P., Ågren, A., & Brahme, A. (1992). Tumour and normal tissue responses to fractionated non-uniform dose delivery. International journal of radiation biology, 62(2), 249-262.

Kan, M. W., Leung, L. H., & Yu, P. K. (2014). The use of biologically related model (Eclipse) for the intensity-modulated radiation therapy planning of nasopharyngeal carcinomas. *PLoS One*, *9*(11), e112229.

Kang, S. W., Chung, J. B., Kim, J. S., Kim, I. A., Eom, K. Y., Song, C., ... & Suh, T. S. (2017). Optimal planning strategy among various arc arrangements for prostate stereotactic body radiotherapy with volumetric modulated arc therapy technique. *Radiology and Oncology*, *51*(1), 112.

Karger CP (2006) 18 Biological Models in Treatment Planning. *New Technologies in Radiation Oncology: 221*.

Karia, D. (2018). *Radiobiological Optimization of Lung and Prostate Radiotherapy Treatments-A Macroscopic Approach*. The University of Liverpool (United Kingdom).

Kostakopoulos, A., Argiropoulos, V., Protogerou, V., Tekerlekis, P., & Melekos, M. (2004). Vesicourethral anastomotic strictures after radical retropubic prostatectomy: the experience of a single institution. *Urologia internationalis*, *72*(1), 17-20.

Kutcher, G.J., Burman, C., Brewster, L., Goitein, M. and Mohan, R., 1991. Histogram reduction method for calculating complication probabilities for three-dimensional treatment planning evaluations. International Journal of Radiation Oncology* Biology* Physics, 21(1), pp.137-146.

Kutcher, G. J., & Burman, C. (1989). Calculation of complication probability factors for non-uniform normal tissue irradiation: The effective volume method gerald. *International Journal of Radiation Oncology* Biology* Physics*, *16*(6), 1623-1630.

Lawton, C. A., Won, M., Pilepich, M. V., Asbell, S. O., Shipley, W. U., Hanks, G. E., ... & Rubin, P. (1991). Long-term treatment sequelae following external beam irradiation for adenocarcinoma of the prostate: analysis of RTOG studies 7506 and 7706. *International Journal of Radiation Oncology* Biology* Physics*, *21*(4), 935-939.

Lea, D. E., & Catcheside, D. G. (1942). The mechanism of the induction by radiation of chromosome aberrations in Tradescantia. Journal of genetics, 44, 216-245.

Leskinen, K., & Jero, J. (2005). Acute complications of otitis media in adults. *Clinical Otolaryngology*, *30*(6), 511-516.

Limb, C. J., Lustig, L. R., & Klein, J. O. (2017). Acute otitis media in adults. *Up To Date Apr*, *19*.

Lu, Y., Song, P. Y., Li, S. D., Spelbring, D. R., Vijayakumar, S., Haraf, D. J., & Chen, G. T. (1995). A method of analyzing rectal surface area irradiated and rectal complications in prostate conformal radiotherapy. International journal of radiation oncology, biology, physics, 33(5), 1121-1125.

Lustig, L. R., Limb, C. J., Baden, R., & LaSalvia, M. T. (2018). Chronic otitis media, cholesteatoma, and mastoiditis in adults. *UpToDate Waltham, MA (citirano 145, 2019)*.

Lyman, J. T., & Wolbarst, A. B. (1987). Optimization of radiation therapy, III: A method of assessing complication probabilities from dose-volume histograms. International Journal of Radiation Oncology* Biology* Physics, 13(1), 103-109.

Lyman, J. T. (1985). Complication probability as assessed from dose-volume histograms. *Radiation Research*, *104*(2s), S13-S19.

Marzi, S., Iaccarino, G., Pasciuti, K., Soriani, A., Benassi, M., Arcangeli, G., ... & Marucci, L. (2009). Analysis of salivary flow and dose–volume modeling of complication incidence in patients with head-and-neck cancer receiving intensity-modulated radiotherapy. *International Journal of Radiation Oncology* Biology* Physics*, *73*(4), 1252-1259.

Mazonakis, M., Lyraraki, E., Tolia, M., & Damilakis, J. (2022). 3D-CRT, IMRT and VMAT for flank irradiation due to pediatric Wilms tumor: A comparative planning study with XCAT phantoms. Physica Medica, *103*, 89-97.

Meherali, S., Campbell, A., Hartling, L., & Scott, S. (2019). Understanding parents' experiences and information needs on pediatric acute otitis media: a qualitative study. *Journal of patient experience*, *6*(1), 53-61.

McLaughlin, P. W., Troyer, S., Berri, S., Narayana, V., Meirowitz, A., Roberson, P. L., & Montie, J. (2005). Functional anatomy of the prostate: Implications for treatment planning. International Journal of Radiation Oncology*Biology*Physics, 63(2), 479–491.

McNeal, J. E. (1980). Anatomy of the prostate: An historical survey of divergent views. The Prostate, 1(1), 3–13.

Mohan, R., Mageras, G. S., Baldwin, B., Brewster, L. J., Kutcher, G. J., Leibel, S., ... & Fuks, Z. (1992). Clinically relevant optimization of 3-D conformal treatments. *Medical physics*, *19*(4), 933-944.

Nahum, A. E., & Hill, R. P. (2018). The radiobiological aspects of altered fractionation. *Alternate Fractionation in Radiotherapy: Paradigm Change*, 5-19.

Nahum, A. E., & Chapman, J. D. (2015). Radiotherapy Treatment Planning: Linear-Quadratic Radiobiology. CRC Press.

Nahum, A. E., Movsas, B., Horwitz, E. M., Stobbe, C. C., & Chapman, J. D. (2003). Incorporating clinical measurements of hypoxia into tumor local control modeling of prostate cancer: implications for the α/β ratio. *International Journal of Radiation Oncology* Biology* Physics*, *57*(2), 391-401.

Nahum, A. E., & Sanchez-Nieto, B. (2001). Tumour control probability modelling: basic principles and applications in treatment planning. *Physica Medica*, *17*, 13-23.

Neriishi, K., Nakashima, E., Minamoto, A., Fujiwara, S., Akahoshi, M., Mishima, H. K., ... & Shore, R. E. (2007). Postoperative cataract cases among atomic bomb survivors: radiation dose response and threshold. *Radiation research*, *168*(4), 404-408.

Nickers, P., Hermesse, J., Deneufbourg, J.M., Vanbelle, S. and Lartigau, E., 2010. Which α/β ratio and half-time of repair are useful for predicting outcomes in prostate cancer?. Radiotherapy and Oncology, 97(3), pp.462-466.

Niemierko, A., & Goitein, M. (1993). Modeling of normal tissue response to radiation: the critical volume model. *International Journal of Radiation Oncology* Biology* Physics*, *25*(1), 135-145.

Noël, G., & Antoni, D. (2022). Organs at risk radiation dose constraints. *Cancer/Radiothérapie*, *26*(1-2), 59-75.

Ohkura, H. (2015). Meiosis: an overview of key differences from mitosis. *Cold Spring Harbor Perspectives in Biology*, *7*(5), a015859.

Oinam, A. S., Singh, L., Shukla, A., Ghoshal, S., Kapoor, R., & Sharma, S. C. (2011). Dose volume histogram analysis and comparison of different radiobiological models using in-house developed software. *Journal of Medical Physics*, *36*(4), 220-229.

Okunieff, P., Morgan, D., Niemierko, A., & Suit, H. D. (1995). Radiation dose-response of human tumors. *International Journal of Radiation Oncology* Biology* Physics*, *32*(4), 1227-1237.

Orton, C. G. (2004). In regard to Nahum et al.(int j radiat oncol biol phys 2003; 57: 391–401): incorporating clinical measurements of hypoxia into tumor control modeling of prostate cancer: implications for the α/β ratio. *International journal of radiation oncology, biology, physics*, *58*(5), 1637.

Pandya, S., & Moore, R. G. (2011). Breast development and anatomy. Clinical obstetrics and gynecology, 54(1), 91-95.

Pasqualini, J. R. (Ed.). (2002). Breast cancer: prognosis, treatment, and prevention. CRC Press.

Pedicini, P., Strigari, L., & Benassi, M. (2013). Estimation of a self-consistent set of radiobiological parameters from hypofractionated versus standard radiation therapy of prostate cancer. *International Journal of Radiation Oncology* Biology* Physics*, *85*(5), e231-e237.

Podgorsak, E. B. (2005). *Radiation oncology physics: a handbook for teachers and students*.

Podgorsak, E. B. (2003). Review of radiation oncology physics: a handbook for teachers and students. *Vienna, Austria: IAE Agency*, *19*, 133.

Poncyljusz, M., Kukołowicz, P., Chorąży, J., Czyżew, B., Jankowska, A., Paciorkiewicz, A., ... & Zawadzka, A. (2016). Comparison of 3D-CRT and IMRT techniques in radiotherapy for post-prostatectomy patients with a higher risk of nodal involvement. *Biuletyn Polskiego Towarzystwa Onkologicznego Nowotwory*, *1*(3), 223-227.

Purdy, J. A. (1999). 3D treatment planning and intensity-modulated radiation therapy. Oncology (Williston Park, NY), *13(10 Suppl 5)*, 155-168.

Rana, S., & Cheng, C. Y. (2014). Radiobiological impact of planning techniques for prostate cancer in terms of tumor control probability and normal tissue complication probability. *Annals of medical and health sciences research*, *4*(2), 167-172.

Sanchez-Nieto, B., & Nahum, A. E. (2000). BIOPLAN: software for the biological evaluation of radiotherapy treatment plans. *Medical Dosimetry*, *25*(2), 71-76.

Semenenko, V. A., & Li, X. A. (2008). Lyman–Kutcher–Burman NTCP model parameters for radiation pneumonitis and xerostomia based on combined analysis of published clinical data. *Physics in Medicine & Biology*, *53*(3), 737.

Shah, S. (2022). Common terminology criteria for adverse events.

Shimizuguchi, T., Nihei, K., Okano, T., Machitori, Y., Ito, K., & Karasawa, K. (2017). A comparison of clinical outcomes between three-dimensional conformal radiotherapy and intensity-modulated radiotherapy for prostate cancer. *International journal of clinical oncology*, *22*, 373-379.

Simhan, J., Ramirez, D., Hudak, S. J., & Morey, A. F. (2014). Bladder neck contracture. *Translational andrology and urology*, *3*(2), 214.

Steel GG (2002a) Cell survival as a determinant of tumour response. In: Steel GG (ed) Basic clinical radiobiology, 3rd ed. Arnold, London, pp 52–63.

Steel, G. G. (2007a) Radiobiology of tumours. In: Mayles P, Nahum AE, Rosenwald J-C(eds) Handbook of radiotherapy physics—theory and practice. Taylor and Francis, London, pp 127–148.

Steel, G. G. (1993). Dose-rate effects in brachytherapy. *European Journal of Cancer*, *29*, S36.

Thor, M., Olsson, C., Oh, J. H., Petersen, S. E., Alsadius, D., Bentzen, L., ... & Deasy, J. O. (2016). Urinary bladder dose–response relationships for patient-reported genitourinary morbidity domains following prostate cancer radiotherapy. *Radiotherapy and Oncology*, *119*(1), 117-122.

US Department of Health and Human Services (2017). Common terminology criteria for adverse events. *National Institutes of Health, National Cancer Institute*.

Uzan, J., & Nahum, A. E. (2012). Radiobiologically guided optimisation of the prescription dose and fractionation scheme in radiotherapy using BioSuite. *The British journal of radiology*, *85*(1017), 1279-1286.

Valdagni, R., Italia, C., Montanaro, P., Lanceni, A., Lattuada, P., Magnani, T., Fiorino, C. and Nahum, A., 2005. Is the alpha–beta ratio of prostate cancer really low? A prospective, non-randomized trial comparing standard and hyperfractionated conformal radiation therapy. Radiotherapy and Oncology, 75(1), pp.74-82.

Viani, G., Hamamura, A. C., & Faustino, A. C. (2019). Intensity modulated radiotherapy (IMRT) or conformational radiotherapy (3D-CRT) with conventional fractionation for prostate cancer: Is there any clinical difference?. *International braz j urol*, *45*, 1105-1112.

Wadasadawala, T., Lewis, S., Gaikwad, U., Gayake, U., Phurailatpam, R., Tambe, S., & Sarin, R. (2022). Mono versus dual isocentric technique for breast cancer radiotherapy: Evaluation of planning, dosimetry and treatment delivery. Journal of Radiotherapy in Practice, *21(1)*, 1-6.

Walsh, S., Roelofs, E., Kuess, P., Lambin, P., Jones, B., Georg, D., & Verhaegen, F. (2016). A validated tumor control probability model based on a meta-analysis of low, intermediate, and high-risk prostate cancer patients treated by photon, proton, or carbon-ion radiotherapy. *Medical physics*, *43*(2), 734-747.

Wang, H., Cooper, B. T., Schiff, P., Sanfilippo, N. J., Wu, S. P., Hu, K. S., ... & Xue, J. (2019). Dosimetric assessment of tumor control probability in intensity and

volumetric modulated radiotherapy plans. *The British Journal of Radiology*, *92*(1094), 20180471.

Warkentin, B., Stavrev, P., Stavreva, N., Field, C., & Fallone, B. G. (2004). A TCP-NTCP estimation module using DVHs and known radiobiological models and parameter sets. *Journal of Applied Clinical Medical Physics*, *5*(1), 50-63.

Weigelt, B., Geyer, F. C., & Reis-Filho, J. S. (2010). Histological types of breast cancer: how special are they?. Molecular oncology, 4(3), 192-208.

Williams, M. V., Denekamp, J., & Fowler, J. F. (1985). A review of αβ ratios for experimental tumors: implications for clinical studies of altered fractionation. *International Journal of Radiation Oncology* Biology* Physics*, *11*(1), 87-96.

Williams, S.G., Taylor, J.M., Liu, N., Tra, Y., Duchesne, G.M., Kestin, L.L., Martinez, A., Pratt, G.R. and Sandler, H., 2007. Use of individual fraction size data from 3756 patients to directly determine the α/β ratio of prostate cancer. International Journal of Radiation Oncology* Biology* Physics, 68(1), pp.24-33.

Withers, H. R. (1975). The four R's of radiotherapy. In *Advances in radiation biology* (Vol. 5, pp. 241-271). Elsevier.

Withers, H. R., Taylor, J. M. G., & Maciejewski, B. (1988). The hazard of accelerated tumor clonogen repopulation during radiotherapy. Acta oncologica, 27(2), 131-146.

LENT/Soma, (1995) Tables. Radiation Oncology, 35, 17-60.

Wolbarst, A. B., Chin, L. M., & Svensson, G. K. (1982). Optimization of radiation therapy: integral-response of a model biological system. *International Journal of Radiation Oncology* Biology* Physics*, *8*(10), 1761-1769.

Zaider, M., & Minerbo, G. N. (2000). Tumour control probability: a formulation applicable to any temporal protocol of dose delivery. *Physics in Medicine & Biology*, *45*(2), 279.

Zelefsky, M. J., Levin, E. J., Hunt, M., Yamada, Y., Shippy, A. M., Jackson, A., & Amols, H. I. (2008). Incidence of late rectal and urinary toxicities after three-dimensional conformal radiotherapy and intensity-modulated radiotherapy for localized prostate cancer. *International Journal of Radiation Oncology* Biology* Physics*, *70*(4), 1124-1129.

Zhu, J. (2013). Modèles prédictifs de toxicité en radiothérapie par modulation d'intensité (Doctoral dissertation, Rennes 1).

Zhu, J., Simon, A., Haigron, P., Lafond, C., Acosta, O., Shu, H., ... & De Crevoisier, R. (2016). The benefit of using bladder sub-volume equivalent uniform dose constraints in prostate intensity-modulated radiotherapy planning. *OncoTargets and therapy*, 7537-7544.

Résumé

En plus de l'évaluation dosimétrique des plans de traitement, nous avons effectué une évaluation radiobiologique à l'aide des indices NTCP, TCP et UTCP. Cette évaluation est intégrée dans le programme développé, Radbio-For, qui nous a permis de calculer des modèles radiobiologiques pour divers paramètres de l'organe primaire limitant la dose. Cette approche globale nous a permis d'évaluer et de prédire efficacement les effets précoces et tardifs. Dans une autre section de notre analyse, nous avons effectué une comparaison de notre programme développé avec les logiciels RADBIOMOD et BioSuite.

Notre analyse a indiqué que le NTCP modélise efficacement les différences de contraintes de dose entre les trois modèles : RS, LKB et LM. Le modèle RS démontre une capacité supérieure à caractériser les effets tardifs et précoces. En outre, les valeurs TCP dérivées des modèles : MP, SP et LM ont montré des attentes prometteuses pour le contrôle local de la tumeur après la planification du traitement, dépassant 90 %. Les évaluations radiobiologiques actuelles fournissent des indications claires sur les organes particulièrement sensibles et critiques au cours du processus de validation du plan de traitement, offrant une compréhension plus précise que les indices dosimétriques.

Le critère de comparaison de la contrainte de dose calculée avec le TPS à la contrainte de dose clinique pertinente pour chaque OAR dans le cancer de haut grade de nasopharynx et le cancer de la prostate était un outil prédictif précieux pour évaluer la fiabilité des calculs des complications précoces et tardives attendues ; Ce résultat important trouve son application directe dans la radiothérapie personnalisée dans la prévention des toxicités à long terme et est un outil précieux pour le physicien avant le traitement. En outre, notre outil d'optimisation pour les plans isotoxiques s'est révélé puissant pour prédire un fractionnement alternatif et réduire le nombre de fractions.

***Mots-clés** : Radiobiologie ; radiothérapie ; fractionnement ; plan de traitement ; tumeur ; probabilité de contrôle de la tumeur ; probabilité de complication du tissu normal.*

ملخص

بالإضافة إلى إجراء تقييم جرعات لخطط العلاج الإشعاعي ، أجرينا تقييما بيولوجيا باستخدام مؤشرات NTCP , TCPو UTCP المدمجه في برنامجنا المطور ، Radbio-For ، والذي سمح لنا بحساب النماذج الإشعاعية الحيوية لنقاط النهاية المختلفة للعضو الأساسي الذي يحد من الجرعة. مكننا هذا النهج الشامل من تقييم الآثار المبكرة والمتأخرة والتنبؤ بها بشكل فعال. في قسم آخر من تحليلنا ، أجرينا مقارنة بين برنامجنا المطور مع برنامج RADBIOMOD وBioSuite للتحقق والتاكد من صحه النتائج التي تحصلنا عليها.

يشير تحليلنا إلى أن NTCP ينمذج بشكل فعال الاختلافات في قيود الجرعة عبر النماذج الثلاثة RS : LKB ,وLM. يظهر نموذج RS قدرة فائقة في وصف كل من التأثيرات المتأخرة والمبكرة. علاوة على ذلك ، تظهر قيم TCP المستمدة من النماذج : MP , SP و LM توقعات واعدة للسيطرة على الورم الموضعي بعد تخطيط العلاج ، تتجاوز 90٪. توفر التقييمات الإشعاعية البيولوجية الحالية رؤى واضحة حول الأعضاء الحساسة والحرجة بشكل خاص أثناء عملية التحقق من صحة خطة العلاج ، مما يوفر فهما أكثر دقة من مؤشرات قياس الجرعات .

يعد معيار المقارنة لقيد الجرعة المحسوب مع TPS على قيود الجرعة السريرية ذات الصلة لكل عضو محيط في سرطان البلعوم الأنفي NPC عالي الدرجة وسرطان البروستاتا أداة تنبؤية قيمة لتقييم موثوقية حسابات المضاعفات المبكرة والمتأخرة المتوقعة. تجد هذه النتيجة المهمة تطبيقها المباشر في العلاج الإشعاعي الشخصي في منع السمية طويلة المدى وهي أداة قيمة للفيزيائي قبل العلاج. بالإضافة إلى ذلك ، تم الكشف عن أن أداة التحسين الخاصة بنا لخطط متساوية السمية قوية في التنبؤ بالتجزئة البديلة وتقليل عدد الكسر.

الكلمات المفتاحية: علم الأحياء الإشعاعي؛ تجزئة العلاج الإشعاعي ؛ خطة علاج الورم ؛ احتمال السيطرة على الورم ؛ احتمال حدوث مضاعفات الأنسجة الطبيعية .

Abstract

In addition to conducting a dosimetric evaluation of the treatment plans, we performed a radiobiological assessment using the NTCP, TCP, and UTCP indices. This is integrated into our developed program, Radbio-For, which allowed us to compute radiobiological models for various endpoints of the primary dose-limiting organ. This comprehensive approach enabled us to effectively evaluate and predict both early and late effects. In another section of our analysis, we conducted a comparison of our developed program with the RADBIOMOD and BioSuite software.

Our analysis indicated that the NTCP effectively models the differences in dose constraints across the three models: RS, LKB, and LM. The RS model demonstrates a superior capability in characterizing both late and early effects. Furthermore, the TCP values derived from the models: MP, SP, and LM showed promising expectations for local tumor control following treatment planning, exceeding 90%. Current radiobiological assessments provide clear insights into which organs are particularly sensitive and critical during the treatment plan validation process, offering a more precise understanding than dosimetric indices.

The comparison criterion of the calculated dose constraint with TPS to the relevant clinical dose constraint for each OAR in high-grade NPC and prostate cancer was a valuable predictive tool for assessing the reliability of the calculations of expected early and late complications; This important outcome finds its direct application in personalized radiotherapy in preventing long-term toxicities and is a valuable tool for the physicist before the treatment. In addition, Our optimization tool for isotoxic plans was revealed to be powerful in predicting alternate fractionation and reducing the fraction number.

Keywords*: Radiobiology; radiotherapy; fractionation; treatment plan; tumor; tumor control probability; normal tissue complication probability*.